NASA TECHNICAL NOTE

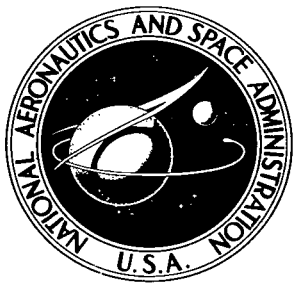

LOW-SPEED WIND-TUNNEL TESTS OF 1/10-SCALE MODEL OF A BLENDED-ARROW SUPERSONIC CRUISE AIRCRAFT

H. Clyde McLemore and Lysle P. Parlett

Langley Research Center
Hampton, Va. 23665

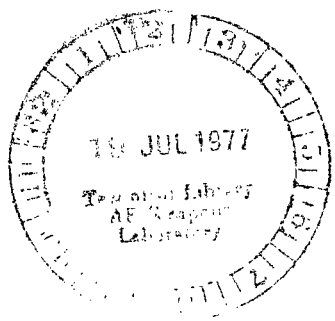

NATIONAL AERONAUTICS AND SPACE ADMINISTRATION • WASHINGTON, D. C. • JUNE 1977

1. Report No.	2. Government Accession No.	3. Recipient's Catalog No.
NASA TN D-8410		

4. Title and Subtitle	5. Report Date
LOW-SPEED WIND-TUNNEL TESTS OF 1/10-SCALE MODEL OF A BLENDED-ARROW SUPERSONIC CRUISE AIRCRAFT	June 1977
	6. Performing Organization Code
7. Author(s)	8. Performing Organization Report No.
H. Clyde McLemore and Lysle P. Parlett	L-11086
	10. Work Unit No. 743-04-12-02
9. Performing Organization Name and Address	11. Contract or Grant No.
NASA Langley Research Center Hampton, VA 23665	
	13. Type of Report and Period Covered
12. Sponsoring Agency Name and Address	Technical Note
National Aeronautics and Space Administration Washington, DC 20546	14. Sponsoring Agency Code

15. Supplementary Notes

16. Abstract

Low-speed static force tests have been conducted in the Langley full-scale tunnel to determine the low-speed aerodynamic characteristics of a 1/10-scale model of a blended-arrow supersonic cruise aircraft. A clean configuration and a high-lift configuration with several combinations of leading- and trailing-edge flaps to provide improved lift and longitudinal stability in the landing and take-off modes were used. The tests were made at angles of attack from about -6° to 30°, sideslip angles from -5° to 10°, and Reynolds numbers from 6.78×10^{6} to 13.85×10^{6} corresponding to test velocities of 41 to 85 knots.

17. Key Words (Suggested by Author(s))	18. Distribution Statement
Aerodynamics Low-speed stability and control Supersonic cruise aircraft	Unclassified - Unlimited Subject Category 01

19. Security Classif. (of this report)	20. Security Classif. (of this page)	21. No. of Pages	22. Price*
Unclassified	Unclassified	64	$4.50

* For sale by the National Technical Information Service, Springfield, Virginia 22161

LOW-SPEED WIND-TUNNEL TESTS OF 1/10-SCALE MODEL OF A BLENDED-ARROW SUPERSONIC CRUISE AIRCRAFT

H. Clyde McLemore and Lysle P. Parlett
Langley Research Center

SUMMARY

Low-speed static force tests have been conducted in the Langley full-scale tunnel to determine the low-speed aerodynamic characteristics of a 1/10-scale model of a blended-arrow supersonic cruise aircraft. A clean configuration and a high-lift configuration with several combinations of leading- and trailing-edge flaps to provide improved lift and longitudinal stability in the landing and take-off modes were used. The tests were made at angles of attack from about -6° to 30°, sideslip angles from -5° to 10°, and Reynolds numbers from 6.78×10^{6} to 13.85×10^{6} corresponding to test velocities of 41 to 85 knots.

The clean configuration exhibited static longitudinal instability (pitch-up) at angles of attack greater than about 3°; however, deflecting inboard and outboard wing leading-edge flaps delayed the pitch-up to an angle of attack of about 18°. Deflecting full-span trailing-edge flaps and leading-edge flaps increased the untrimmed lift coefficient from about 0.35 for the clean configuration to about 0.50 at an angle of attack of 9.5° (estimated tail-scrape angle). The model exhibited satisfactory lateral-directional characteristics for angles of attack to about 16°. Above this angle of attack the directional stability increased markedly; however, the effective dihedral decreased to nearly zero at an angle of attack of about 24°.

INTRODUCTION

The present study is part of an overall effort by the National Aeronautics and Space Administration to provide a technology base for the formulation and development of supersonic cruise vehicles. This paper presents the results of low-speed tests of a supersonic cruise aircraft concept designed to utilize very low wing weight (blended wing-fuselage contours), variable-cycle engines or quiet duct-burning fan engines, and thrust vectoring.

The distinguishing features of the present concept are the platypus-nose all-wing planform and the four-engine propulsion package mounted on the center line. The planform with its long root chord was selected to keep sonic-boom levels low by spreading lift in the axial direction at supersonic speeds as discussed in reference 1. The location of the propulsion system was dictated, in part, by the desire to avoid aeroelastic problems associated with the placing of mass outboard and rearward of the torsional axis of the flexible lightweight structure. The propulsion system was designed to incorporate a thrust vectoring capability which was intended to provide increased circulation and thereby improve lift and lift-drag ratio (refs. 2 and 3), and to provide additional

longitudinal control. In order to use vectored thrust effectively to improve airframe flight efficiency in the critical low-speed mode, where thrust reduction is important to noise alleviation, active controls are also required. Beyond the features cited, the aerodynamic design philosophy is largely that reported in references 4 and 5.

The objectives of these tests are to determine some of the low-speed static aerodynamic characteristics of the basic configuration concept and to provide a data base from which configuration modifications might be made to alleviate any low-speed aerodynamic problems.

The tests were conducted in the Langley full-scale tunnel on a 1/10-scale model of a blended-arrow supersonic cruise aircraft. The tests were made at Reynolds numbers from 6.78×10^6 to 13.85×10^6 based on the mean aerodynamic chord, angles of attack from about -6° to 30°, and sideslip angles from -5° to 10°. The configuration variables included combinations of leading- and trailing-edge flap deflection angles, engine nozzle deflection angles, and a range of thrust levels. A few tests were conducted with the vertical tails removed to determine the contribution of the tails to lateral-directional stability, and in addition, tests were conducted to determine rudder effectiveness. A few tests were also conducted with a canard.

SYMBOLS

The data are referred to the stability system of axes shown in figure 1. The origin of the axis corresponds to the 35-percent location of the mean aerodynamic chord.

The dimensional quantities are given in the International System of Units (SI) and parenthetically in U.S. Customary Units. All measurements and calculations were made in U.S. Customary Units. Conversion factors for the two systems are given in reference 6.

b wing span, 4.572 m (15.00 ft)

C_D drag coefficient, $\frac{\text{Drag}}{qS}$

C_L lift coefficient, $\frac{\text{Lift}}{qS}$

C_l rolling-moment coefficient, $\frac{\text{Rolling moment}}{qSb}$

C_{l_β} rolling moment due to sideslip

C_m pitching-moment coefficient, $\frac{\text{Pitching moment}}{qS\bar{c}}$

C_n yawing-moment coefficient, $\frac{\text{Yawing moment}}{qSb}$

C_{n_β} yawing moment due to sideslip

C_T' thrust coefficient ($C_T' = 0$ when engine exhaust total pressure is equal to free-stream total pressure), T/qS (designated T_c' in many reports)

C_Y side-force coefficient, $\frac{\text{Side force}}{qS}$

C_{Y_β} side force due to sideslip

$\bar{c}$ mean aerodynamic chord, 4.602 m (15.10 ft)

i_c canard deflection angle, positive leading edge up, deg

L/D lift-drag ratio

q free-stream dynamic presure, Pa (lb/ft^2)

S wing area, 15.14 m^2 (163.00 ft^2)

T engine thrust (thrust above the value for $C_T' = 0$), N (lb)

V free-stream velocity, m/sec (ft/sec)

X longitudinal stability axis

α angle of attack referred to wing reference line (fig. 1), deg

β angle of sideslip, deg

$\delta_{f,le}$ leading-edge flap deflection referenced to undeflected leading-edge position, deg

$\delta_{f,te}$ trailing-edge flap deflection, deg

δ_N engine exhaust deflection angle, positive downward, deg

δ_r rudder deflection, positive for trailing edge left, deg

Subscripts:

1,2,3,4,5,6,7 wing leading-edge flap segments (used with $\delta_{f,le}$); 1, nearest wing tip and 7, nearest nose of model (see figs. 2 and 3)

1,2,3 wing trailing-edge flap segments (used with $\delta_{f,te}$); 1, inboard, and 3, outboard (see figs. 2 and 3)

Abbreviations:

BS body station (longitudinal distance from model nose)

WL water line

MODEL

The dimensional characteristics of the 1/10-scale model are shown in figures 2 to 4. Photographs of the model mounted for tests in the Langley full-scale tunnel are presented in figures 5 to 7. The model had an aluminum framework filled with a polyurethane foam filler and covered with several layers of fiber glass. The model was essentially rigid for these low-speed tests.

The model was equipped with wing leading- and trailing-edge flaps, twin vertical tails, and, for a few tests, a canard of either 2 or 2.5 percent of wing area. The leading-edge flap segments could be deflected from 0° to 60° downward (referenced normal to the wing leading-edge hinge line and to the mean line of the leading-edge section). The location, length, and chord of the leading-edge flap segments are shown in figures 2 and 3.

As shown in figure 3, the trailing-edge flaps were divided into three segments and each side could be deflected downward 30° perpendicular to the hinge line. This deflection was the maximum estimated allowable angle to prevent scraping the runway on landing or take-off.

The 0.020S canard was equipped with a double slotted full-span flap and a full-span slat. The 0.025S canard had a glove installed over the double slotted flap that closed the flap gaps and increased the canard chord to 28.12 cm (11.07 in.). Each canard was installed at a fixed angle of incidence on the under side of the model nose. The physical characteristics of the canard and their locations on the fuselage are shown in figure 4.

The model was equipped with fixed twin tails with full-span rudders. The size and positioning of fins and rudders are shown in figure 2.

Four 0.140-m (5.50-in.) diameter fans (engines) were mounted in an underslung nacelle. (See fig. 3.) These fans were free to windmill or to be powered by externally supplied compressed air. The fans were tip driven (air ejected from blade tips to cause fan rotation), and for the current installation the fans could be driven to about 18 000 rpm (Total combined static thrust $\approx$ 290 N (65 lb)) with the available compressed air supply.

TESTS

Static force tests were conducted on the 1/10-scale model in the Langley full-scale tunnel for several values of Reynolds number, based on the mean aerodynamic chord, from 6.78×10^6 to 13.85×10^6 (corresponding to test velocities of 41 to 85 knots). Most of the tests were made at about 54 knots (Reynolds

number of 8.92×10^6). For the powered tests, the test speed was restricted to about 23 knots to 34 knots ($C_T' = 0.1$ to 0.2) because of a limited air supply system for the fans.

Tests were conducted for angles of attack from about -6° to 30° and for sideslip angles from -5° to 10°. Tests were made for several combinations of wing leading-edge flap segments and deflections and for combinations of trailing-edge flap segments and deflections - the latter for longitudinal and lateral control as well as for improved lift.

A few tests were conducted (at zero sideslip) to determine the effectiveness of the twin rudders, and a few tests were made with a canard and with vertical tails off.

Most of the tests were conducted with the model drive fans (engines) windmilling with a drag correction being applied to the force data to compensate for the excess drag of the windmilling fans and the internal drag of the fan duct ($C_T' = 0$). The drag correction ($\Delta C_D = 0.004$) was determined by comparing the windmilling drag with the drag measured with the fans operating at sufficient speed to generate free-stream total pressure at the fan nozzle. Tests were conducted for thrust coefficients C_T' to about 0.10 to determine the effects of thrust on the aerodynamic forces and moments. The desired thrust for a particular test was obtained by setting the fans at a particular operating speed. The fan thrust had been previously calibrated as a function of fan rotation speed. Wool tufts were attached to the wing upper surface to aid in the interpretation of force test results.

CORRECTIONS

The test data have been corrected for tunnel airflow angularity, buoyancy, and strut tares. The sidewash angle which was approximately 0.5° ($\beta \approx -0.5^\circ$), has not been accounted for in the data presentation, and this, in general, has resulted in an initial offset, from zero, of the lateral and directional data.

Tunnel wall corrections were found to be negligible by theory (ref. 7) and experiment. The experiments were conducted with a 1/150-scale model tested in the Langley full-scale tunnel and in a 1/15-scale model of the full-scale tunnel.

PRESENTATION OF DATA

RESULTS AND DISCUSSION

Longitudinal Aerodynamic Characteristics

The data of this report are analyzed with regard to the achievement of high lift and adequate stability and control for only the low to moderate angles of attack that would be encountered during landing and take-off maneuvers.

Tuft studies.- As an aid in interpreting the force and moment characteristics, flow studies were made of a few select configurations by observing wool tufts that were attached to the upper surface of the wing. Photographs of the tuft studies are presented in figures 8 to 14. The absence of photographs for a few angles of attack was caused by camera malfunction.

Flow over the clean wing ($\delta_{f,te} = \delta_{f,le} = 0^\circ$) at zero sideslip and with vertical tails removed (fig. 8) develops into a large chordwise vortex that sweeps the flow outboard for angles of attack above 10°. Installing the vertical tails (fig. 9) constrains the large vortices and causes rough flow outboard of the fins at $\alpha = 14^\circ$. Some stall exists outboard of the tails at $\alpha = 18^\circ$ and the tips are stalled by $\alpha = 28^\circ$. Sideslipping the clean configuration ($\beta = 10^\circ$, fig. 10) caused the advancing wing tip to stall earlier than the unyawed wing, and the retreating wing did not stall through the full angle-of-attack range. This characteristic is related to the dihedral effect exhibited by the configuration and discussed in a later section. Deflecting inboard leading-edge and full-span trailing-edge flaps (high-lift configuration) resulted in spanwise flow at the wing tips by $\alpha = 2^\circ$. (See fig. 11.) The wing tips and the mid-trailing-edge flaps were stalled by $\alpha = 22^\circ$. The effect of deflecting the outboard leading-edge flaps for the high-lift configuration is shown

in figure 12. Stall of the wing tips was delayed to $\alpha \approx 26^{\circ}$ and flow over the remainder of the wing was fairly good to $\alpha = 28^{\circ}$. Sideslipping the high-lift configuration with all leading- and trailing-edge flaps deflected resulted in flow conditions which were markedly different than those exhibited by the clean configuration. (Compare figs. 10 and 13.) The retreating wing of the high-lift configuration was subject to some separated flow at $\alpha = 12^{\circ}$ and the retreating wing tip, including the outboard flap, was stalled at $\alpha = 16^{\circ}$. Installing a small canard on the model had no apparent effect on the wing-flap flow pattern. (See fig. 14.)

Basic configuration.- At the outset of the program, tests were conducted on the clean configuration over a range of wind-tunnel speeds to determine whether there were appreciable effects of Reynolds number on the data. The effect of Reynolds number on the longitudinal aerodynamic characteristics of the clean configuration with vertical tails is shown in figure 15. There was no appreciable Reynolds number effect on the data; therefore, most of the tests were conducted at a Reynolds number of 8.92×10^6.

Perhaps the most significant point concerning the data presented in figure 15 is that the clean configuration exhibited static longitudinal instability (pitch-up) for angles of attack greater than about 3°. The variation of lift with angle of attack indicated an increase in lift-curve slope at moderate angles of attack due to vortex lift, and the lift curve did not exhibit any abrupt changes. A maximum value of lift-drag ratio of about 6 occurred near $\alpha = 3^{\circ}$.

Effect of vertical tails.- The effect of the vertical tails on the longitudinal aerodynamic characteristics of the clean configuration is shown in figure 16. These data indicate that a lift loss occurred at moderate to high angles of attack when the vertical tails were added to the model. The tuft studies of figures 8 and 9 indicate the cause of the reduced lift. At moderate and high angles of attack, the flow outboard of the tails shows a large area of rough and separated flow. This flow condition indicates that the reduction in lift with the tails on is related to the constraining effect of the tails on the spanwise vortex flow. In general, the longitudinal stability characteristics, particularly the pitch-up, are not affected by the tails.

Effect of leading- and trailing-edge flap deflection.- The effect of deflecting the trailing-edge flaps and outboard leading-edge flaps is shown in figures 17 and 18. Lift and L/D increased significantly; however, in figure 17, the configuration still exhibited the pitch-up shown in figure 15 for the clean configuration. Deflecting the inboard leading-edge flaps in addition to the outboard leading-edge flaps (fig. 19) produced a very significant effect in that the pitch-up was delayed to $\alpha \approx 18^{\circ}$ with only a very small loss of lift. (Compare figs. 17 and 19.) Deflection of the trailing-edge flaps and leading-edge flaps increased the untrimmed lift coefficient, at the estimated tail-scrape angle of attack of 9.5°, from about 0.35 for the clean configuration to about 0.50 for a trailing-edge flap deflection of 30°. (See figs. 17 and 18.) For figure 19, the inboard trailing-edge flap was deflected only 20°; this accounts for the apparently lower lift values than those in figure 18. The most significant point shown by the data of figure 19 is that the inboard leading-edge flap segments 5, 6, and 7 must be deflected at least 60° to alleviate the pitch-up at moderate and high angles of attack.

In order to determine the effect of outboard leading-edge flap deflection, the trailing-edge and inboard leading-edge flaps were deflected with and without outboard leading-edge flaps (segments 1, 2, and 3), and the results are shown in figure 20. Deflecting the outboard leading-edge flaps reduced lift and, to a small extent, longitudinal stability.

Effect of canard.- The results of tests, wherein a canard having an area of either 0.020S or 0.025S with an incidence angle of 0° or 15°, respectively, was evaluated to determine the effectiveness of such a surface for reducing longitudinal trim requirements, are presented in figures 21 and 22. The data show that the canard provided substantial positive (favorable) increments of C_m over the angle-of-attack range. The canard produced no noticeable effect on lift; however, the larger canard at 15° incidence did result in a degradation in L/D.

Effect of thrust vectoring.- The effect of engine thrust with no thrust vectoring on the lift and pitch characteristics with the 0.020S canard installed is shown to be small in figure 23. The effect of thrust vectoring is shown in figure 24. Directly comparable data were not obtained during the tests, that is, canard on, $\delta_{f,te} = 20^{\circ}$ and 30° with $C_T' = 0.10$ without thrust vectoring. However, since thrust was shown in figure 23 to have only a small effect on lift and pitch and since the small effect shown in figure 24 is about the same as that shown in figure 23, it may be assumed that the effects shown in figure 24 are mainly attributable to thrust and not thrust vectoring. The rather minor effects of thrust vectoring for the present configuration can be explained by the poor nozzle deflection technique of the tests (only the upper half of the nozzle was deflected), which resulted in poor turning of the exhaust flow, and by the fact that the nozzle area A was larger than desired ($A_{nozzle}/A_{fans} = 1.84$), which resulted in relatively low exhaust velocities. It is expected that an improved nozzle design with increased nozzle velocities would provide substantial gains in lift with nozzle deflection.

Longitudinal control effectiveness.- The longitudinal control effectiveness of the trailing-edge flaps is shown in figures 25 and 26. All combinations of flaps were quite effective in providing longitudinal trim (with attendant reduction in lift) with the exception of the outboard flaps alone (fig. 25(d)). These outboard flaps were relatively ineffective as might be expected based on the tuft studies (fig. 11) which show the flow over the outboard flap to be fairly poor. As expected, the data of figure 26 show that the presence of the canard had no appreciable effect on the longitudinal control effectiveness.

Effect of sideslip.- The effect of sideslip on the longitudinal aerodynamic characteristics of the model is shown in figures 27 to 30. The data show that sideslip tended to make the pitch-up characteristics of both the clean and high-lift configurations more severe.

Lateral-Directional Stability Characteristics

The lateral-directional stability characteristics of the model are shown in figures 31 to 38. An analysis of lateral-directional data obtained for

the clean configuration over the Reynolds number range previously discussed for the longitudinal aerodynamic data indicated that the effects of Reynolds number were also negligible for the lateral-directional tests. As a result, most of the tests were conducted at a Reynolds number of 8.92×10^6 (the same value that was used for the longitudinal tests).

The variations of side-force, rolling-moment, and yawing-moment coefficients with sideslip for the clean configuration, the high-lift configuration, and the high-lift configuration with canard are presented in figures 31 to 33. The data show that the variation of C_l with β was generally linear for angles of attack to about 20°, whereas the variation of C_n with β became nonlinear near $\alpha = 8^\circ$ with increasing nonlinearity at higher angles of attack. In addition, the data show large yawing- and rolling-moment asymmetries for angles of attack greater than 20°. These asymmetric moments, which are believed to be caused by asymmetric vortex shedding off the highly swept nose, would have a significant effect on the lateral-directional control of the configuration at high angles of attack, as is discussed in the following section. As shown in figure 34, the magnitudes and directions of the C_n and C_l asymmetries varied over the range of Reynolds number.

The lateral-directional stability characteristics of the model are summarized in figures 35 to 38 in terms of the side force due to sideslip C_{Y_β}, the yawing moment due to sideslip C_{n_β}, and the rolling moment due to sideslip C_{l_β}. The magnitudes of the derivatives were determined from values of the respective coefficients at values of β from -5° to 5°. In general, the model exhibited satisfactory static lateral-directional characteristics for angles of attack to about 16°.

The data of figure 35 show that the clean configuration was directionally stable at low angles of attack and that the level of directional stability increased markedly as angle of attack was increased, so that the configuration was extremely stable at high angles of attack. It should be noted that the marked increase in C_{n_β} at high angles of attack was produced in conjunction with a positive increment of C_{Y_β}. An analysis of the relative signs of the two derivatives indicates that the aerodynamic stabilizing moment was produced forward of the center-of-gravity position. Past investigations have shown that the foregoing characteristics may be related to the aerodynamic effects of a pair of strong vortices shed off the highly swept flat nose of the model. (See refs. 8 to 12.) The data of figure 35 also show that the magnitude of C_{l_β} increased with increasing α up to 12°. Above this angle, the value of the derivative decreased rapidly and approached zero at $\alpha \approx 24^\circ$. This decrease in C_{l_β} is related to the advancing wing panel stall discussed in the section on flow visualization ("Tuft Studies"). As previously noted, variations in Reynolds number had no significant effect on the lateral-directional characteristics.

The effect of the vertical tails on the lateral-directional stability derivatives of the clean configuration is presented in figure 36. The data show that the tail contribution to C_{n_β} was essentially constant over the angle-of-attack range and that the tails had a significant effect on the magnitude of C_{l_β} at the higher angles of attack.

Shown in figure 37 is a comparison of the lateral-directional stability derivatives from the clean and high-lift configurations; these data show essentially similar trends although the high-lift configuration did exhibit less stable values of C_{n_β} at extremely high angles of attack.

The effect of the 0.020S canard on the derivatives for the high-lift configuration is presented in figure 38. The data show that although the canard caused a large reduction in C_{n_β} at angles of attack above 4°, the configuration still had a high level of directional stability at all angles of attack.

Lateral-Directional Control Characteristics

In the present investigation, the outboard trailing-edge flaps (trailing-edge segment 3) were evaluated as a possible source of roll control. Presented in figure 39 are the variations of C_Y, C_n, and C_l with deflections of the left-hand outboard flap. The data show that a total deflection of $\pm 30^\circ$ of the outboard surface produced an increment of C_l of only about 0.01. This magnitude of roll-control effectiveness is generally similar to values obtained from the deflection of outboard surfaces on other highly swept configurations in previous investigations (refs. 13 and 14). An evaluation of roll-control requirements for satisfactory handling qualities indicates that this level of control effectiveness may be insufficient for some operational conditions. For example, in terms of the roll control required to trim the rolling moments resulting from sideslip, an examination of the effective dihedral characteristics of the present model (see fig. 38) shows that a 10° sideslip angle would require a value of C_l of 0.03 for roll trim near $\alpha = 10^\circ$. On this basis, it appears that additional means of roll control would be required for satisfactory operation in the landing and take-off modes where cross winds could produce sideslip angles of this magnitude. It is possible that differential deflection of full-span trailing-edge flaps or various combinations of the trailing-edge flaps could produce adequate roll control; however, no data of this type were obtained for the present model.

The variations of C_Y, C_n, and C_l with deflections of the twin rudders are presented in figure 40. The data show that the rudder effectiveness decreases with increasing angle of attack. For angles of attack to about 8°, rudder deflections of $\pm 20^\circ$ produced a value of C_n of about ± 0.01. This control effectiveness is generally similar to that shown in references 13 and 14 for configurations having geometric characteristics generally similar to those of the present model. An examination of the directional stability data for the present model (fig. 38) indicates that a value of C_n of 0.01 is only adequate for trimming the yawing moments resulting from about 5° of sideslip

for angles of attack near 0°. It should also be noted that at extremely high angles of attack the asymmetric yawing moments were much larger than the yaw control provided by the rudders. (Compare figs. 39 and 40.)

CONCLUSIONS

The results of static force tests of a 1/10-scale model of a blended-arrow supersonic cruise aircraft in the Langley full-scale tunnel indicate the following conclusions:

1. The clean configuration exhibited static longitudinal instability (pitch-up) at angles of attack greater than 3°; however, deflecting inboard and outboard wing leading-edge flaps delayed the pitch-up to an angle of attack of about 18°.

2. Deflecting full-span trailing-edge flaps and leading-edge flaps increased the untrimmed lift coefficient from about 0.35 for the clean configuration to about 0.50 at an angle of attack of 9.5° (estimated tail-scrape angle).

3. The thrust vectoring nozzle used was not effective for increasing lift because of poor turning of the exhaust flow. An improved nozzle design, however, should provide some increase in lift with thrust vectoring.

4. The model exhibited satisfactory lateral-directional characteristics for angles of attack to about 16°. At higher angles of attack the directional stability increased markedly; however, the effective dihedral decreased to nearly zero near an angle of attack of about 24°.

5. The deflection of leading- and trailing-edge flaps and the addition of a canard for longitudinal trim reduced the level of directional stability at high angles of attack.

6. Outboard trailing-edge flaps were relatively ineffective for roll control, particularly for roll trim during take-off and landing in a cross wind.

Langley Research Center
National Aeronautics and Space Administration
Hampton, VA 23665
April 8, 1977

REFERENCES

1. Carlson, Harry W.; Barger, Raymond L.; and Mack, Robert J.: Application of Sonic-Boom Minimization Concepts in Supersonic Transport Design. NASA TN D-7218, 1973.

2. Corson, Blake W., Jr.; Capone, Francis J.; and Putnam, Lawrence E.: Lift Induced on a Swept Wing by a Two-Dimensional Partial-Span Deflected Jet at Mach Numbers From 0.20 to 1.30. NASA TM X-2309, 1971.

3. Capone, Francis J.: Exploratory Investigation of Lift Induced on a Swept Wing by a Two-Dimensional, Partial Span Deflected Jet at Mach Numbers From 0.20 to 1.30. NASA TM X-2529, 1972.

4. Robins, A. Warner; Morris, Odell A.; and Harris, Roy V., Jr.: Recent Research Results in the Aerodynamics of Supersonic Vehicles. J. Aircr., vol. 3, no. 6, Nov.-Dec. 1966, pp. 573-577.

5. Baals, Donald D.; Robins, A. Warner; and Harris, Roy V., Jr.: Aerodynamic Design Integration of Supersonic Aircraft. J. Aircr., vol 7, no. 5, Sept.-Oct. 1970, pp. 385-394.

6. Mechtly, E. A.: The International System of Units - Physical Constants and Conversion Factors (Second Revision). NASA SP-7012, 1973.

7. Heyson, Harry H.: Use of Superposition in Digital Computers To Obtain Wind-Tunnel Interference Factors for Arbitrary Configurations, With Particular Reference to V/STOL Models. NASA TR R-302, 1969.

8. Grafton, Sue B.; Chambers, Joseph R.; and Coe, Paul L., Jr.: Wind-Tunnel Free-Flight Investigation of a Model of a Spin-Resistant Fighter Configuration. NASA TN D-7716, 1974.

9. Johnson, Joseph L.: Damping in Yaw and Static Directional Stability of a Canard Airplane Model and of Several Models Having Fuselages of Relatively Flat Cross Section. NACA RM L50H30a, 1950.

10. Paulson, John W.; and Johnson, Joseph L., Jr.: Free-Flight-Tunnel Investigation of the Low-Speed Stability and Control Characteristics of a Model Having a Fuselage of Relatively Flat Cross Section. NACA RM L52L22, 1953.

11. Bates, William R.: Static Stability of Fuselages Having a Relatively Flat Cross Section. NACA TN 3429, 1955. (Supersedes NACA RM L9I06a.)

12. Spencer, Bernard, Jr.; and Phillips, W. Pelham: Effects of Cross-Section Shape on the Low-Speed Aerodynamic Characteristics of a Low-Wave-Drag Hypersonic Body. NASA TN D-1963, 1963.

13. Henderson, William P.: Low-Speed Aerodynamic Characteristics of a Supersonic Transport Model With a Highly Swept, Twisted and Cambered, Fixed Wing. NASA TM X-1249, 1966.

14. Ray, Edward J.; and Henderson, William P.: Low-Speed Aerodynamic Characteristics of a Highly Swept Supersonic Transport Model With Auxiliary Canard and High-Lift Devices. NASA TM X-1694, 1968.

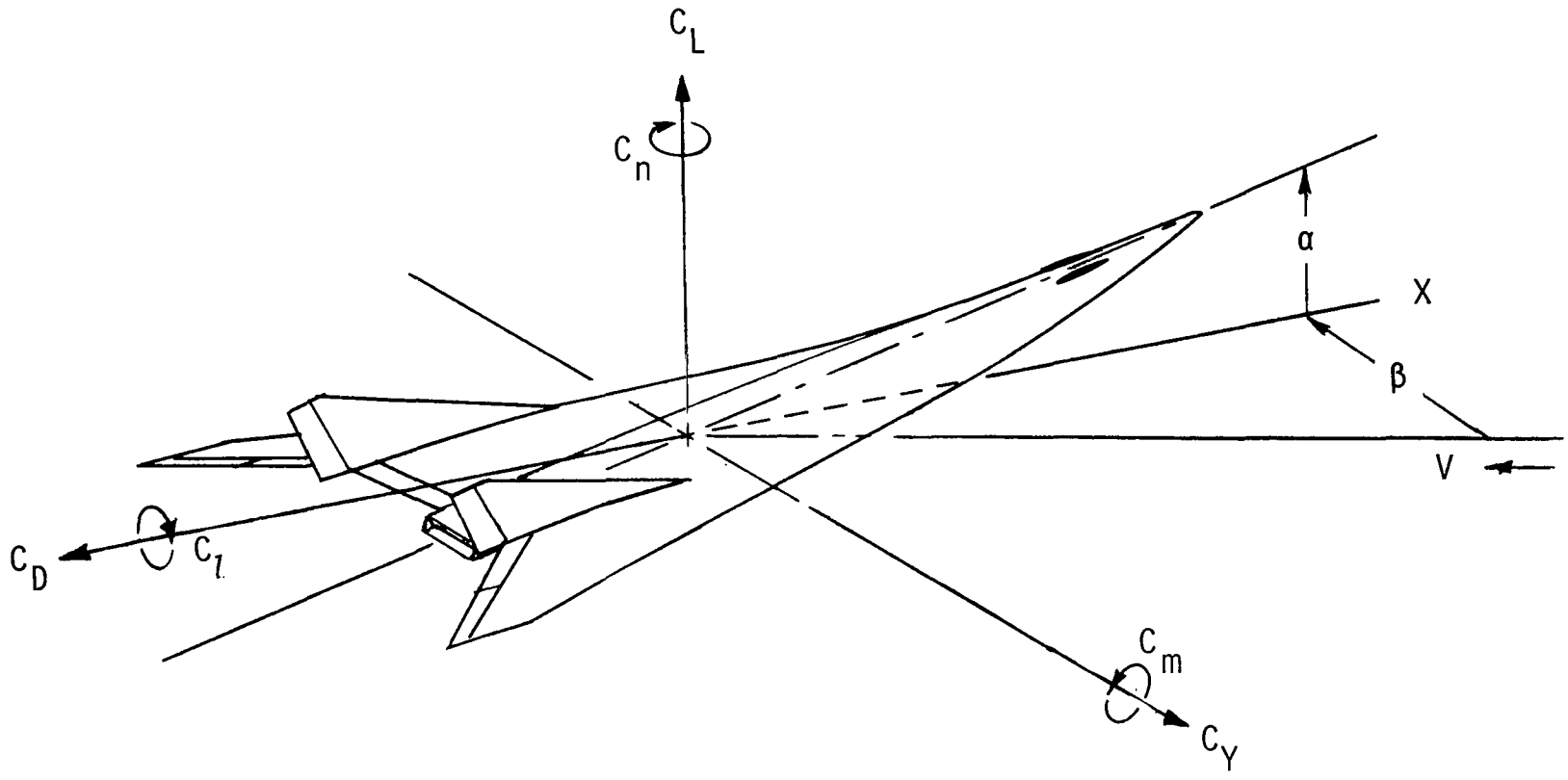

Figure 1.- Stability system of axes and positive sense of angles, forces, and moments.

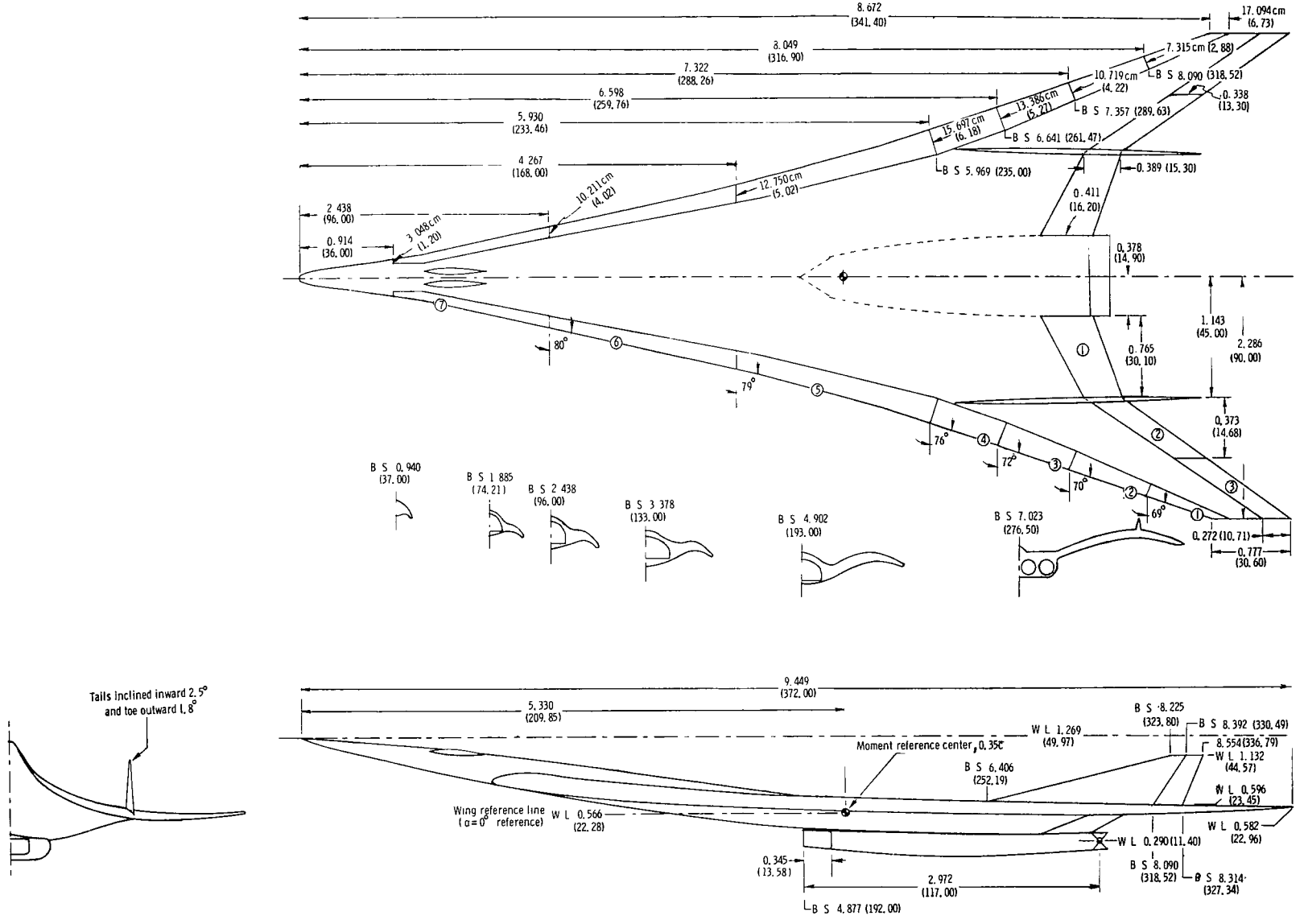

Figure 2.- Geometric characteristics of 1/10-scale arrow-wing model. All dimensions are in m (in.) unless otherwise noted.

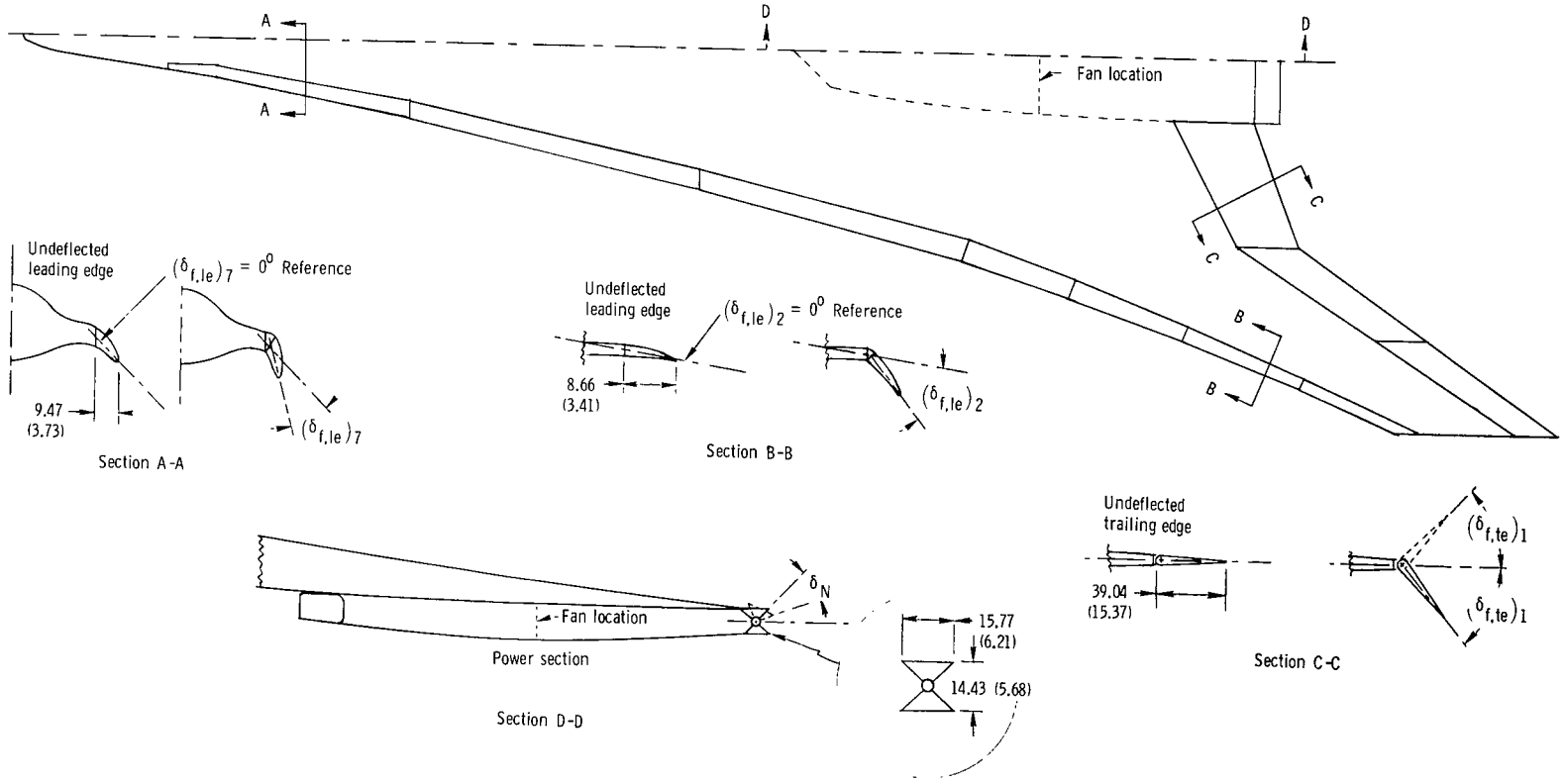

Figure 3.- Schematic arrangements of leading- and trailing-edge flaps and engine exhaust nozzle. (Components not to scale.) Dimensions are in cm (in.).

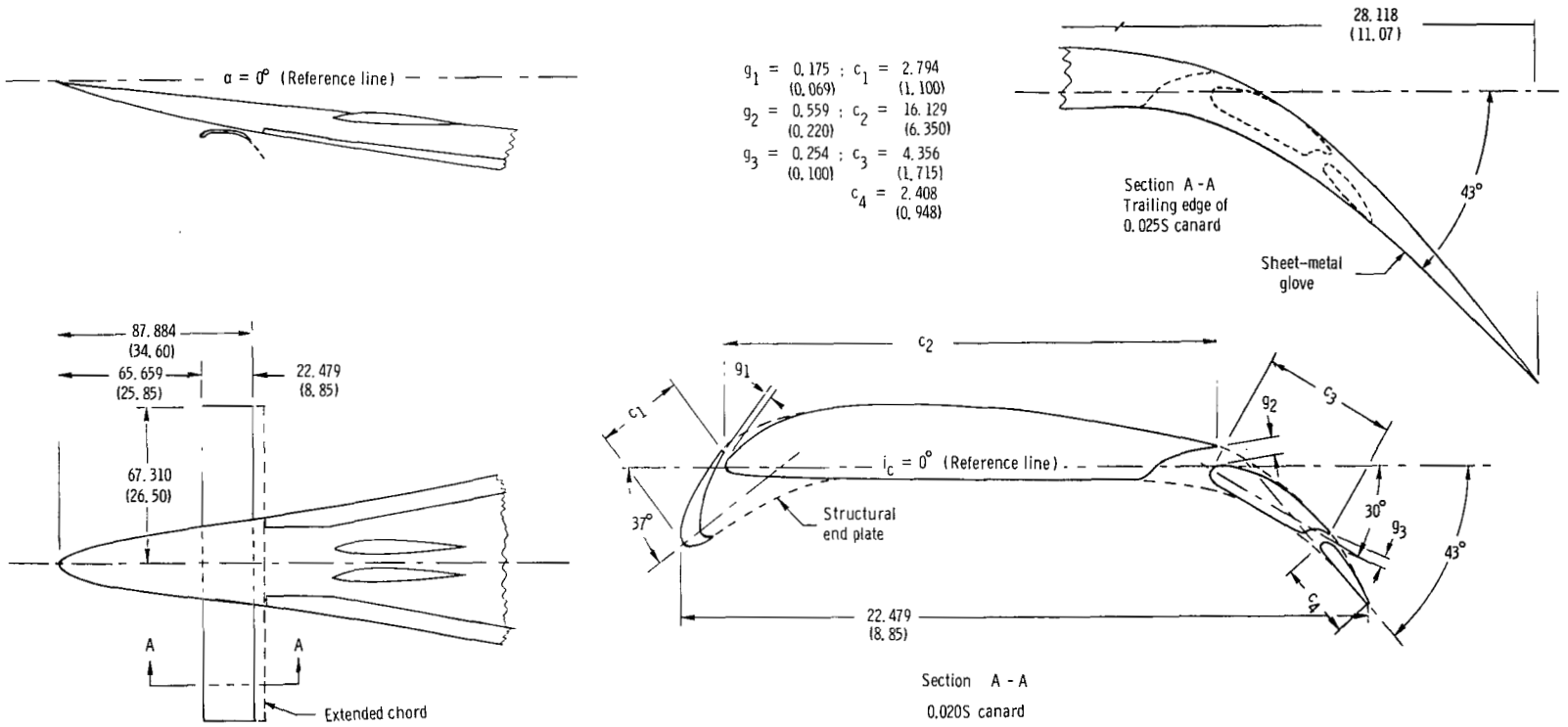

Figure 4.- Geometric characteristics and location of canard. Dimensions are in cm (in.).

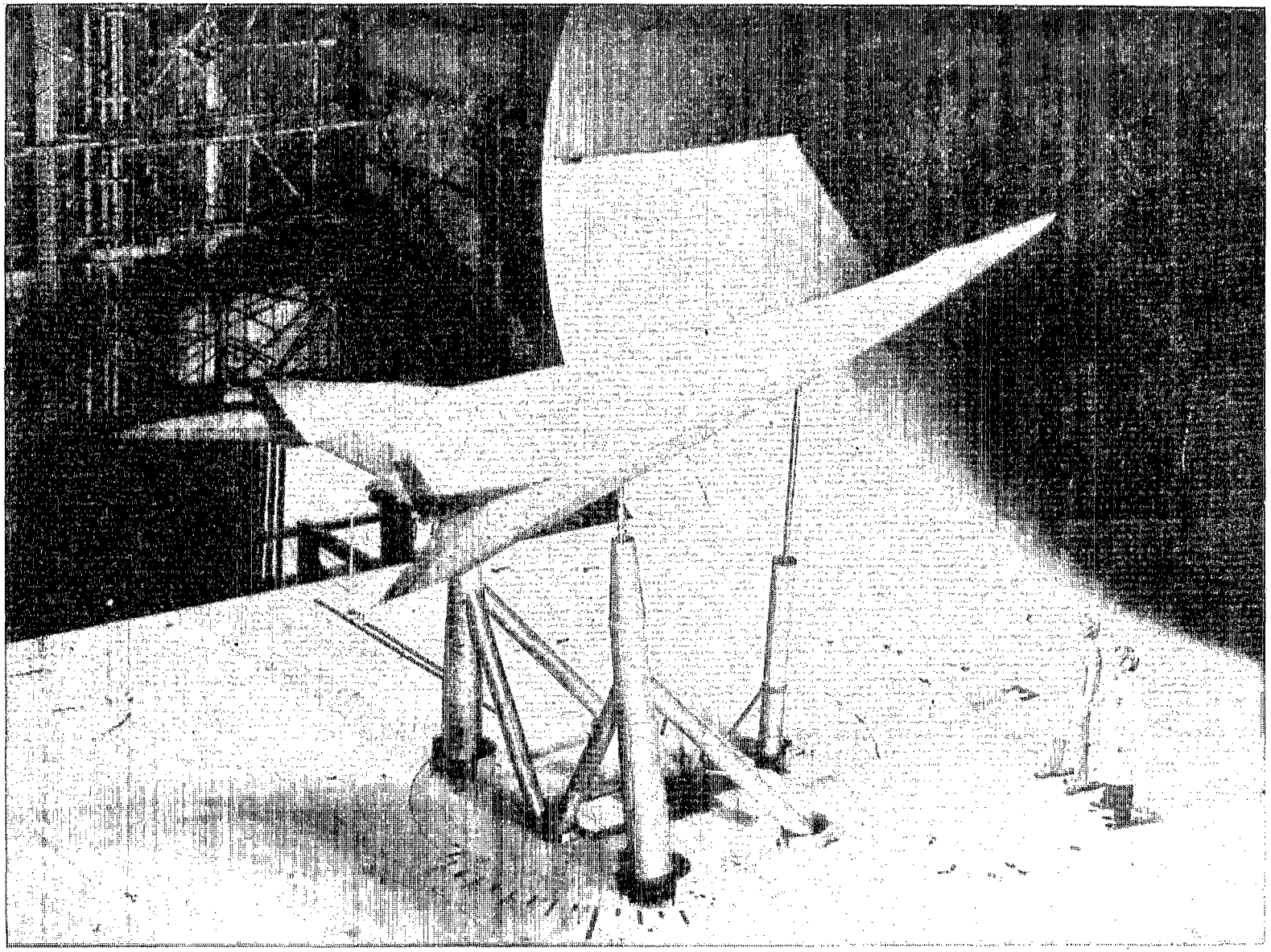

L-73-7547

Figure 5.- Three-quarter rear view of 1/10-scale model mounted for tests in Langley full-scale tunnel.

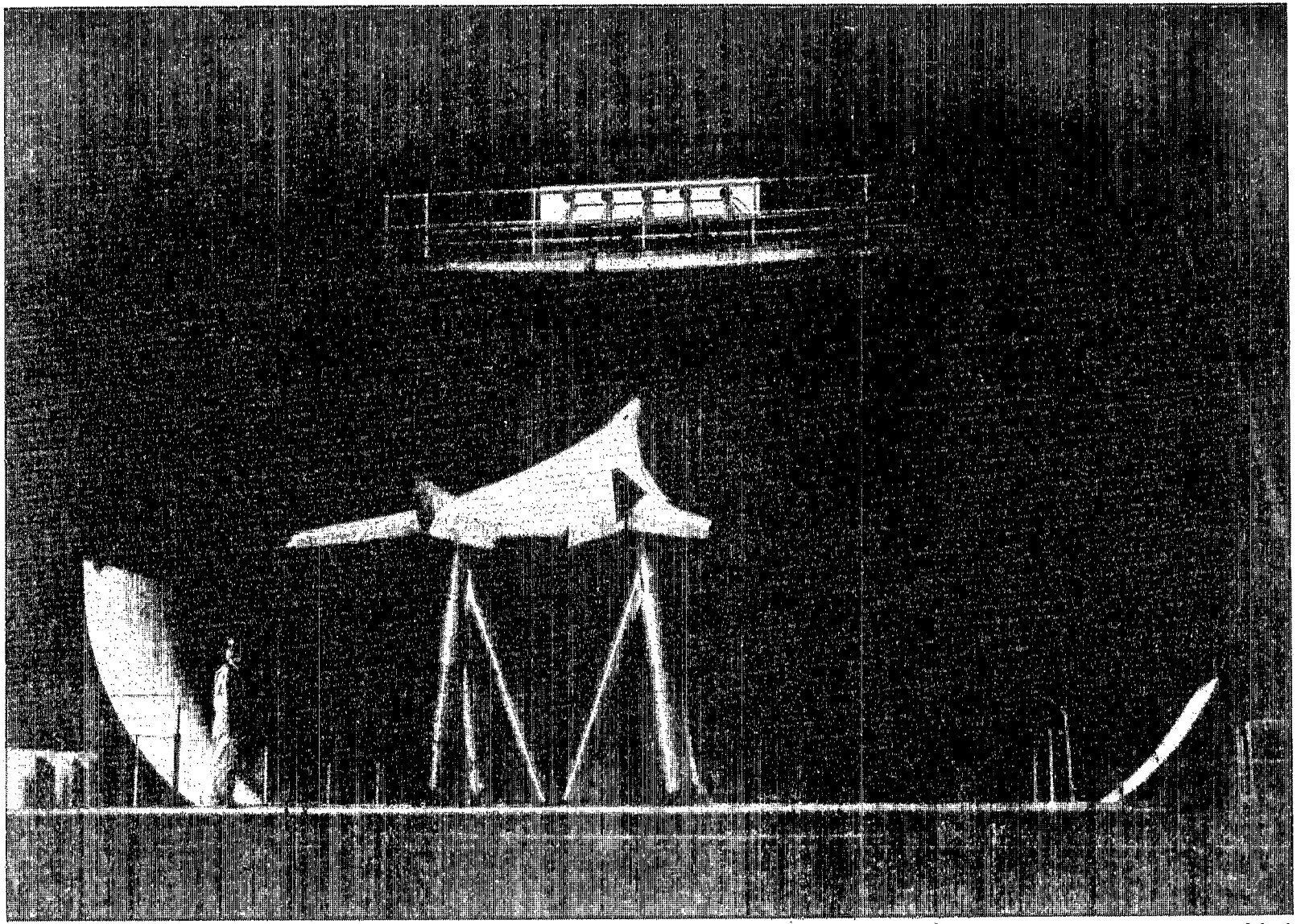

L-73-8616

Figure 6.- Rear view of 1/10-scale model mounted for tests in Langley full-scale tunnel.

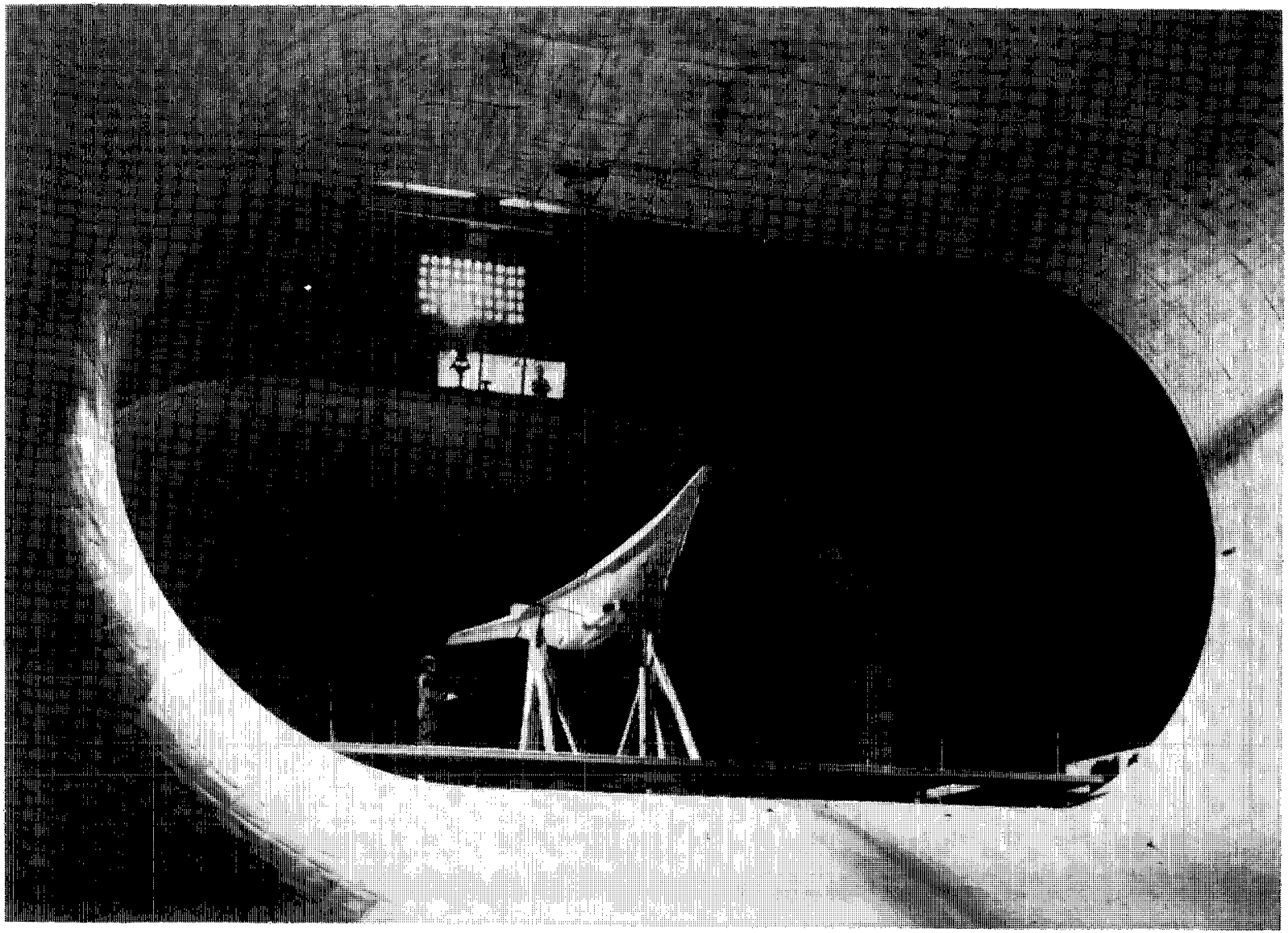

L-73-8617

Figure 7.- Three-quarter front view of 1/10-scale model mounted for tests in Langley full-scale tunnel.

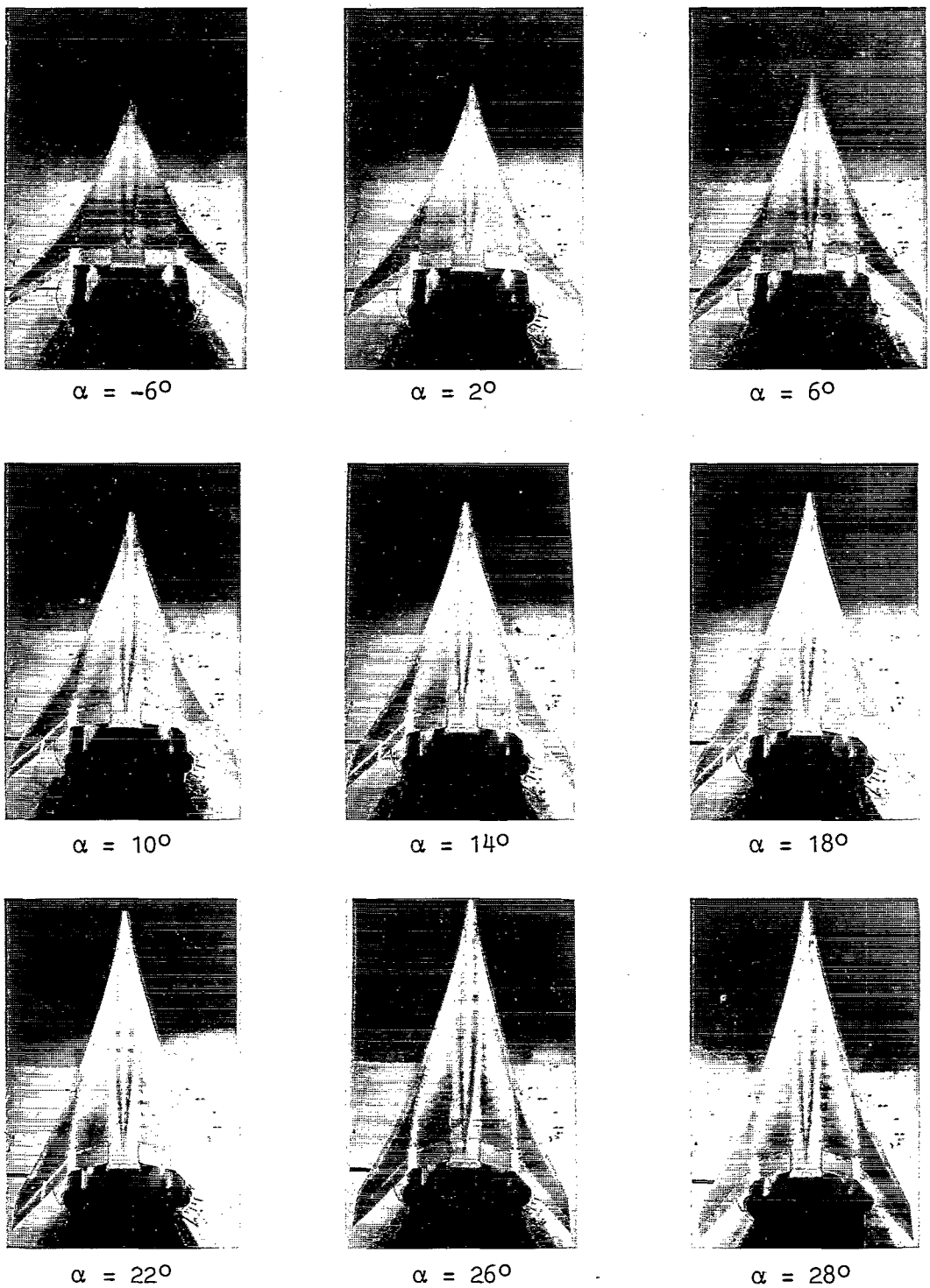

L-77-170

Figure 8.- Tuft studies of clean configuration at $\beta = 0^{\circ}$. $\delta_{f,te} = 0^{\circ}$; $\delta_{f,le} = 0^{\circ}$; $C_T' = 0$; vertical tails off.

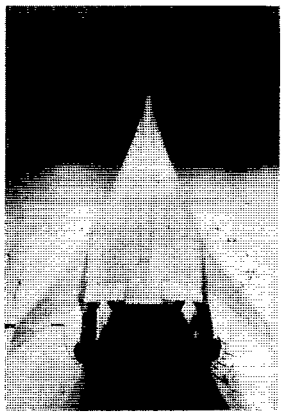

$\alpha = 2^{\circ}$

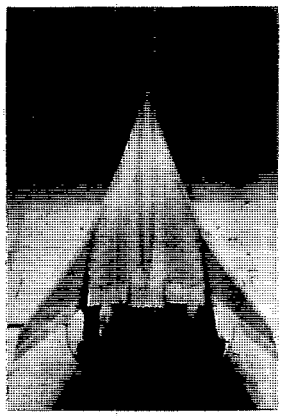

$\alpha = 6^{\circ}$

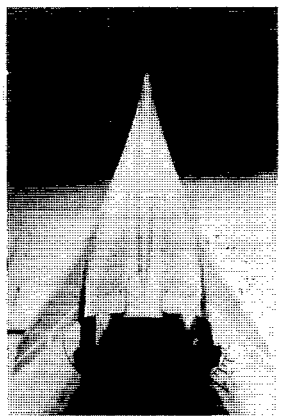

$\alpha = 12^{\circ}$

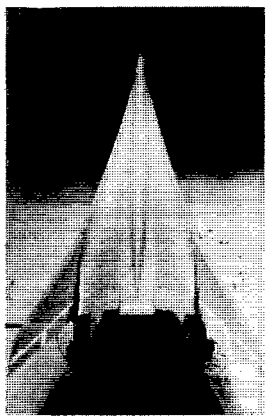

$\alpha = 14^{\circ}$

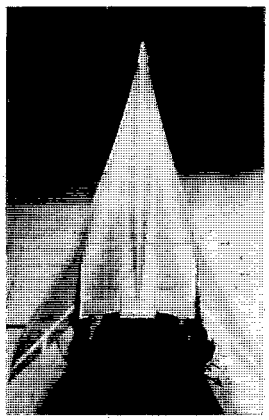

$\alpha = 18^{\circ}$

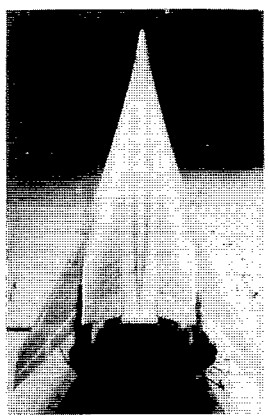

$\alpha = 22^{\circ}$

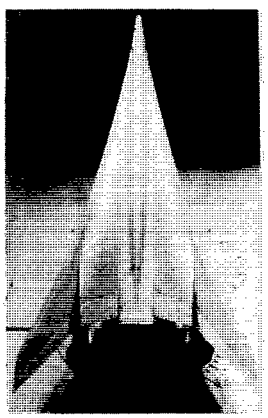

$\alpha = 26^{\circ}$

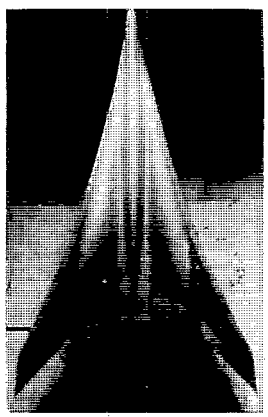

$\alpha = 30^{\circ}$

L-77-171

Figure 9.- Tuft studies of clean configuration at $\beta = 0^{\circ}$. $\delta_{f,te} = 0^{\circ}$; $\delta_{f,le} = 0^{\circ}$; $C_T' = 0$; vertical tails on.

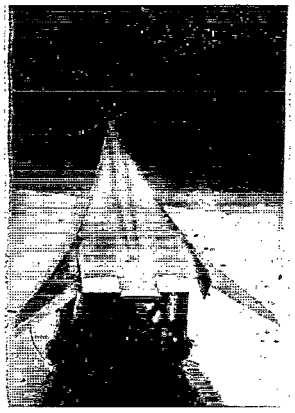

$\alpha = -6^{\circ}$

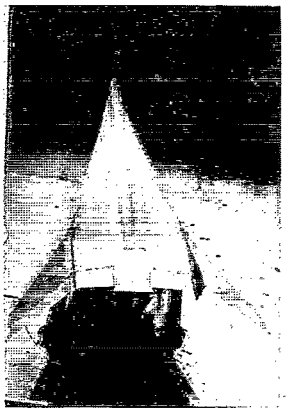

$\alpha = 2^{\circ}$

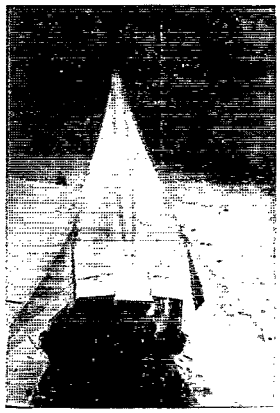

$\alpha = 6^{\circ}$

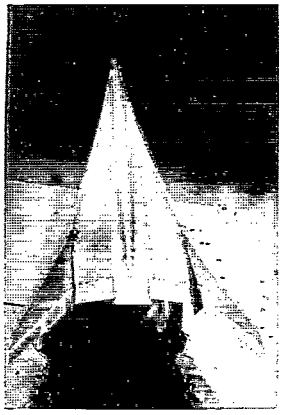

$\alpha = 10^{\circ}$

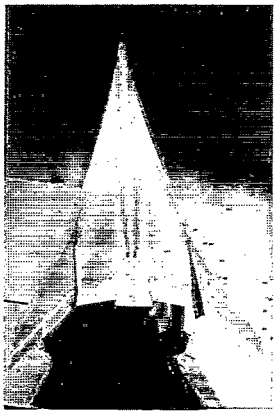

$\alpha = 14^{\circ}$

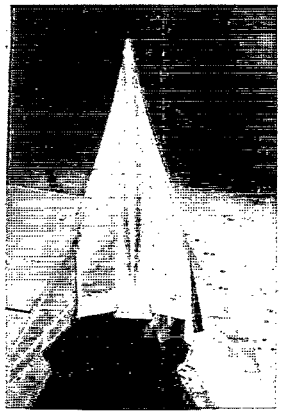

$\alpha = 18^{\circ}$

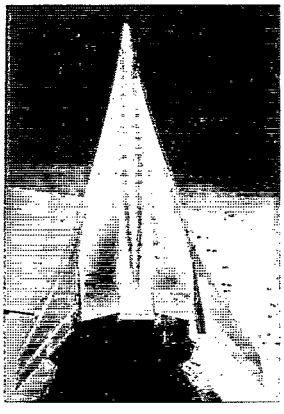

$\alpha = 22^{\circ}$

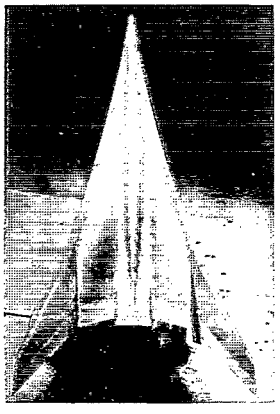

$\alpha = 26^{\circ}$

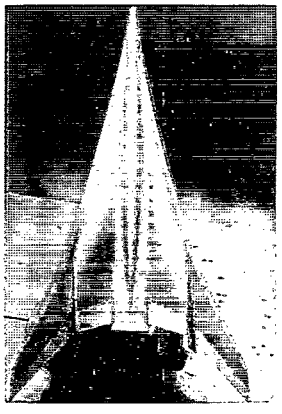

$\alpha = 30^{\circ}$

L-77-172

Figure 10.- Tuft studies of clean configuration at $\beta = 10^{\circ}$. $\delta_{f,te} = 0^{\circ}$; $\delta_{f,le} = 0^{\circ}$; $C_T' = 0$; vertical tails on.

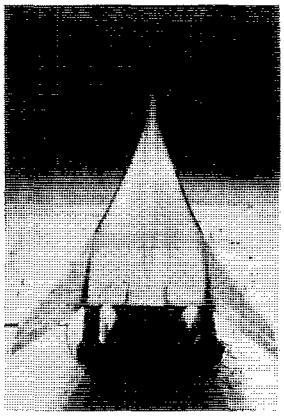

$\alpha = 2^{\circ}$

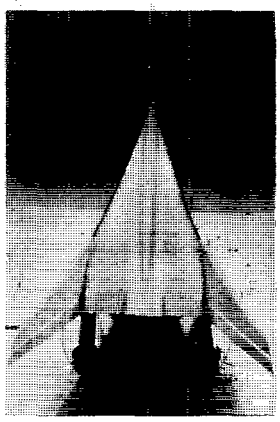

$\alpha = 6^{\circ}$

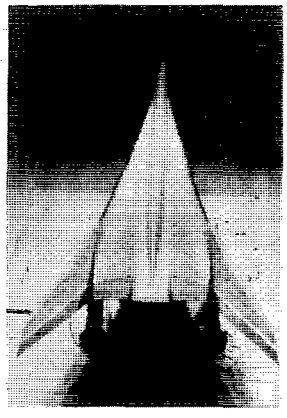

$\alpha = 10^{\circ}$

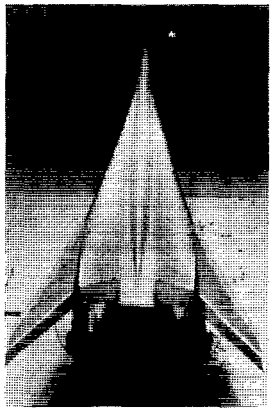

$\alpha = 14^{\circ}$

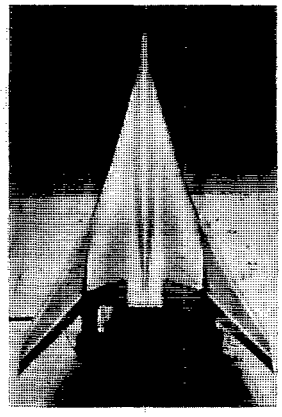

$\alpha = 18^{\circ}$

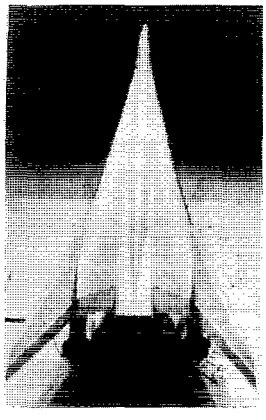

$\alpha = 22^{\circ}$

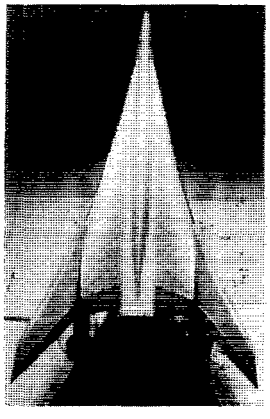

$\alpha = 26^{\circ}$

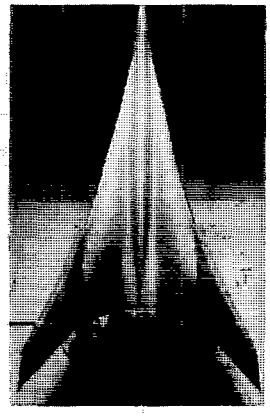

$\alpha = 30^{\circ}$

L-77-173

Figure 11.- Tuft studies of high-lift configuration at $\beta = 0^{\circ}$. $(\delta_{f,te})_{1,2,3} = 20.5^{\circ}$; 30.0°, 30.5°; $(\delta_{f,le})_{1,2,3,4} = 0^{\circ}$; $(\delta_{f,le})_{5,6,7} = 60^{\circ}$; $C_T' = 0$; vertical tails on.

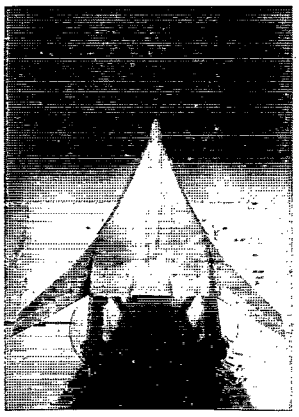

$\alpha = -6^{\circ}$

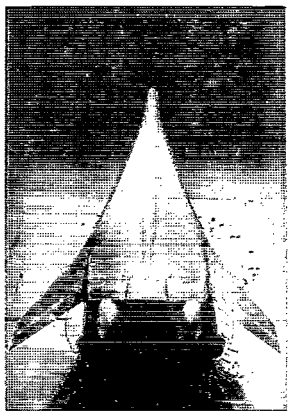

$\alpha = 2^{\circ}$

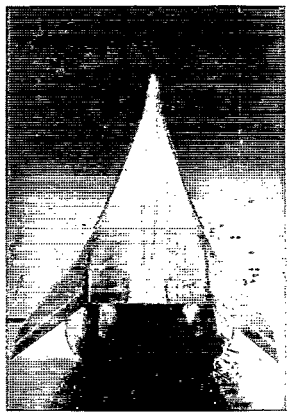

$\alpha = 6^{\circ}$

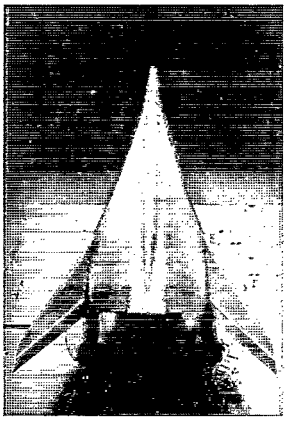

$\alpha = 12^{\circ}$

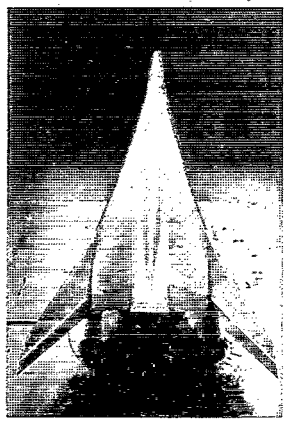

$\alpha = 14^{\circ}$

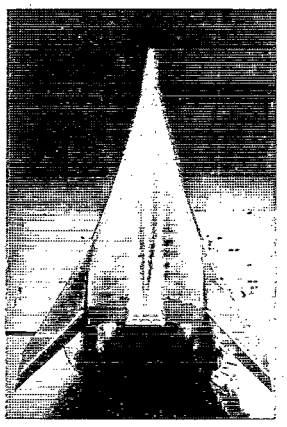

$\alpha = 18^{\circ}$

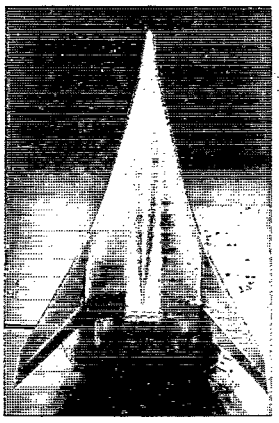

$\alpha = 22^{\circ}$

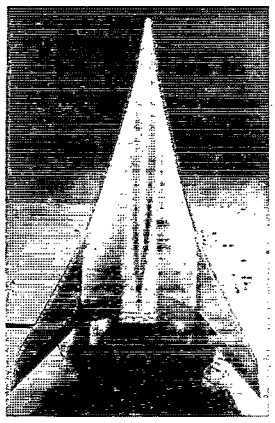

$\alpha = 26^{\circ}$

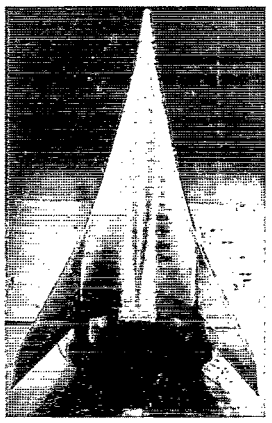

$\alpha = 28^{\circ}$

L-77-174

Figure 12.- Tuft studies of high-lift configuration at $\beta = 0^{\circ}$. $(\delta_{f,te})_{1,2,3} = 20.5^{\circ}$, 30.0°, 30.5°; $(\delta_{f,le})_{1,2,3,4} = 45^{\circ}$; $(\delta_{f,le})_{5,6,7} = 60^{\circ}$; $C_T' = 0$; vertical tails on.

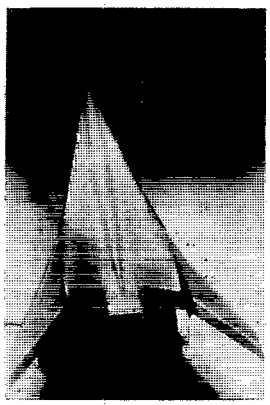

$\alpha = 12^{\circ}$

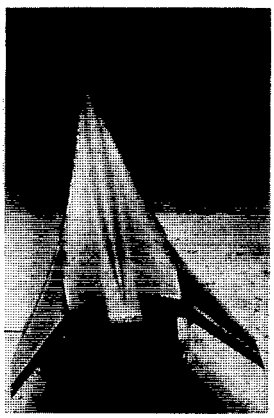

$\alpha = 14^{\circ}$

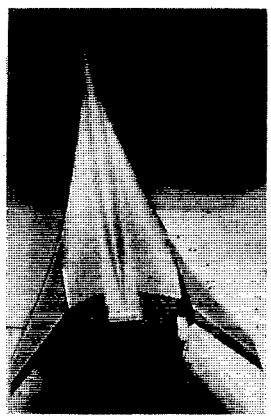

$\alpha = 16^{\circ}$

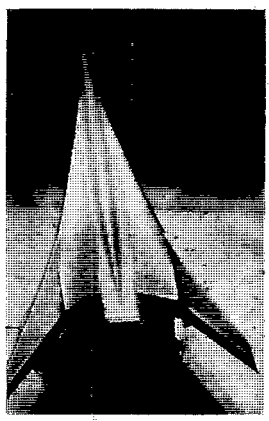

$\alpha = 18^{\circ}$

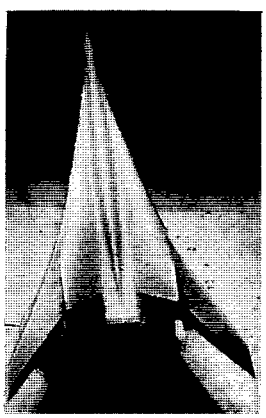

$\alpha = 22^{\circ}$

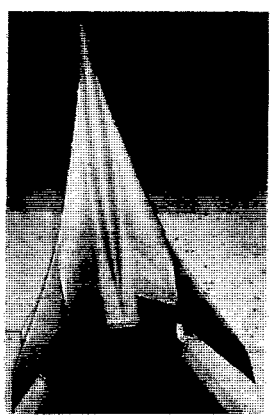

$\alpha = 26^{\circ}$

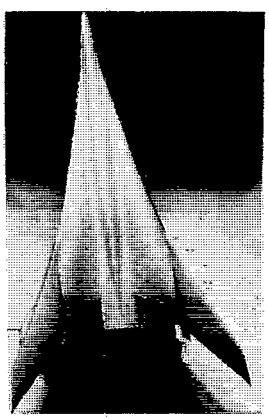

$\alpha = 30^{\circ}$

L-77-175

Figure 13.- Tuft studies of high-lift configuration at $\beta = 10^{\circ}$. $(\delta_{f,te})_{1,2,3} = 20.5^{\circ}$, 30.0°, 30.5°; $(\delta_{f,le})_{1,2,3,4} = 45^{\circ}$; $(\delta_{f,le})_{5,6,7} = 60^{\circ}$; $C_T' = 0$; vertical tails on.

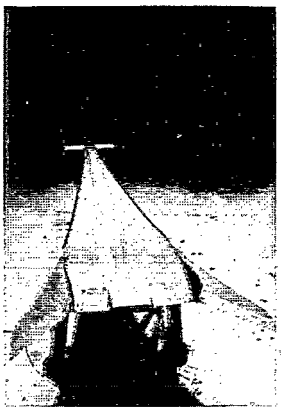

$\alpha = -6^{\circ}$

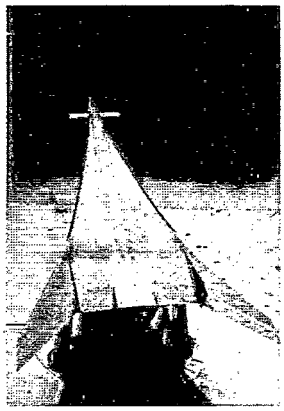

$\alpha = 2^{\circ}$

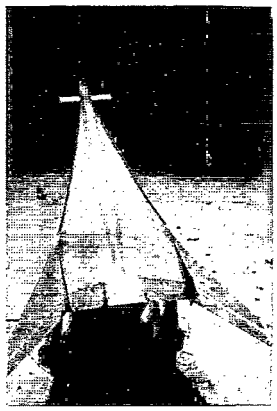

$\alpha = 6^{\circ}$

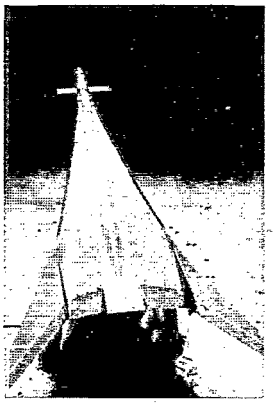

$\alpha = 10^{\circ}$

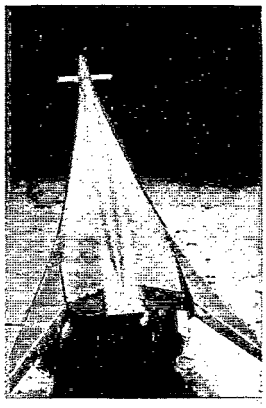

$\alpha = 14^{\circ}$

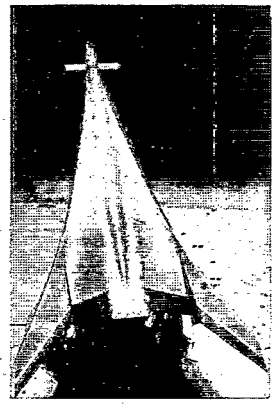

$\alpha = 18^{\circ}$

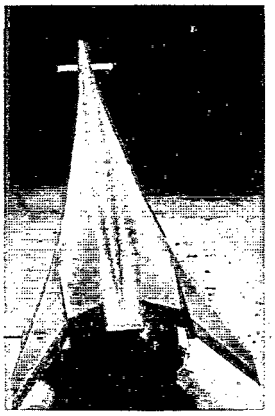

$\alpha = 22^{\circ}$

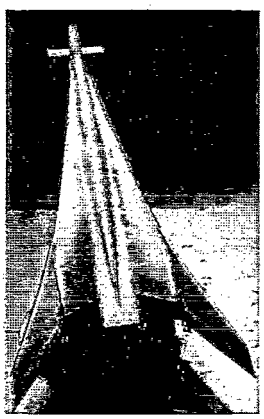

$\alpha = 26^{\circ}$

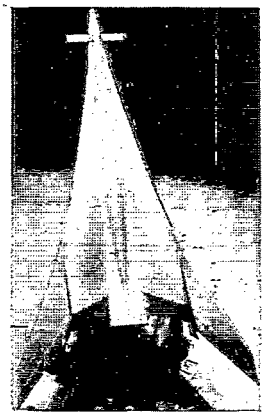

$\alpha = 30^{\circ}$

L-77-176

Figure 14.- Tuft studies of high-lift configuration with canard at $\beta = 10^{\circ}$. $(\delta_{f,te})_{1,2,3} = 30.0^{\circ}$, 30.0°, 30.5°; $(\delta_{f,le})_{1,2,3,4} = 45^{\circ}$; $(\delta_{f,le})_{5,6,7} = 60^{\circ}$; $C_{T'} = 0$; vertical tails on.

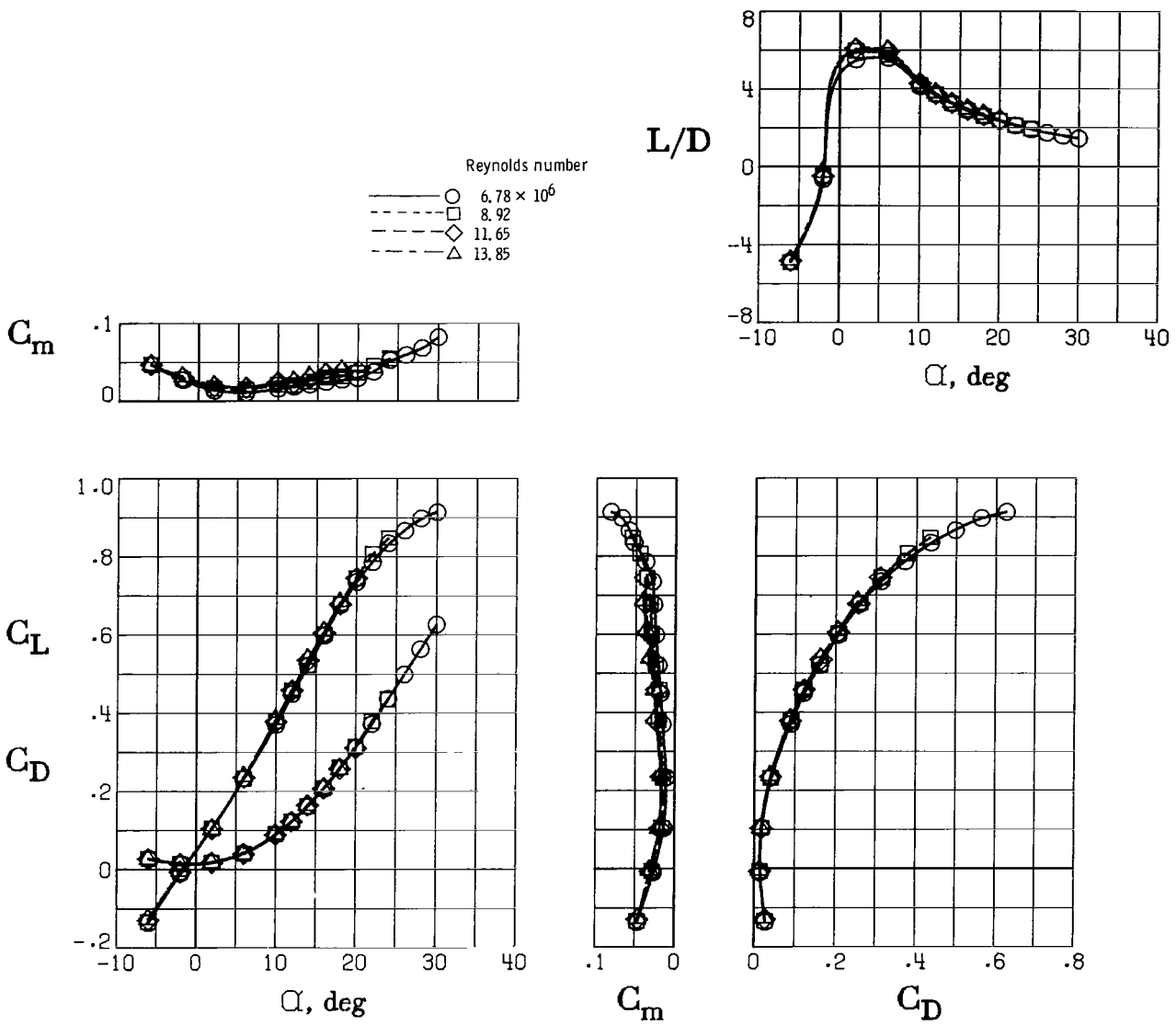

Figure 15.- Effect of Reynolds number on longitudinal aerodynamic characteristics of clean configuration with vertical tails. $\delta_{f,te} = 0^o$; $\delta_{f,le} = 0^o$; $\beta = 0^o$; $C_T' = 0$.

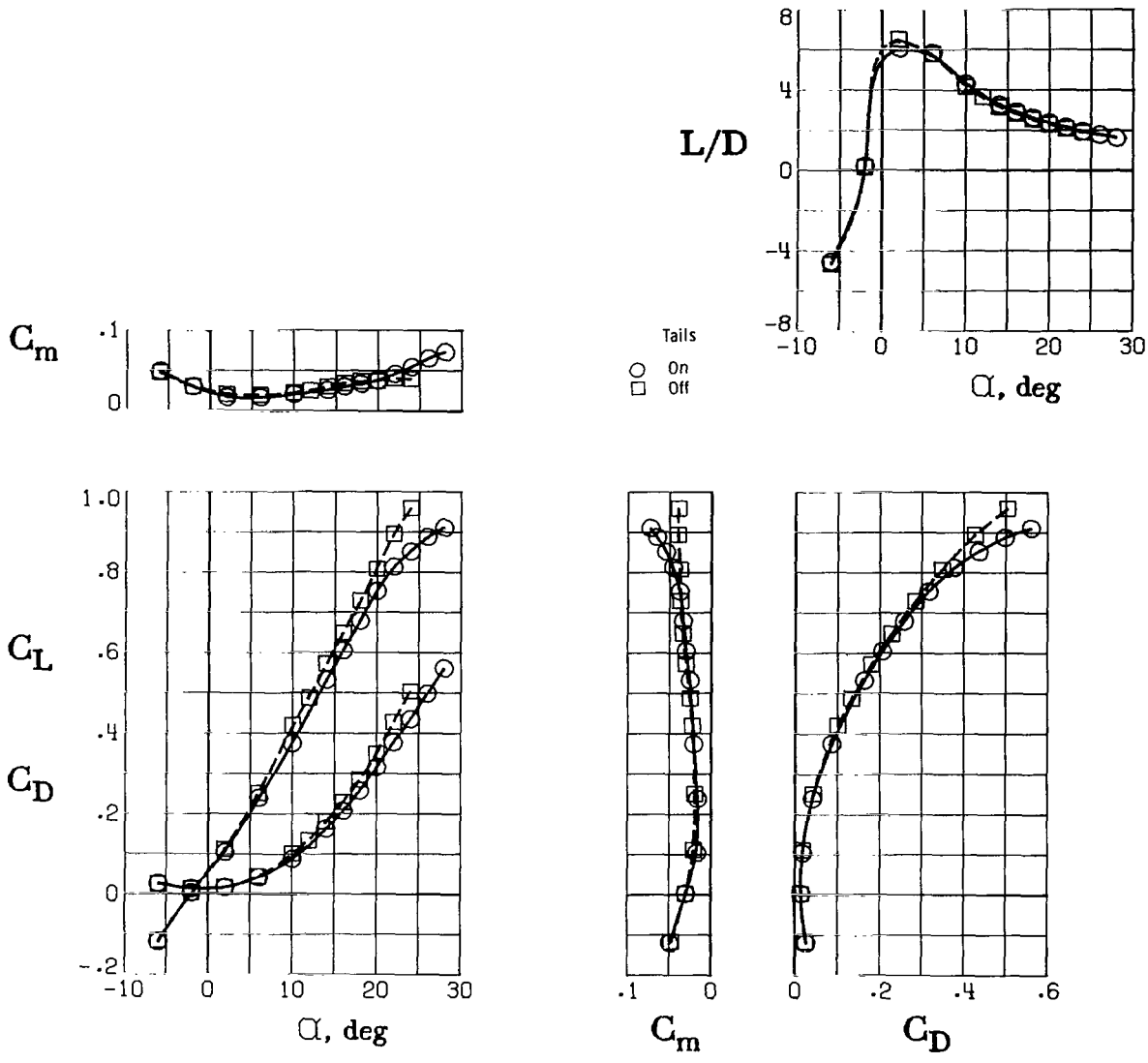

Figure 16.- Effect of vertical tails on longitudinal aerodynamic characteristics of clean configuration. $\delta_{f,te} = 0^{o}$; $\delta_{f,le} = 0^{o}$; $\beta = 0^{o}$; $C_T' = 0$.

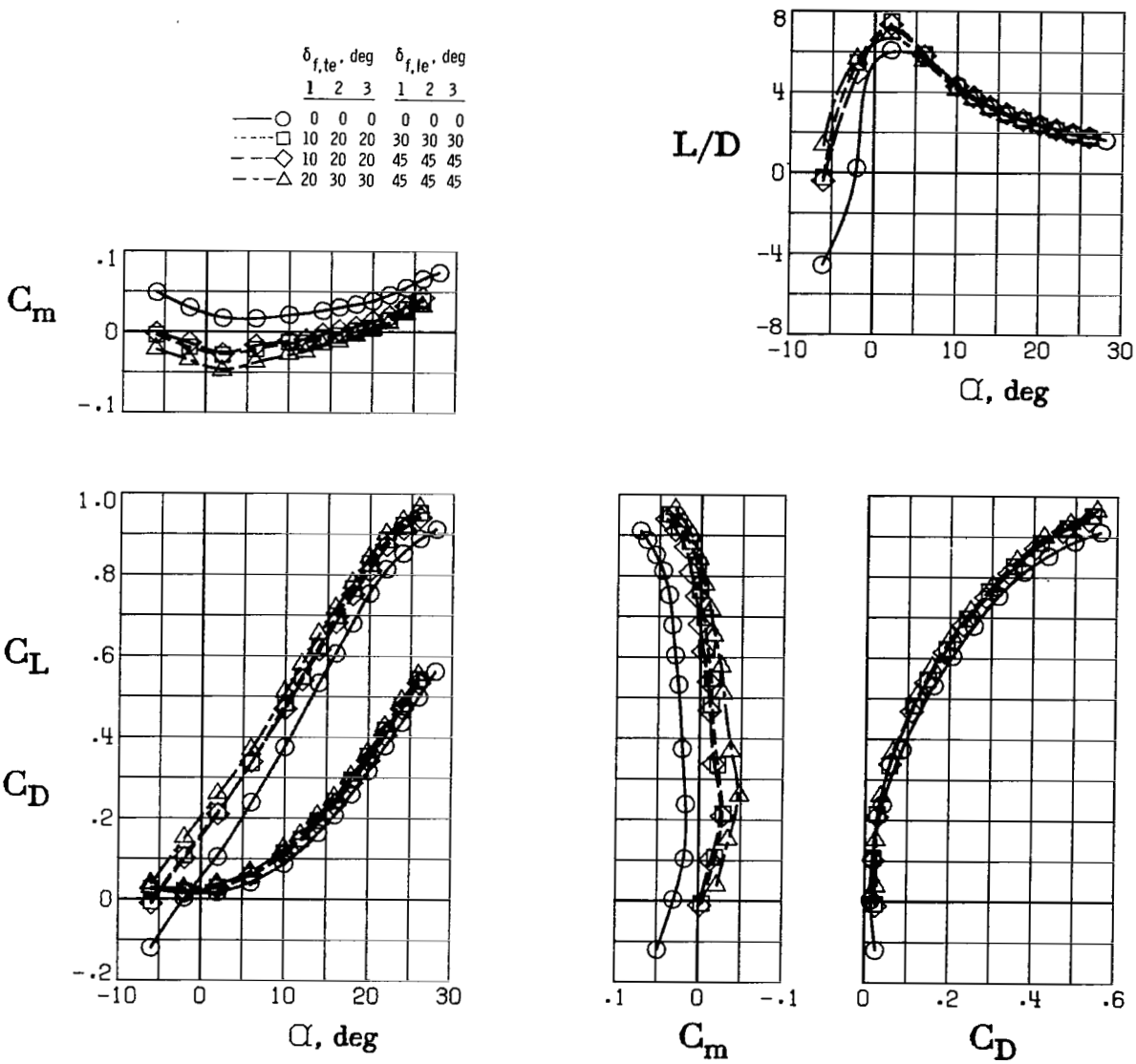

Figure 17.- Effect of wing leading- and trailing-edge flap deflection on longitudinal aerodynamic characteristics of high-lift configuration. $(\delta_{f,le})_{4,5,6,7} = 0^{\circ}$; $\beta = 0^{\circ}$; $C_T' = 0$.

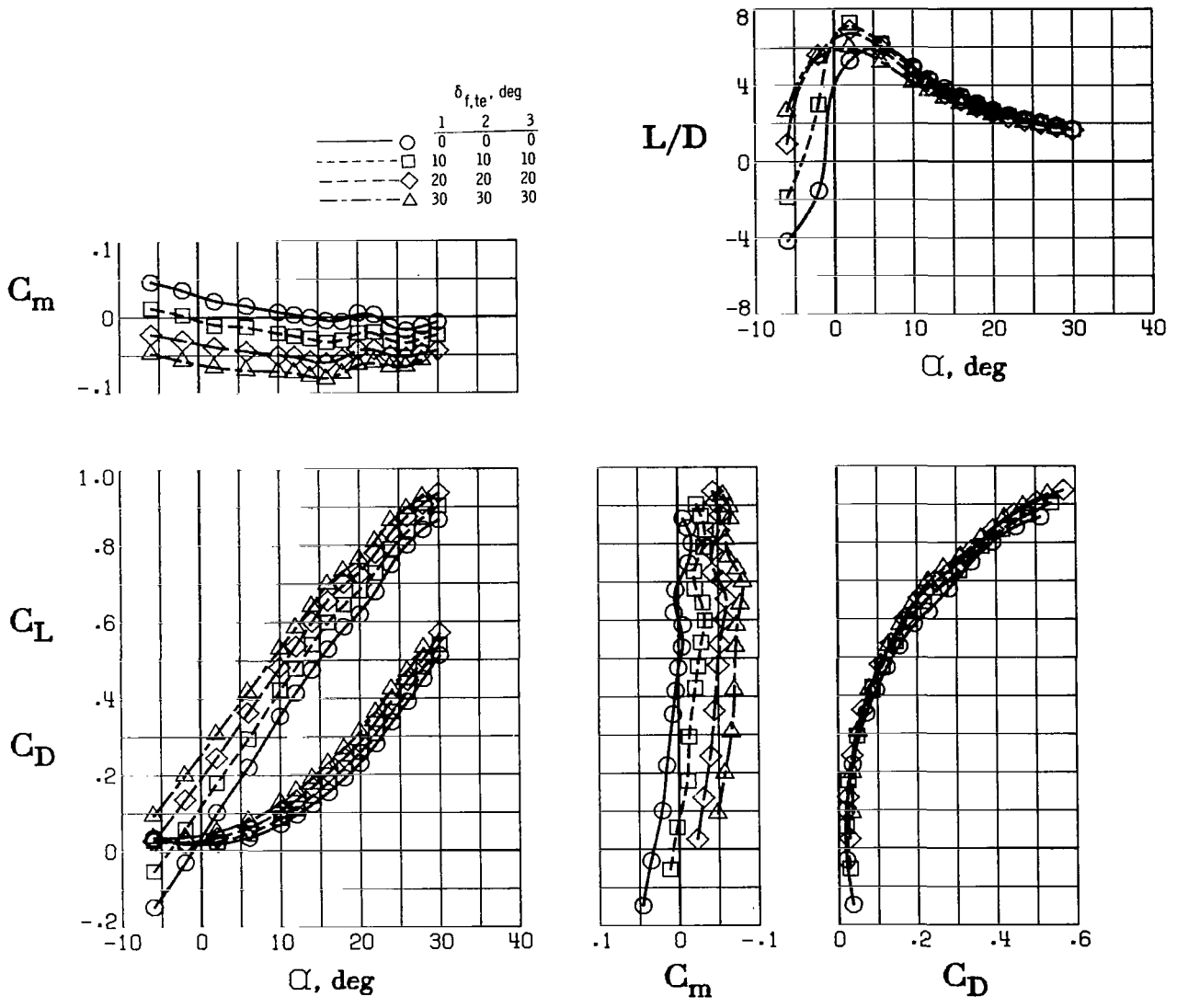

Figure 18.- Effect of full-span trailing-edge flap deflection on longitudinal aerodynamic characteristics of high-lift configuration. $(\delta_{f,le})_{1,2,3,4} = 45°$; $(\delta_{f,le})_{5,6,7} = 60°$; $\beta = 0°$; $C_T' = 0$.

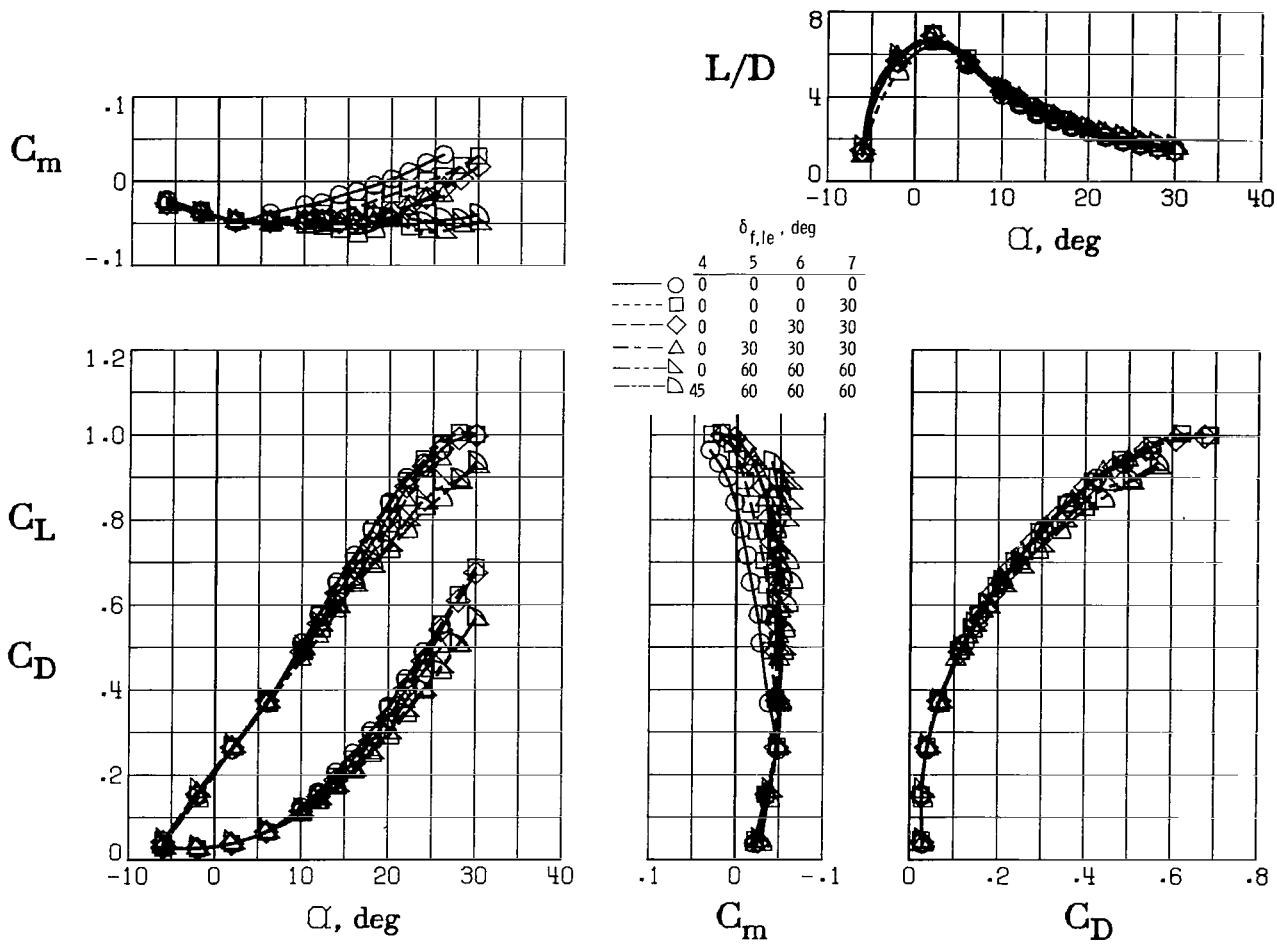

Figure 19.- Effect of inboard leading-edge flap deflection on longitudinal aerodynamic characteristics of high-lift configuration. $(\delta_{f,te})_{1,2,3} = 20^\circ, 30^\circ, 30^\circ$; $(\delta_{f,le})_{1,2,3} = 45^\circ$; $\beta = 0^\circ$; $C_T' = 0$.

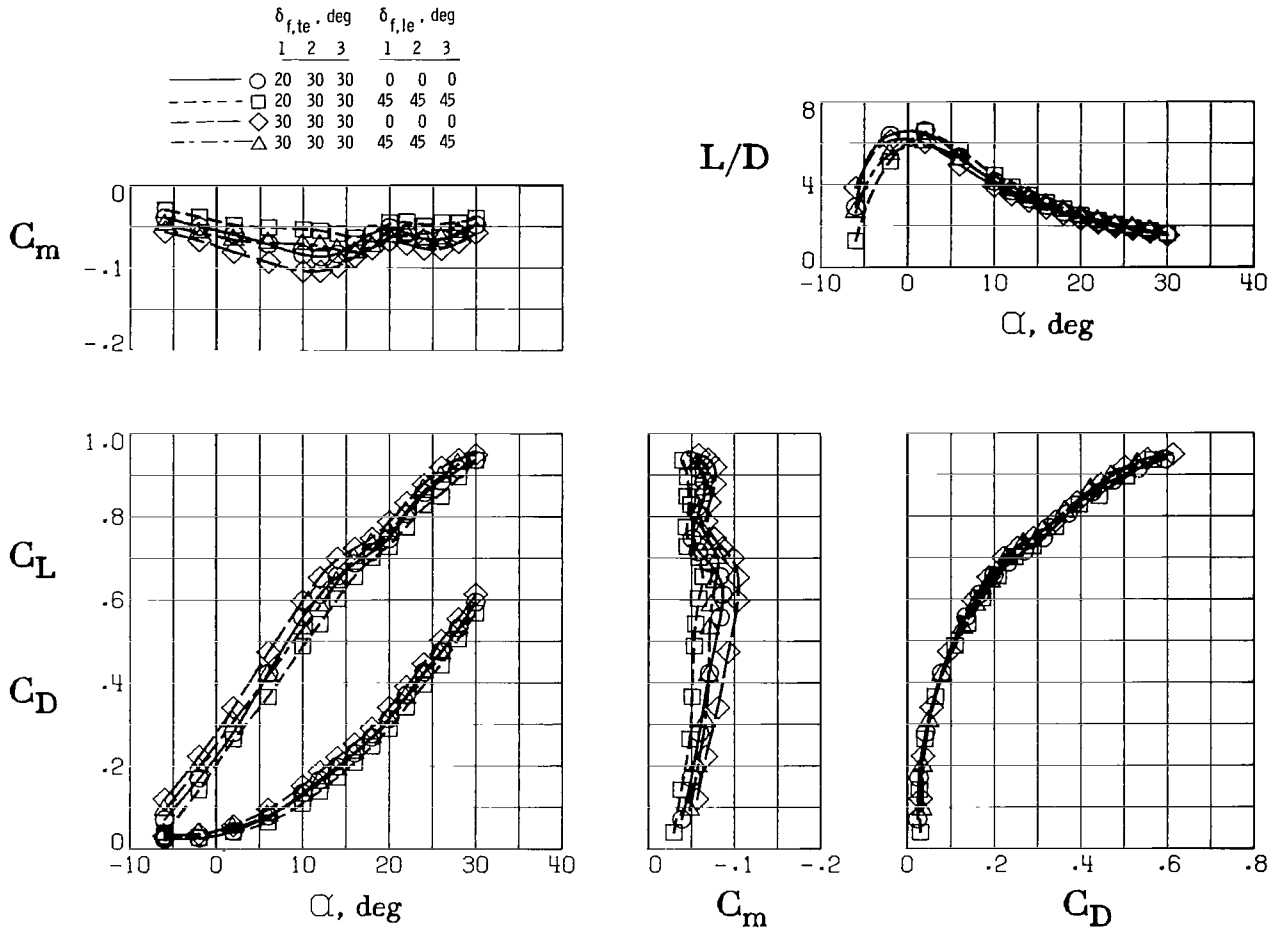

Figure 20.- Effect of outboard leading-edge flap deflection on longitudinal aerodynamic characteristics of high-lift configuration. $(\delta_{f,le})_{5,6,7}$ = 60°; β = 0°; C_T' = 0.

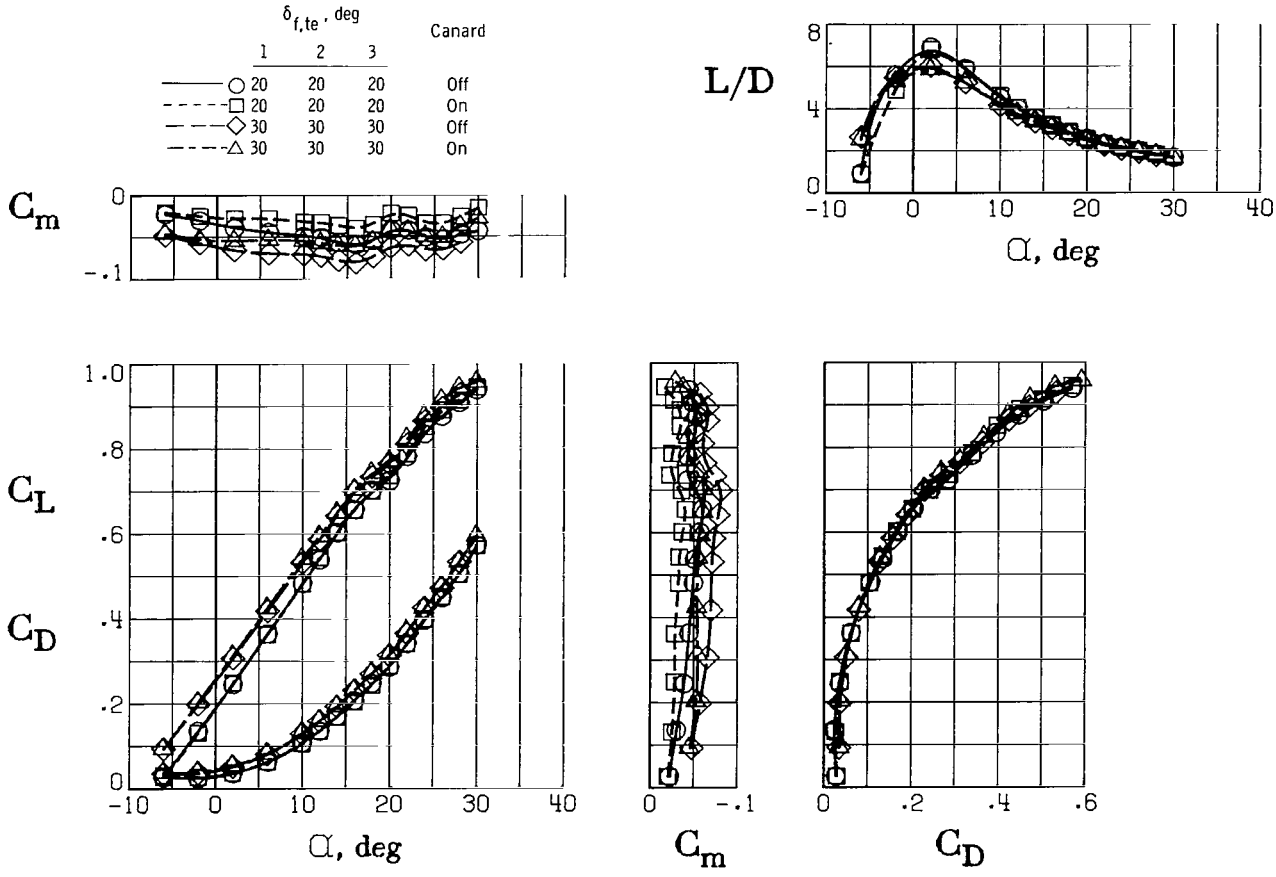

Figure 21.- Effect of 0.020S canard on longitudinal aerodynamic characteristics of high-lift configuration. $(\delta_{f,le})_{1,2,3,4} = 45^o$; $(\delta_{f,le})_{5,6,7} = 60^o$; $\beta = 0^o$; $C_T' = 0$.

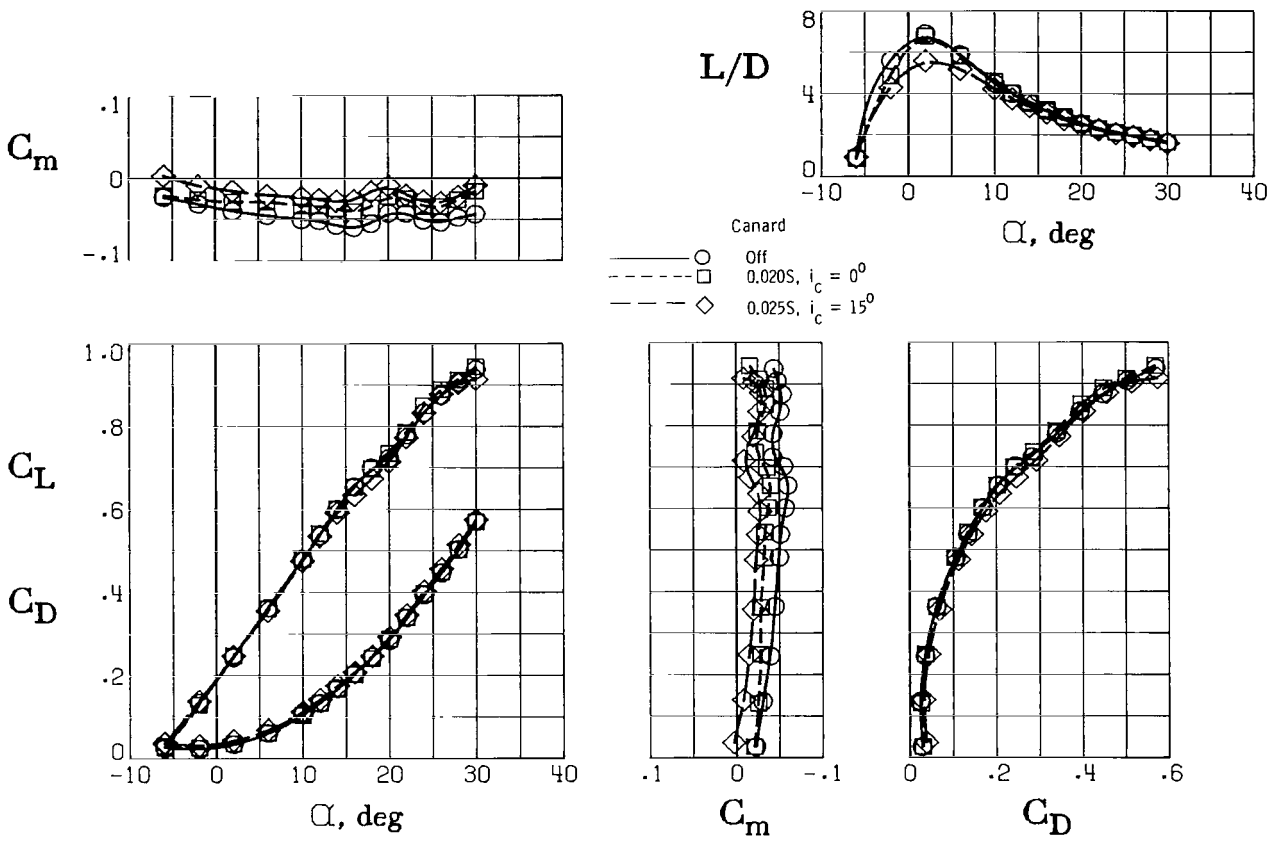

(a) $(\delta_{f,te})_{1,2,3} = 20^{o}$.

Figure 22.- Effect of increasing canard area and incidence on longitudinal aerodynamic characteristics of high-lift configuration. $(\delta_{f,le})_{1,2,3,4} = 45^{o}$; $(\delta_{f,le})_{5,6,7} = 60^{o}$; $\beta = 0^{o}$; $C_T' = 0$.

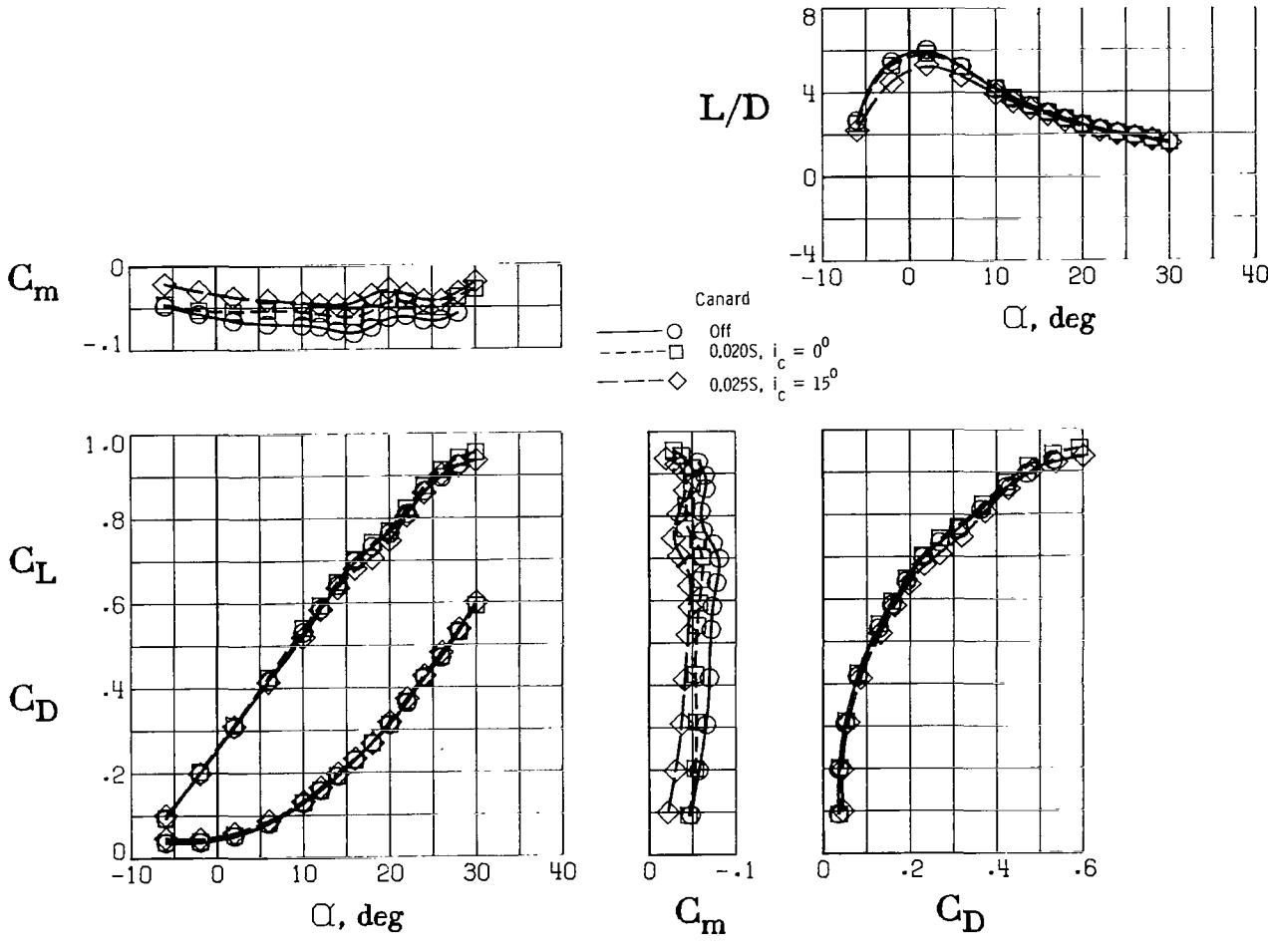

(b) $(\delta_{f,te})_{1,2,3} = 30^o$.

Figure 22.- Concluded.

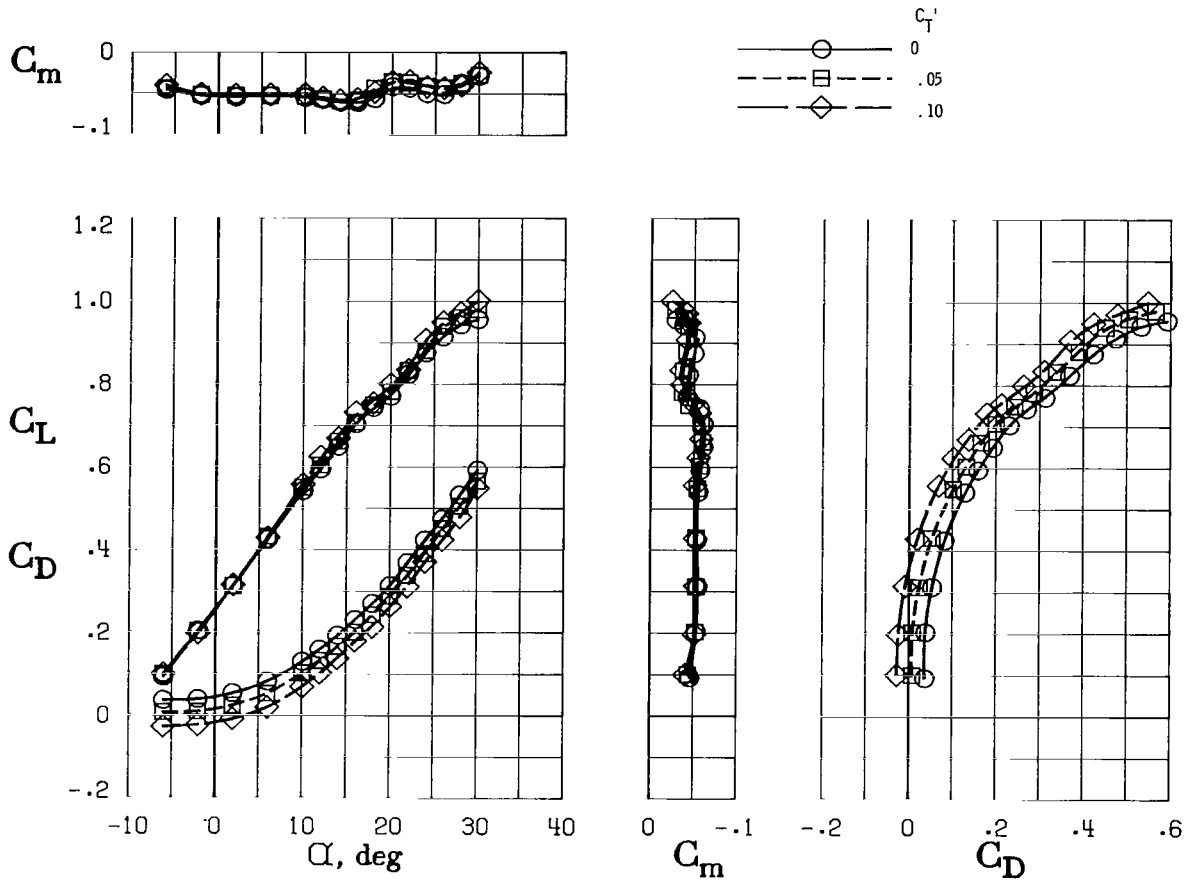

Figure 23.- Effect of engine thrust on longitudinal aerodynamic characteristics of high-lift configuration. $(\delta_{f,te})_{1,2,3} = 30^o$; $(\delta_{f,le})_{1,2,3,4} = 45^o$; $(\delta_{f,le})_{5,6,7} = 60^o$; 0.020S canard; $\beta = 0^o$.

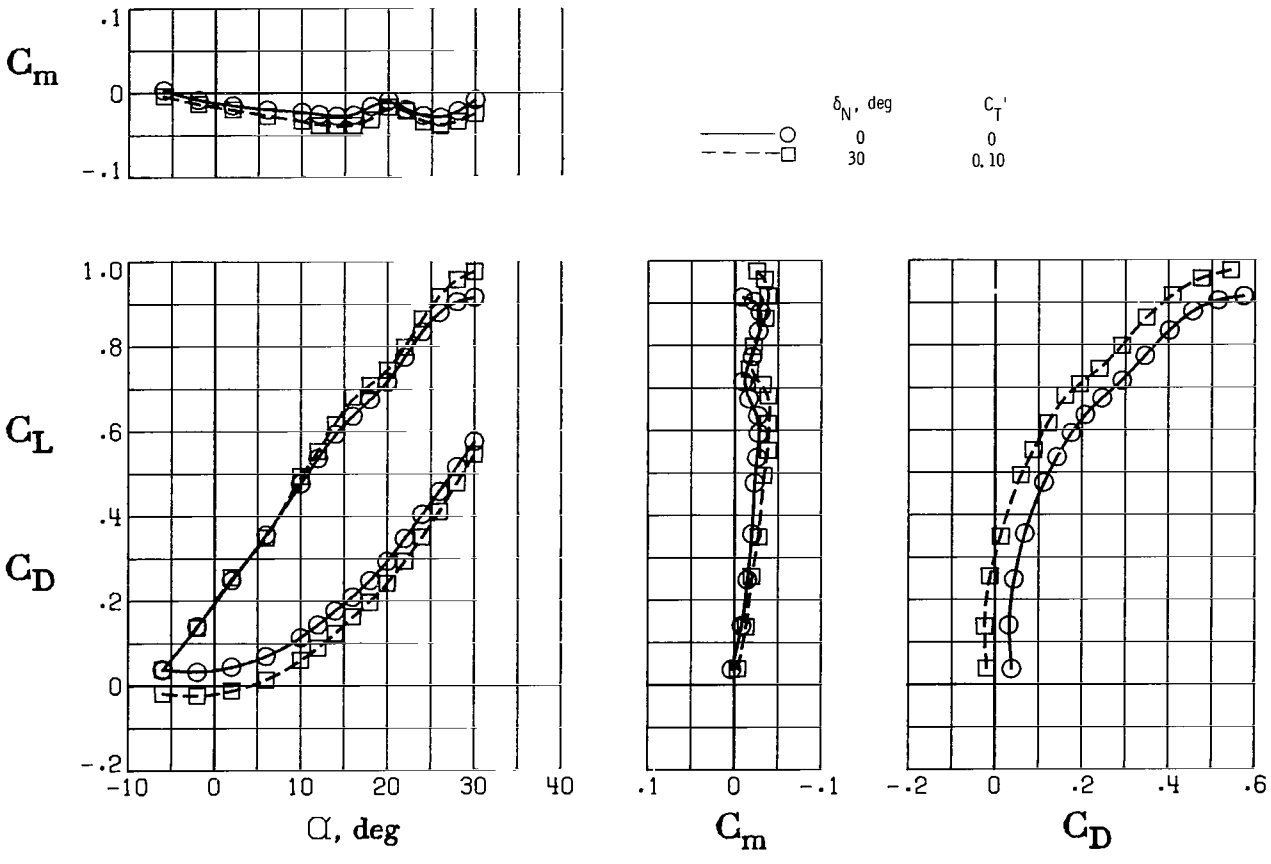

(a) $(\delta_{f,te})_{1,2,3} = 20^{o}$.

Figure 24.- Effect of thrust vectoring on longitudinal aerodynamic characteristics of high-lift configuration. $(\delta_{f,le})_{1,2,3,4} = 45^{o}$; $(\delta_{f,le})_{5,6,7} = 60^{o}$; 0.020S canard; $\beta = 0^{o}$.

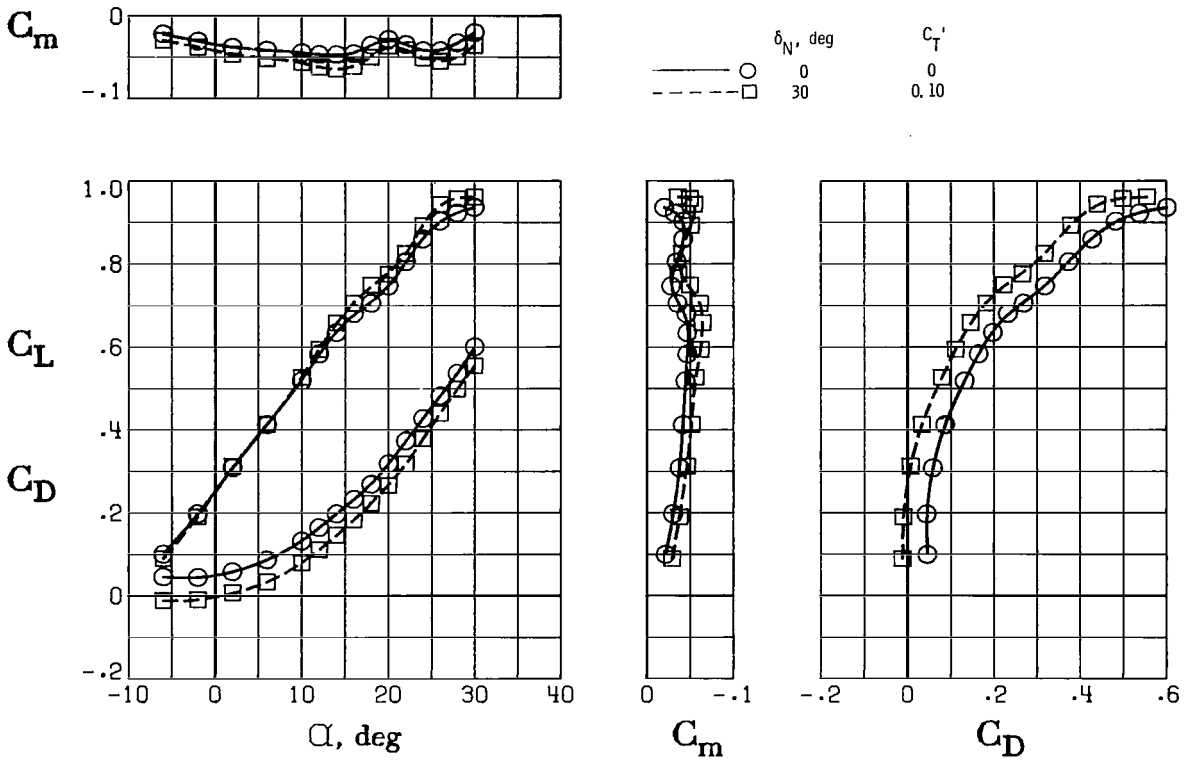

(b) $(\delta_{f,te})_{1,2,3} = 30^{\circ}$.

Figure 24.- Concluded.

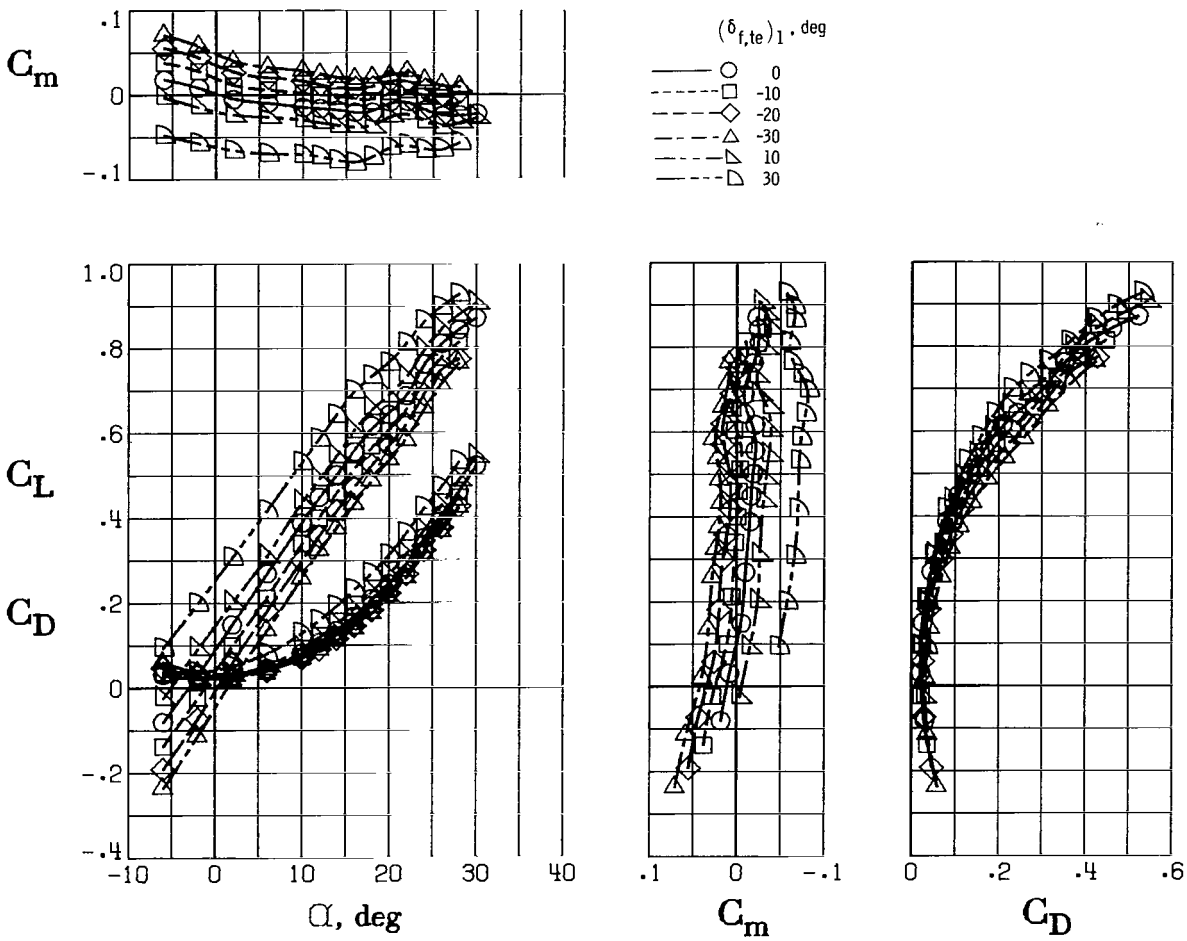

(a) $(\delta_{f,te})_{2,3} = 30^\circ$ (inboard flap variable).

Figure 25.- Longitudinal control effectiveness of trailing-edge flaps on longitudinal aerodynamic characteristics of high-lift configuration. $(\delta_{f,le})_{1,2,3,4} = 45^\circ$; $(\delta_{f,le})_{5,6,7} = 60^\circ$; $\beta = 0^\circ$; $C_T' = 0$.

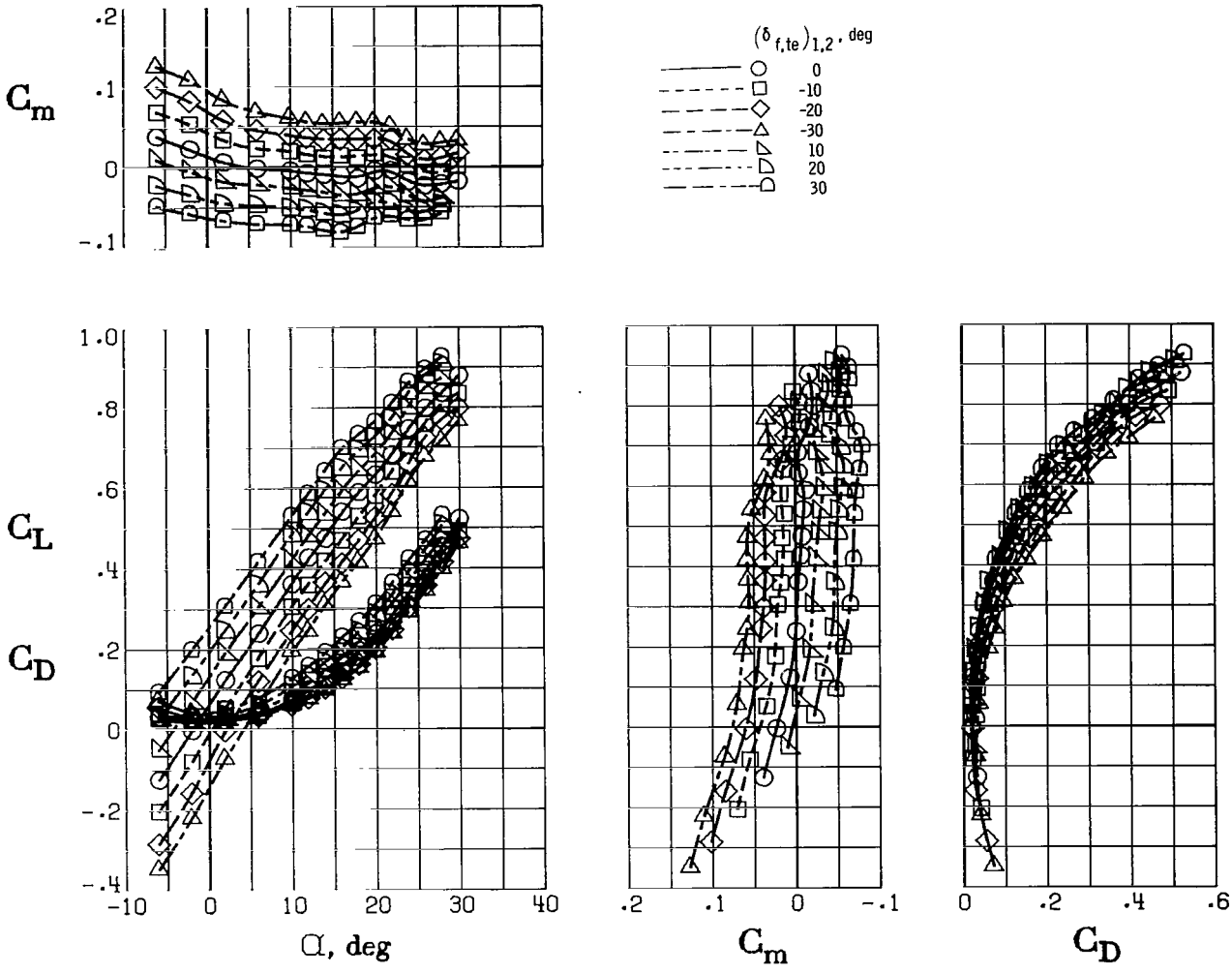

(b) $(\delta_{f,te})_3 = 30^\circ$ (inboard and center flap variable).

Figure 25.- Continued.

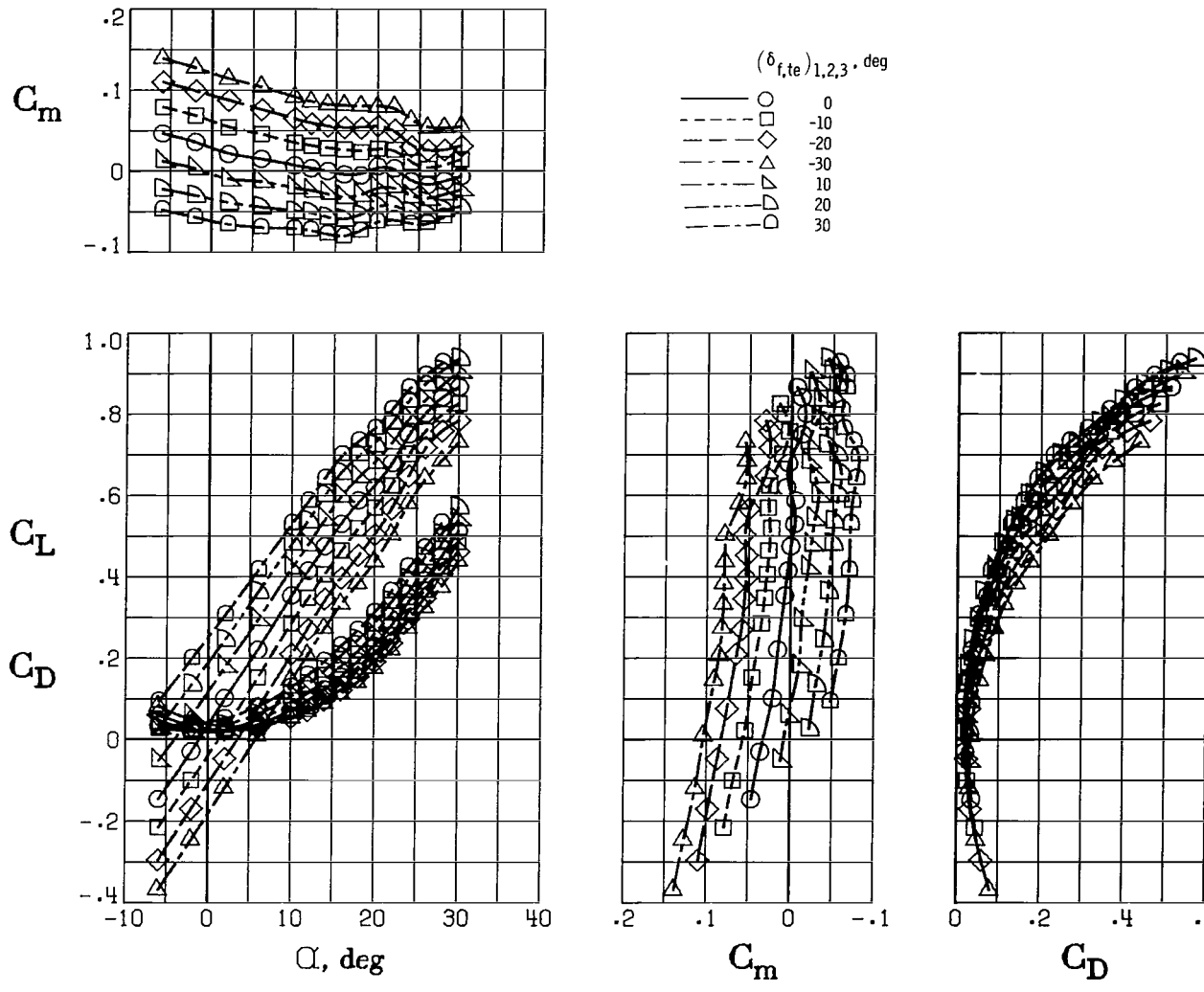

(c) Inboard, center, and outboard flap variable.

Figure 25.- Continued.

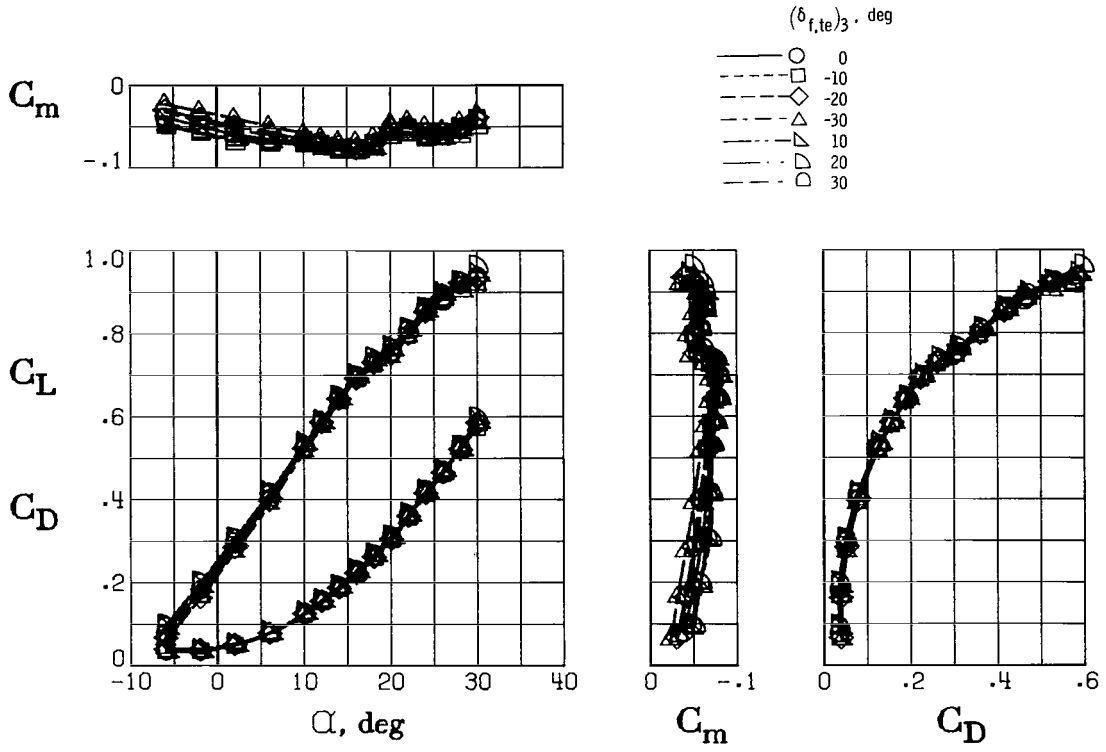

(d) $(\delta_{f,te})_{1,2} = 30^\circ$ (outboard flap variable).

Figure 25.- Concluded.

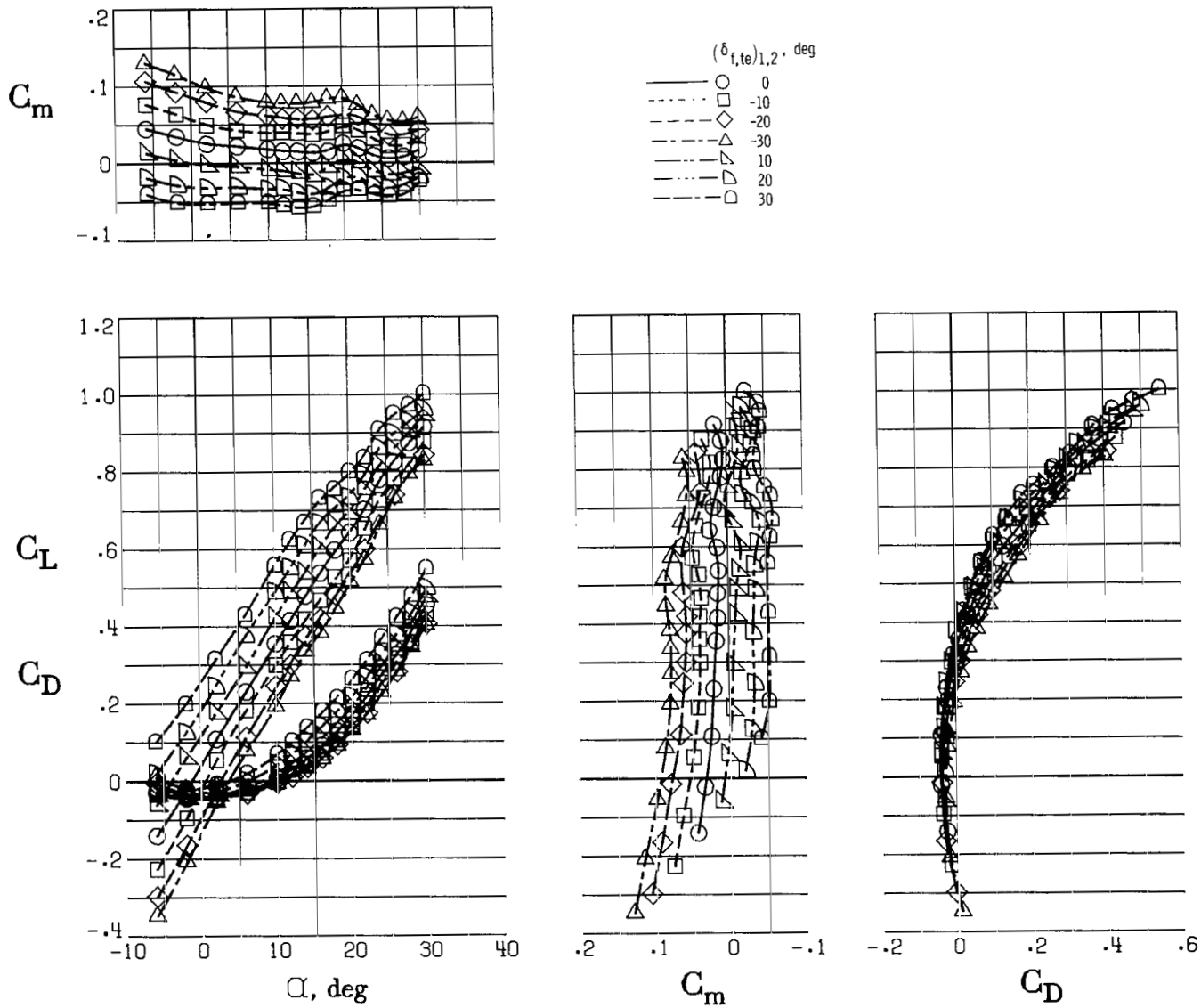

Figure 26.- Longitudinal control effectiveness of trailing-edge flaps on longitudinal aerodynamic characteristics of high-lift configuration with 0.020S canard and engines operating. $(\delta_{f,te})_3 = 30°$; $(\delta_{f,le})_{1,2,3,4} = 45°$; $(\delta_{f,le})_{5,6,7} = 60°$; $\beta = 0°$; $C_T' = 0.10$.

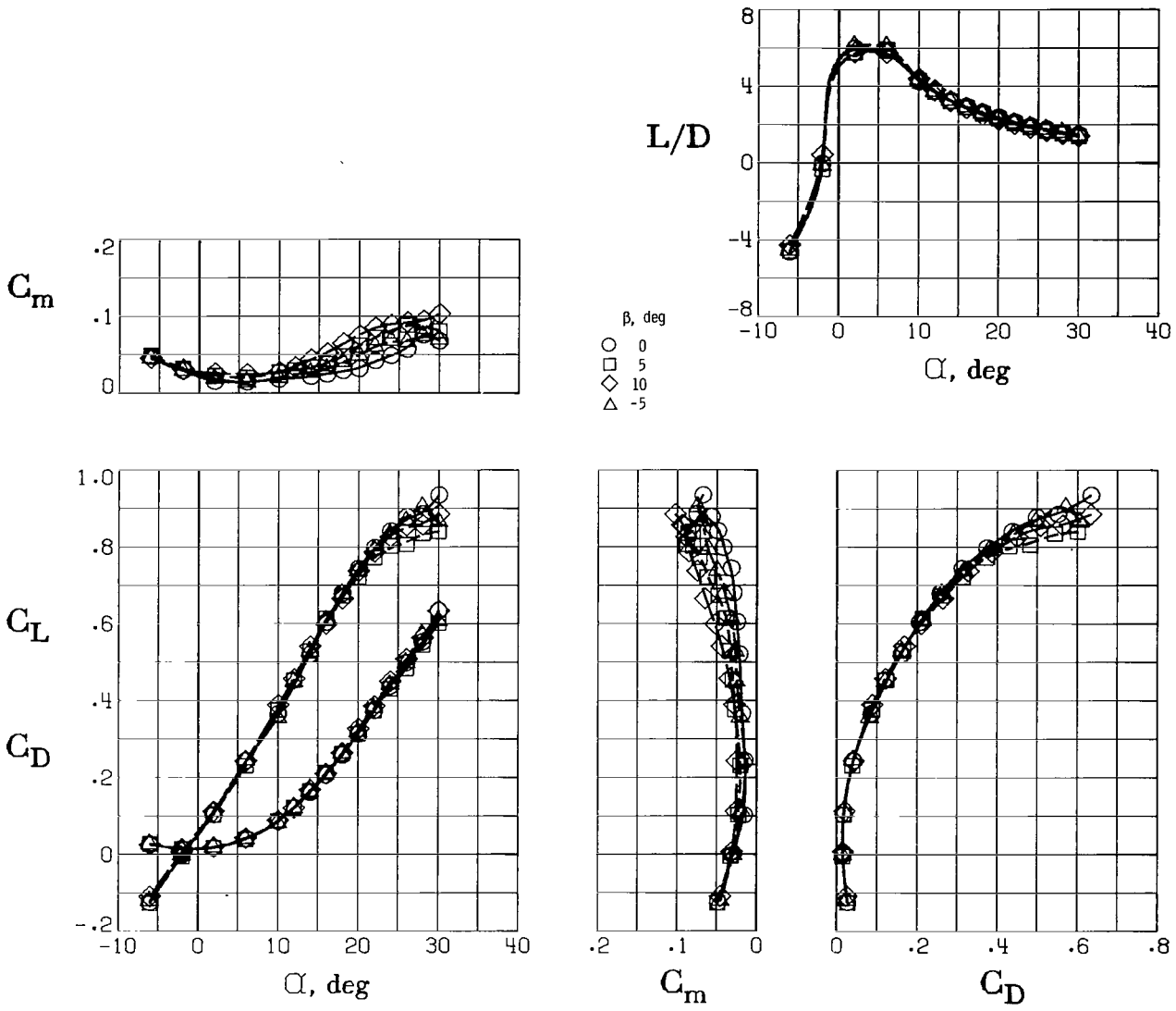

(a) Reynolds number, 6.78×10^6.

Figure 27.- Effect of sideslip on longitudinal aerodynamic characteristics of clean configuration at several Reynolds numbers. $\delta_{f,te} = 0^o$; $\delta_{f,le} = 0^o$; $C_T' = 0$.

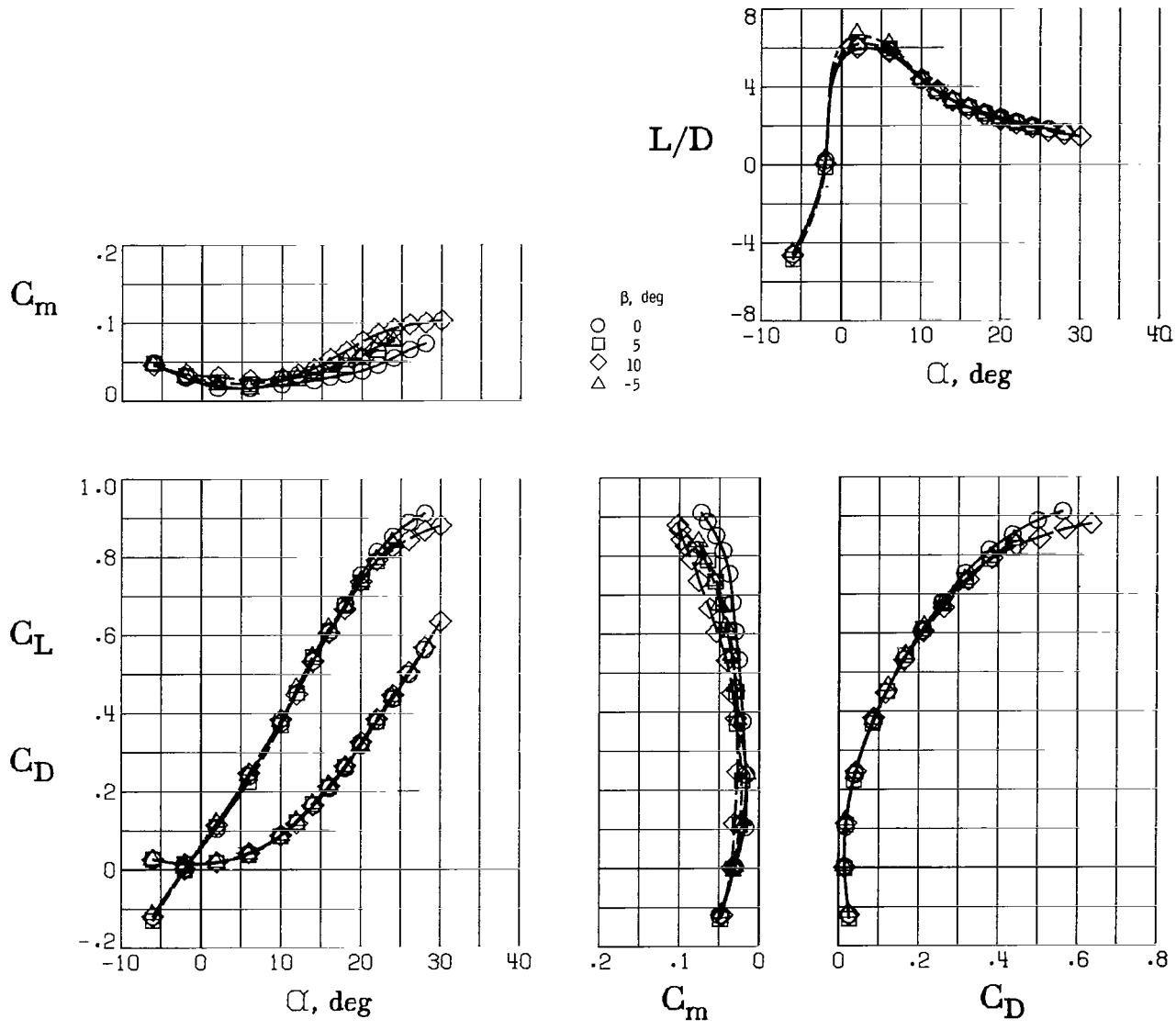

(b) Reynolds number, 8.92×10^6.

Figure 27.- Continued.

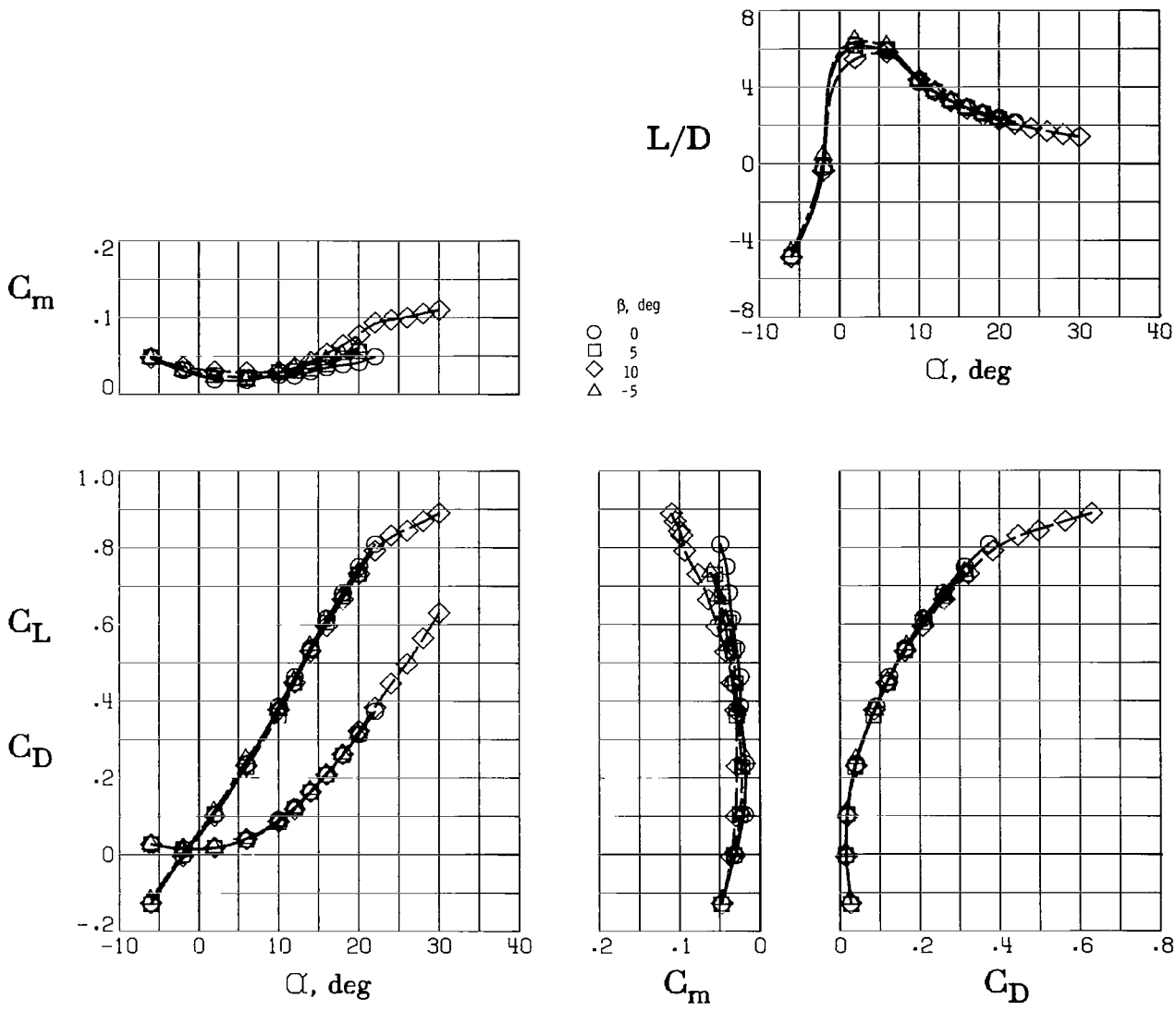

(c) Reynolds number, 11.65×10^6.

Figure 27.- Continued.

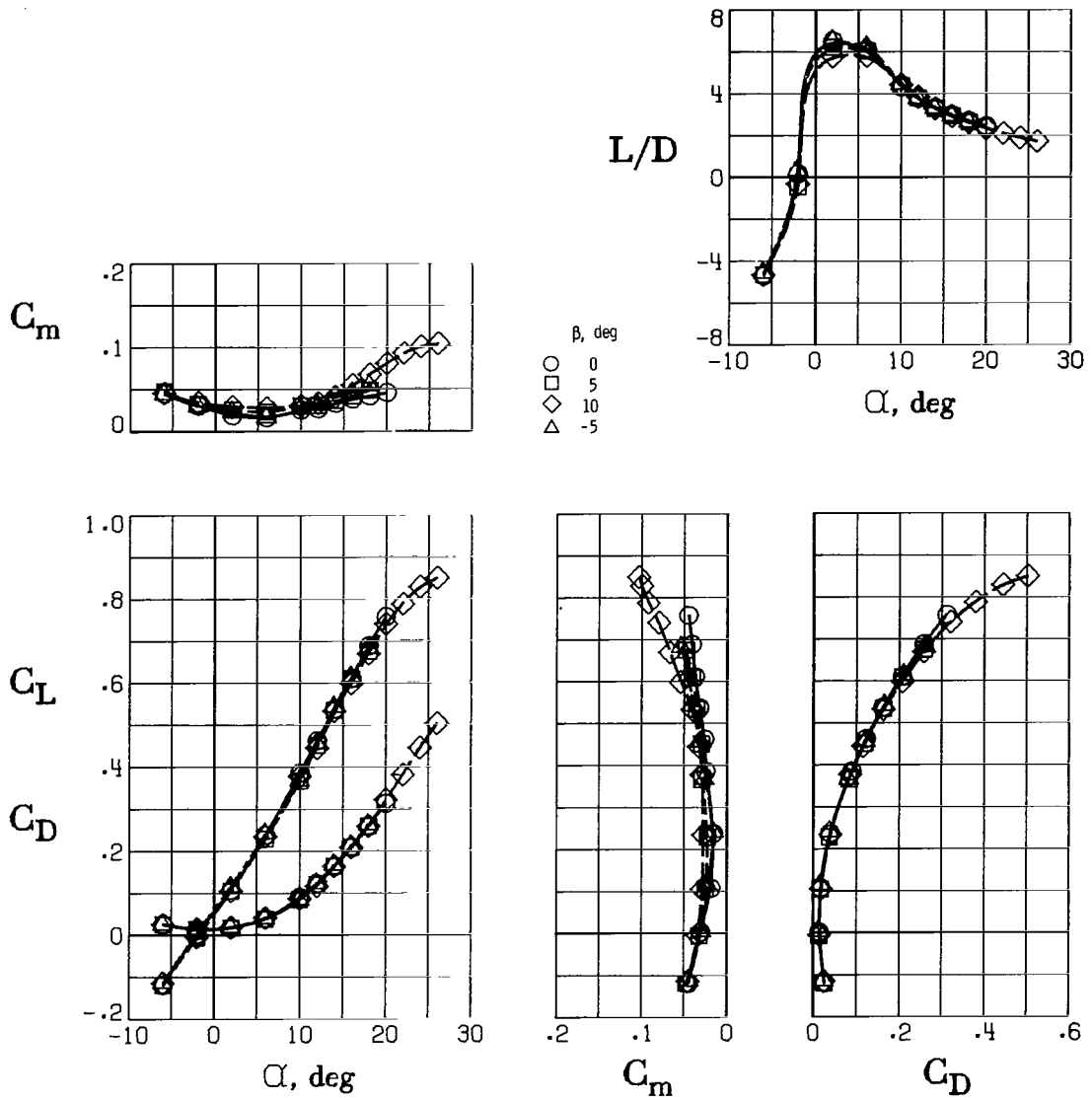

(d) Reynolds number, 13.85×10^6.

Figure 27.- Concluded.

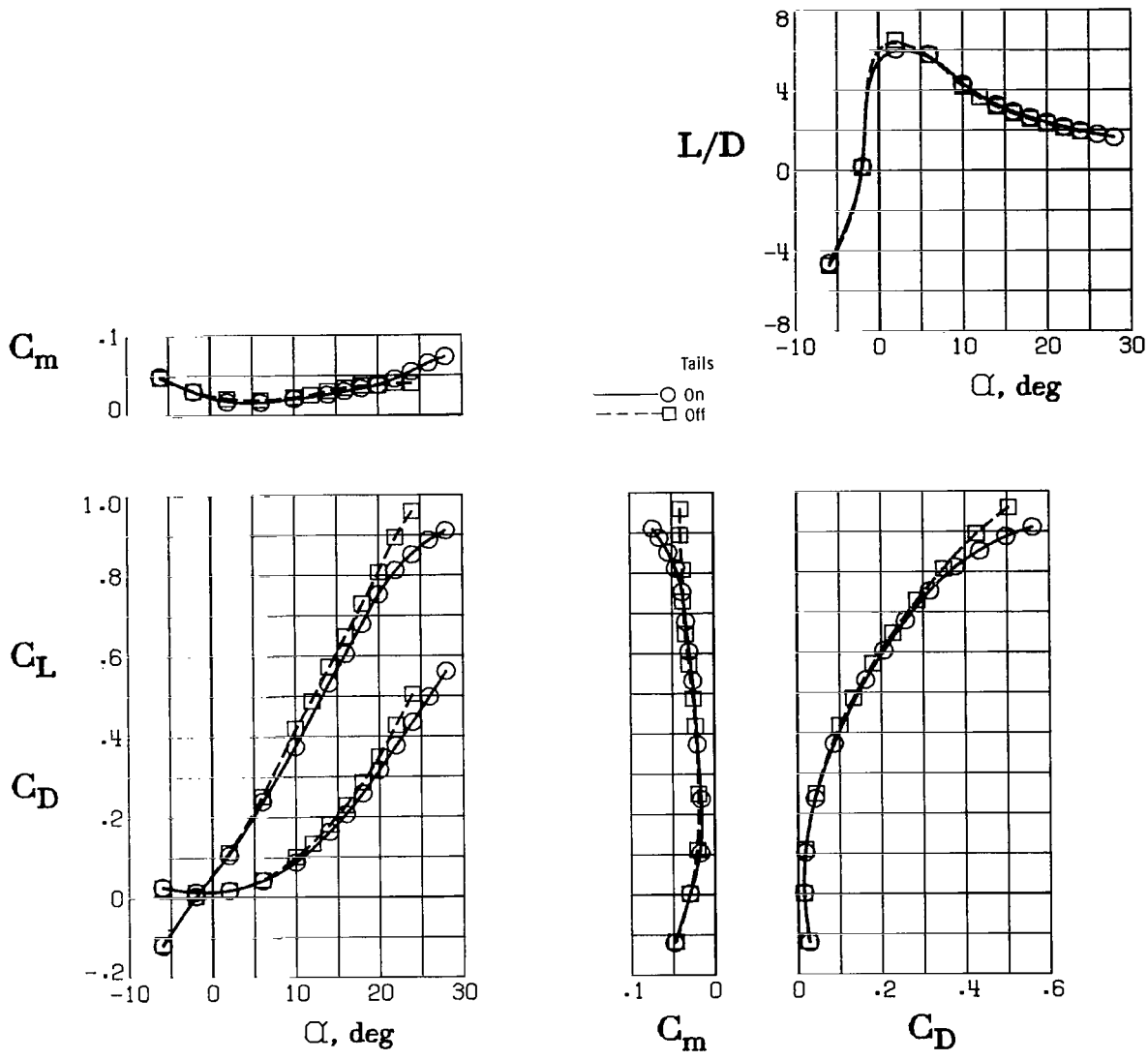

(a) $\beta = 0^{\circ}$.

Figure 28.- Effect of vertical tails on longitudinal aerodynamic characteristics of clean configuration at several sideslip angles. $\delta_{f,te} = 0^{\circ}$; $\delta_{f,le} = 0^{\circ}$; $C_{T'} = 0$.

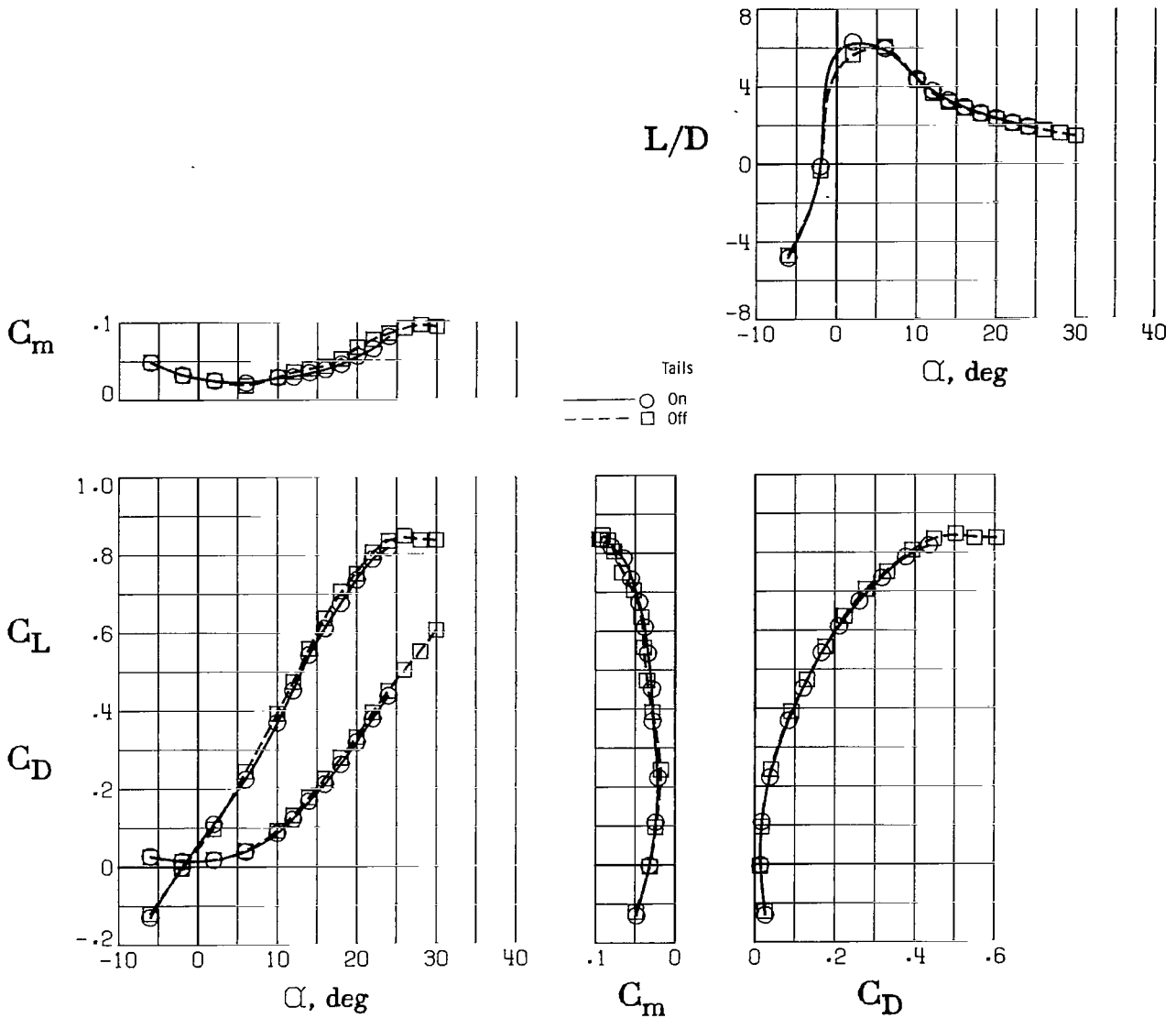

(b) $\beta = 5^{\circ}$.

Figure 28.- Continued.

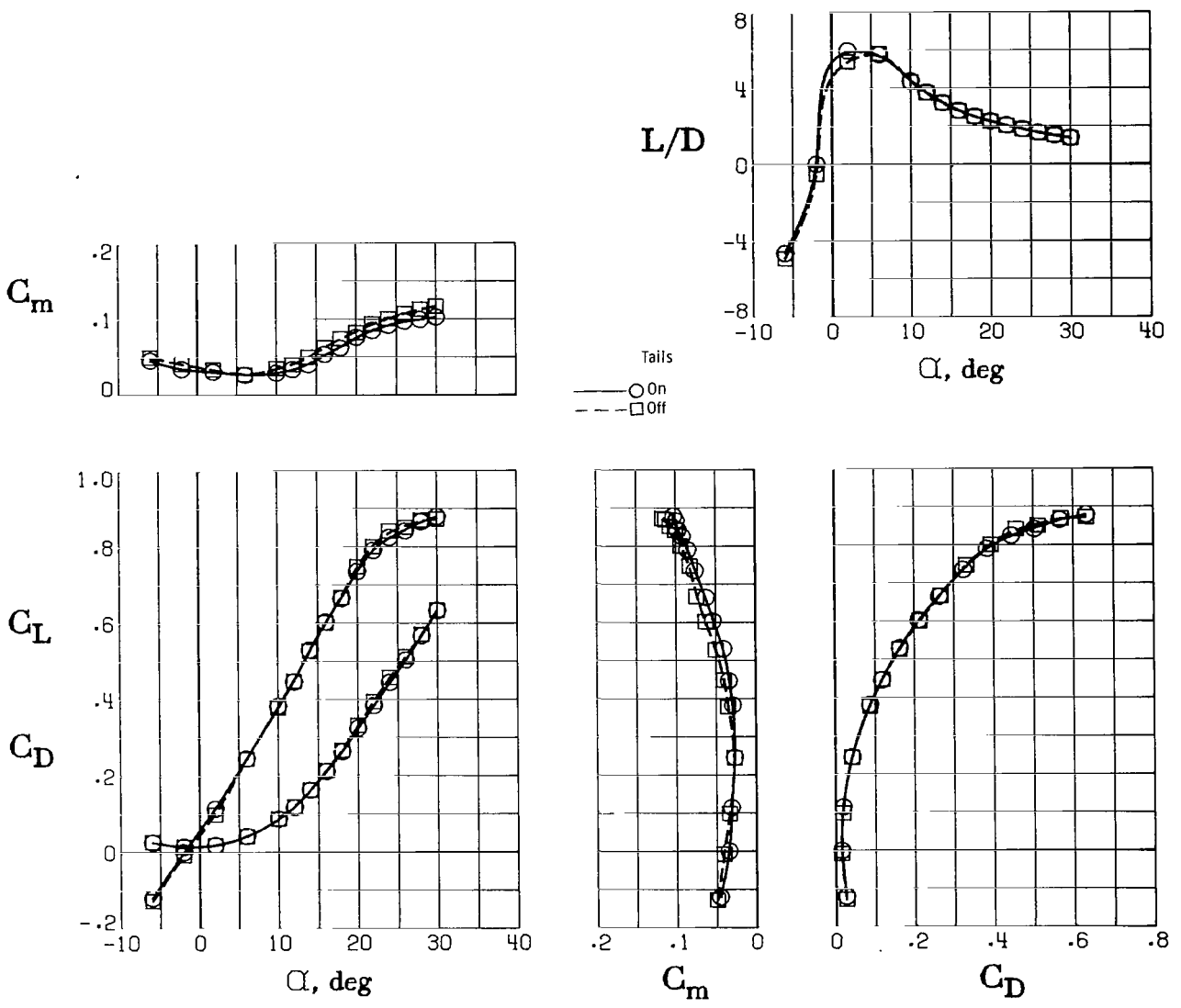

(c) $\beta = 10^{\circ}$.

Figure 28.- Continued.

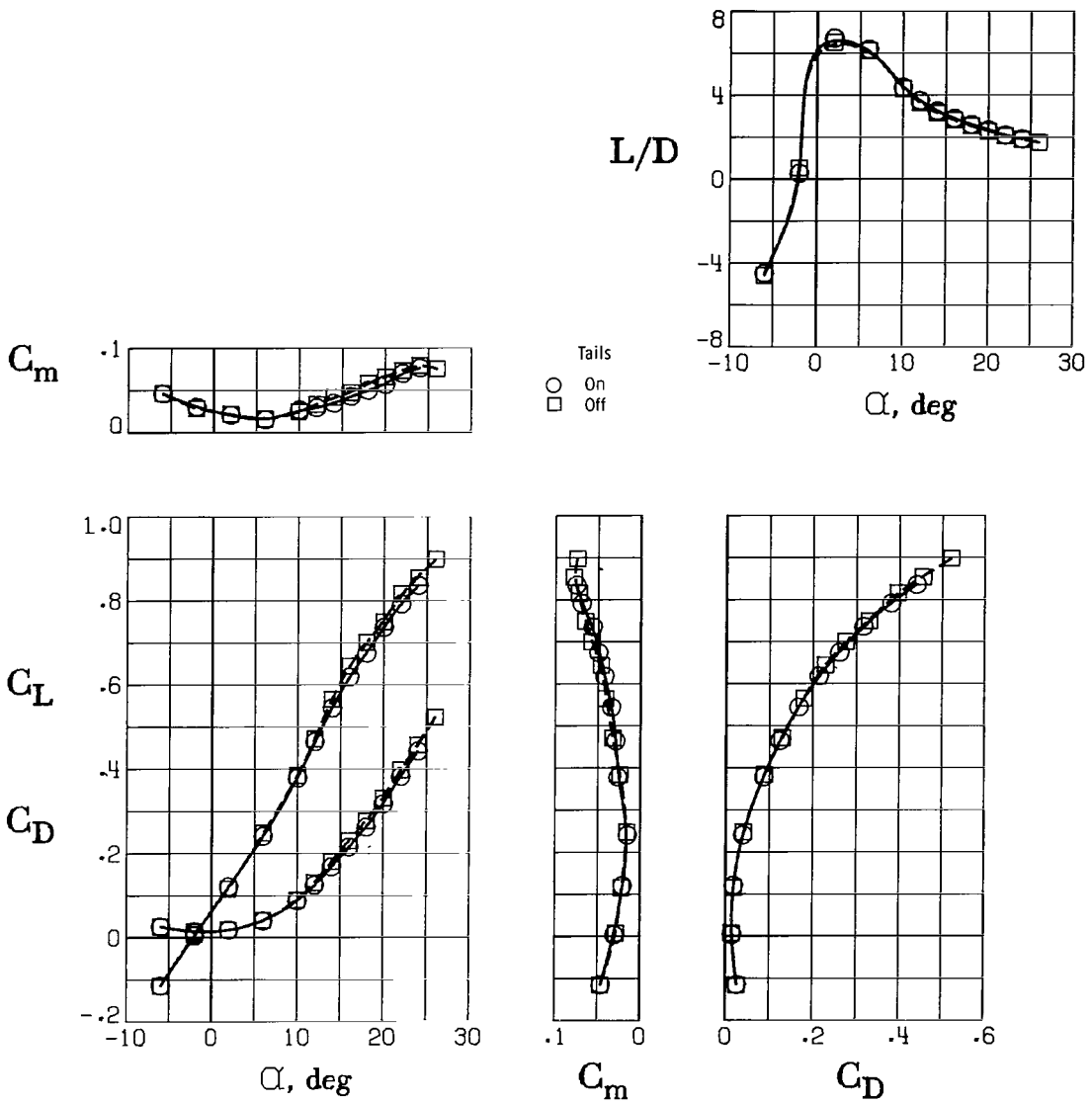

(d) $\beta = -5^{\circ}$.

Figure 28.- Concluded.

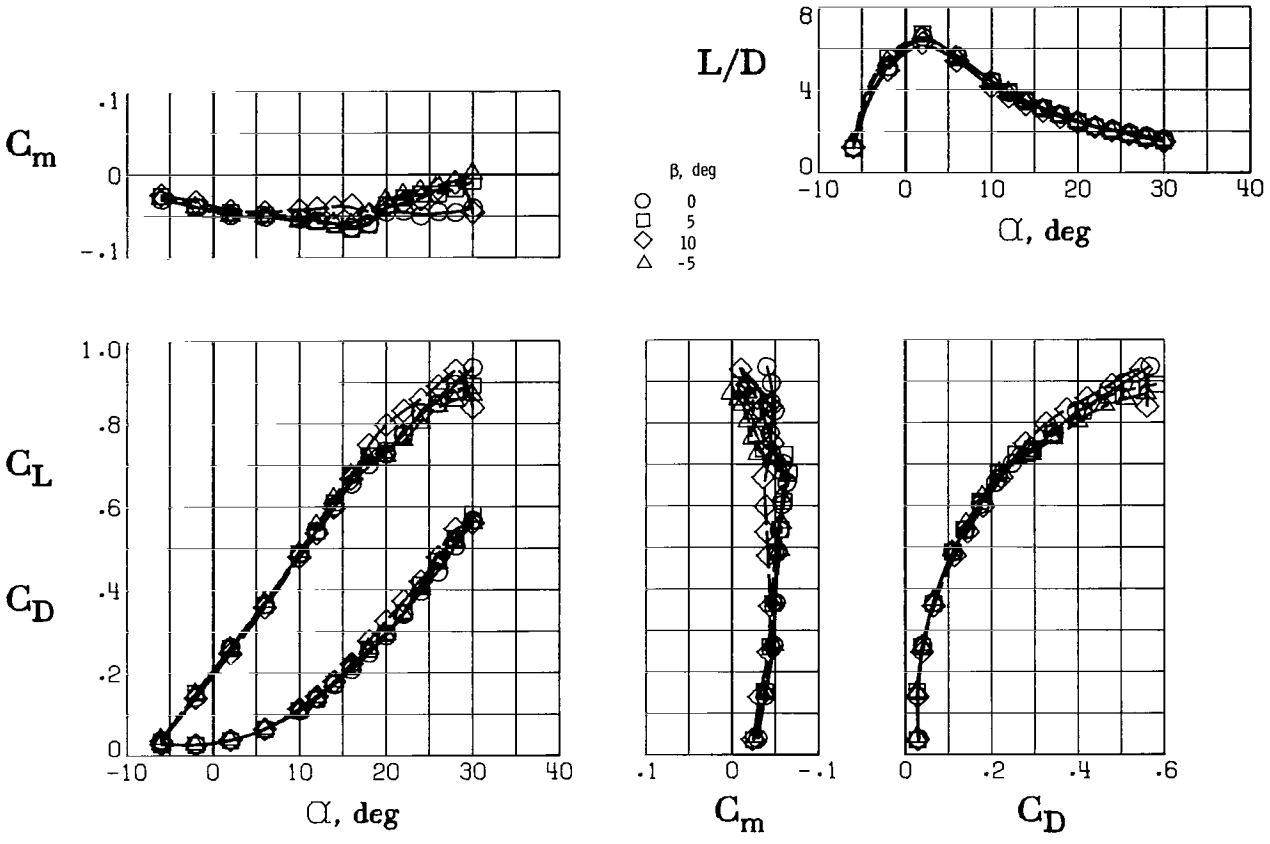

Figure 29.- Effect of sideslip on longitudinal aerodynamic characteristics of high-lift configuration. $(\delta_{f,te})_{1,2,3} = 20^o, 30^o, 30^o$; $(\delta_{f,le})_{1,2,3,4} = 45^o$; $(\delta_{f,le})_{5,6,7} = 60^o$; $C_T' = 0$.

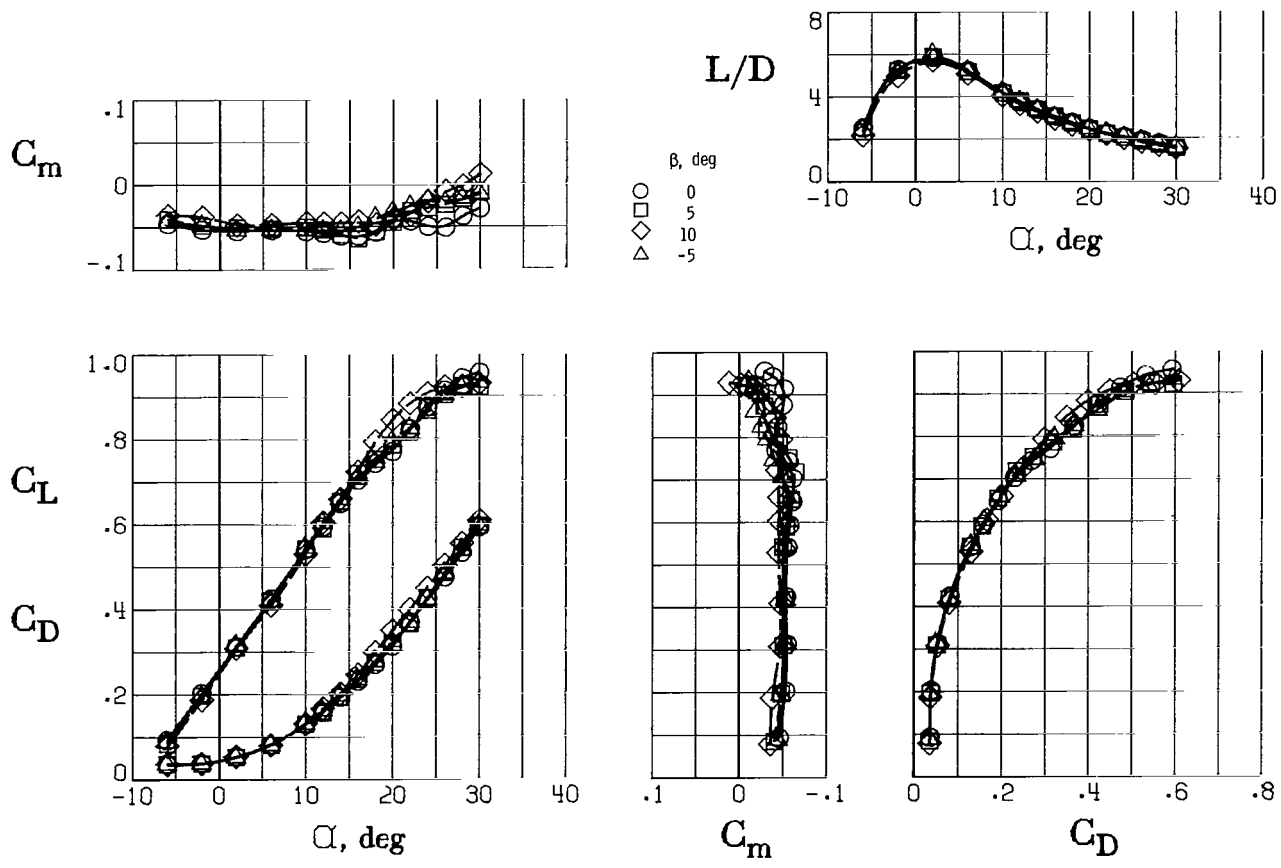

Figure 30.- Effect of sideslip on longitudinal aerodynamic characteristics of high-lift configuration with 0.020S canard. $(\delta_{f,te})_{1,2,3} = 30^{\circ}$; $(\delta_{f,le})_{1,2,3,4} = 45^{\circ}$; $(\delta_{f,le})_{5,6,7} = 60^{\circ}$; $C_T' = 0$.

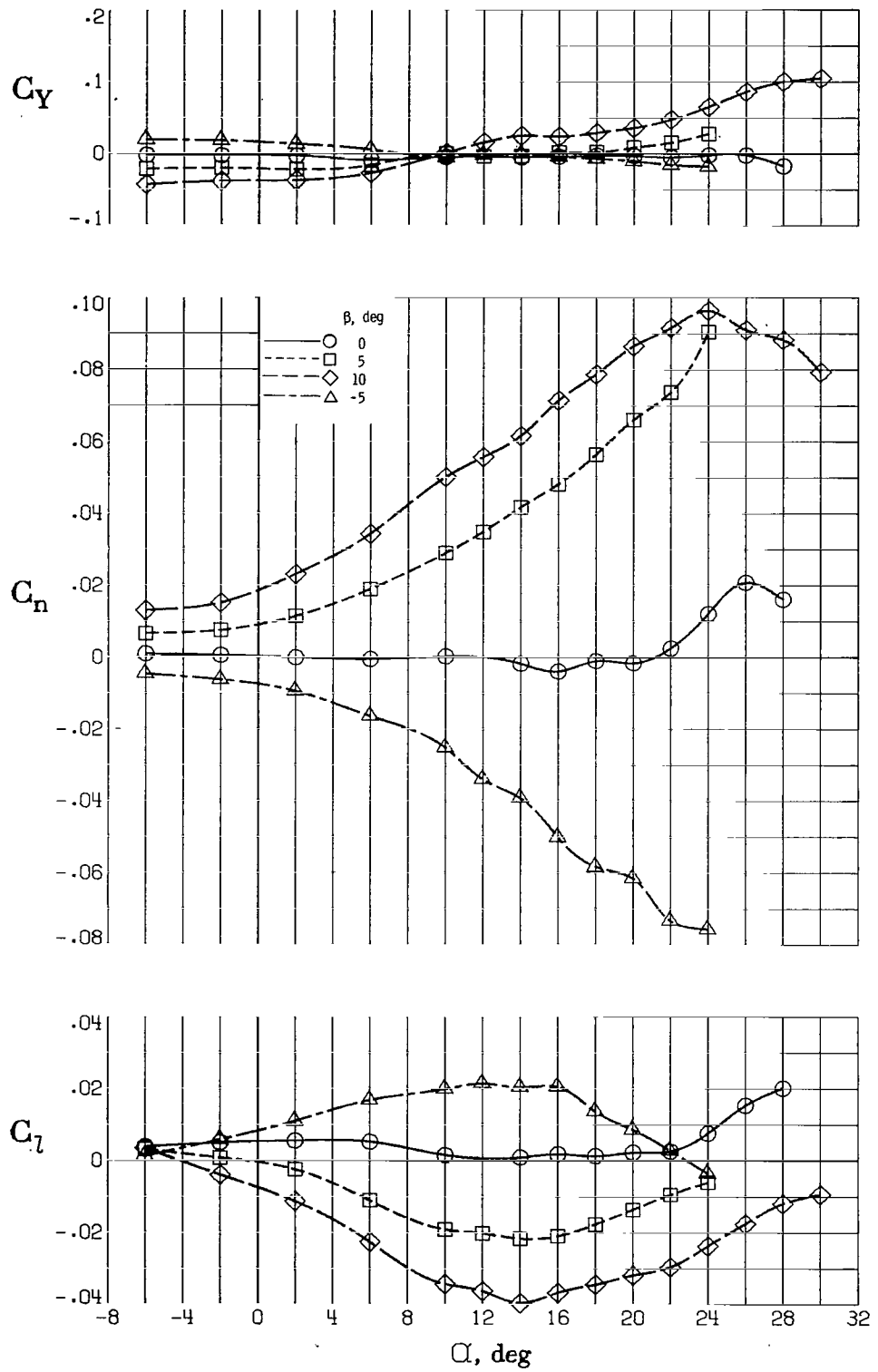

Figure 31.- Effect of sideslip on lateral-directional aerodynamic characteristics of clean configuration with vertical tails. $C_{T'} = 0$.

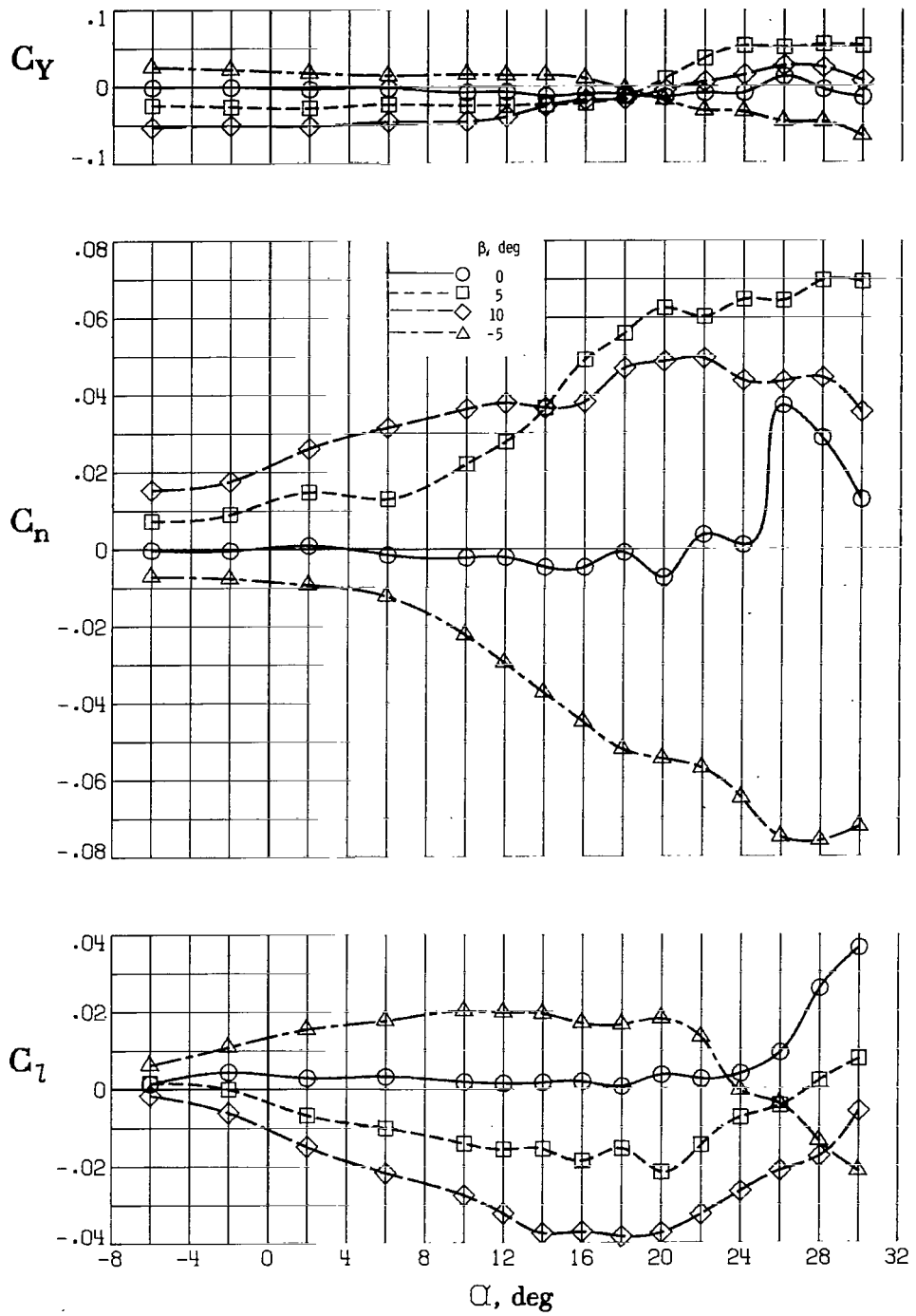

Figure 32.- Effect of sideslip on lateral-directional aerodynamic characteristics of high-lift configuration with vertical tails. $(\delta_{f,te})_{1,2,3} = 20^\circ$, 30°, 30°; $(\delta_{f,le})_{1,2,3,4} = 45^\circ$; $(\delta_{f,le})_{5,6,7} = 60^\circ$; $C_T' = 0$.

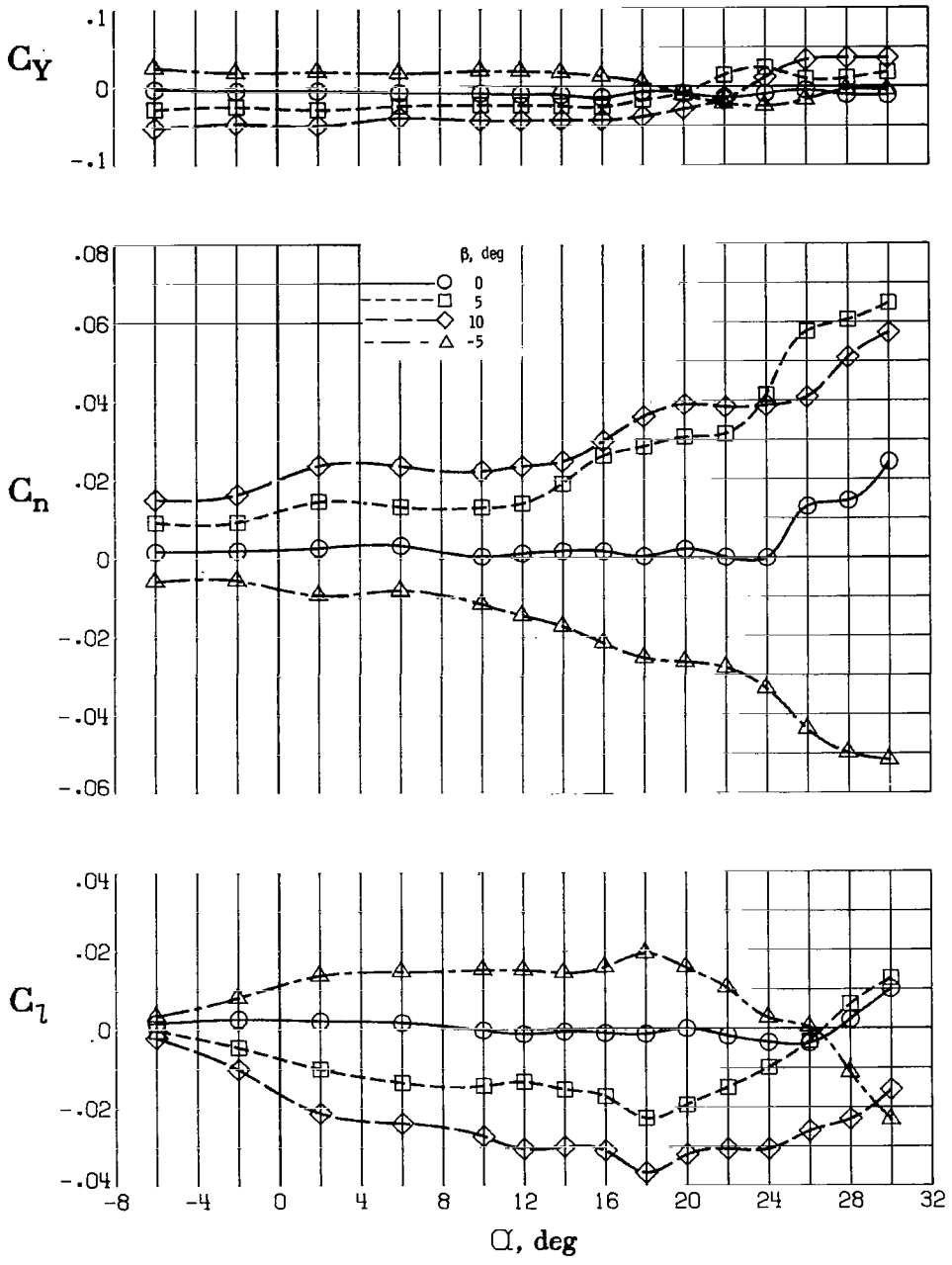

Figure 33.- Effect of sideslip on lateral-directional aerodynamic characteristics of high-lift configuration with 0.020S canard and vertical tails. $(\delta_{f,te})_{1,2,3} = 30^{o}$; $(\delta_{f,le})_{1,2,3,4} = 45^{o}$; $(\delta_{f,le})_{5,6,7} = 60^{o}$; $C_T' = 0$.

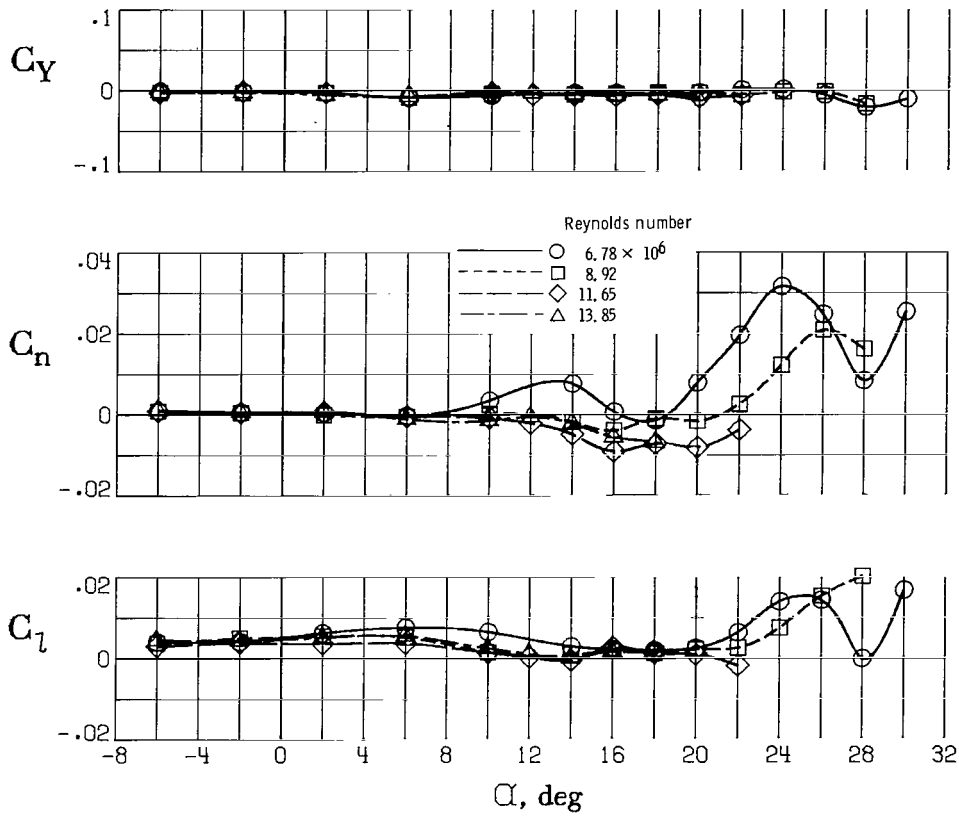

Figure 34.- Effect of Reynolds number on lateral-directional aerodynamic characteristics of clean configuration with vertical tails. $\beta = 0^\circ$; $C_{T'} = 0$.

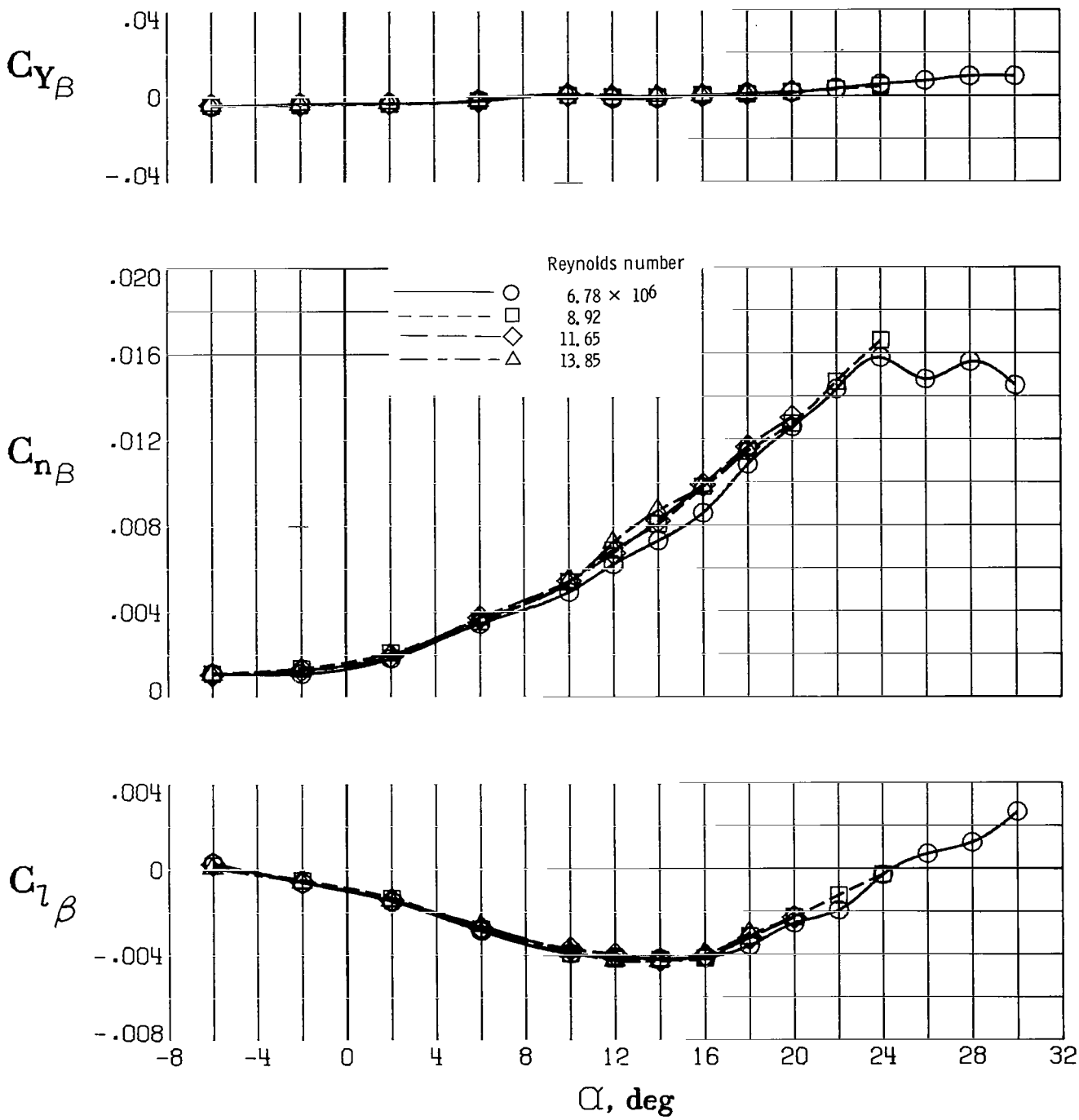

Figure 35.- Effect of Reynolds number on lateral-directional stability derivatives of clean configuration with vertical tails. $C_T' = 0$.

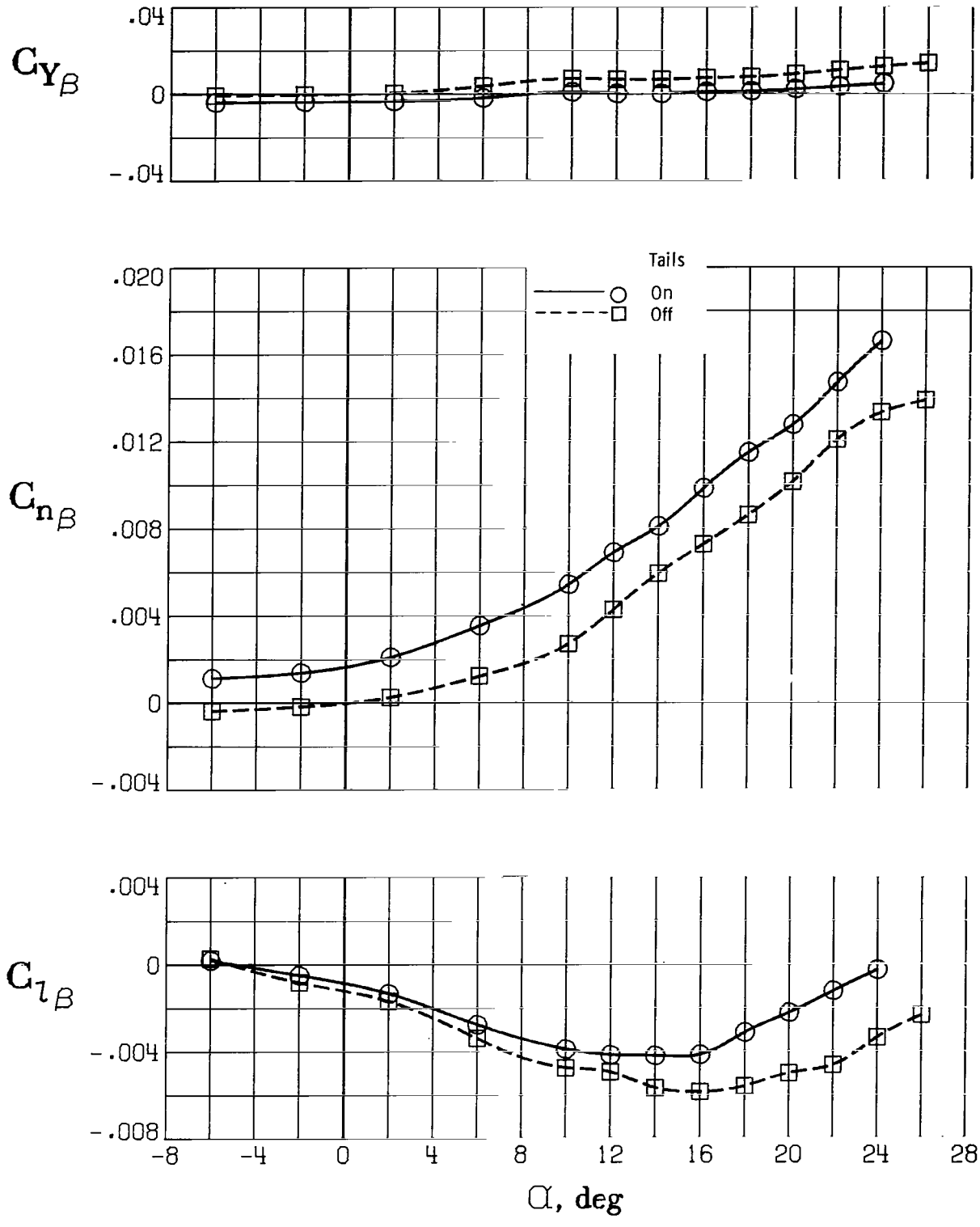

Figure 36.- Effect of vertical tails on lateral-directional stability derivatives of clean configuration. $C_T' = 0$.

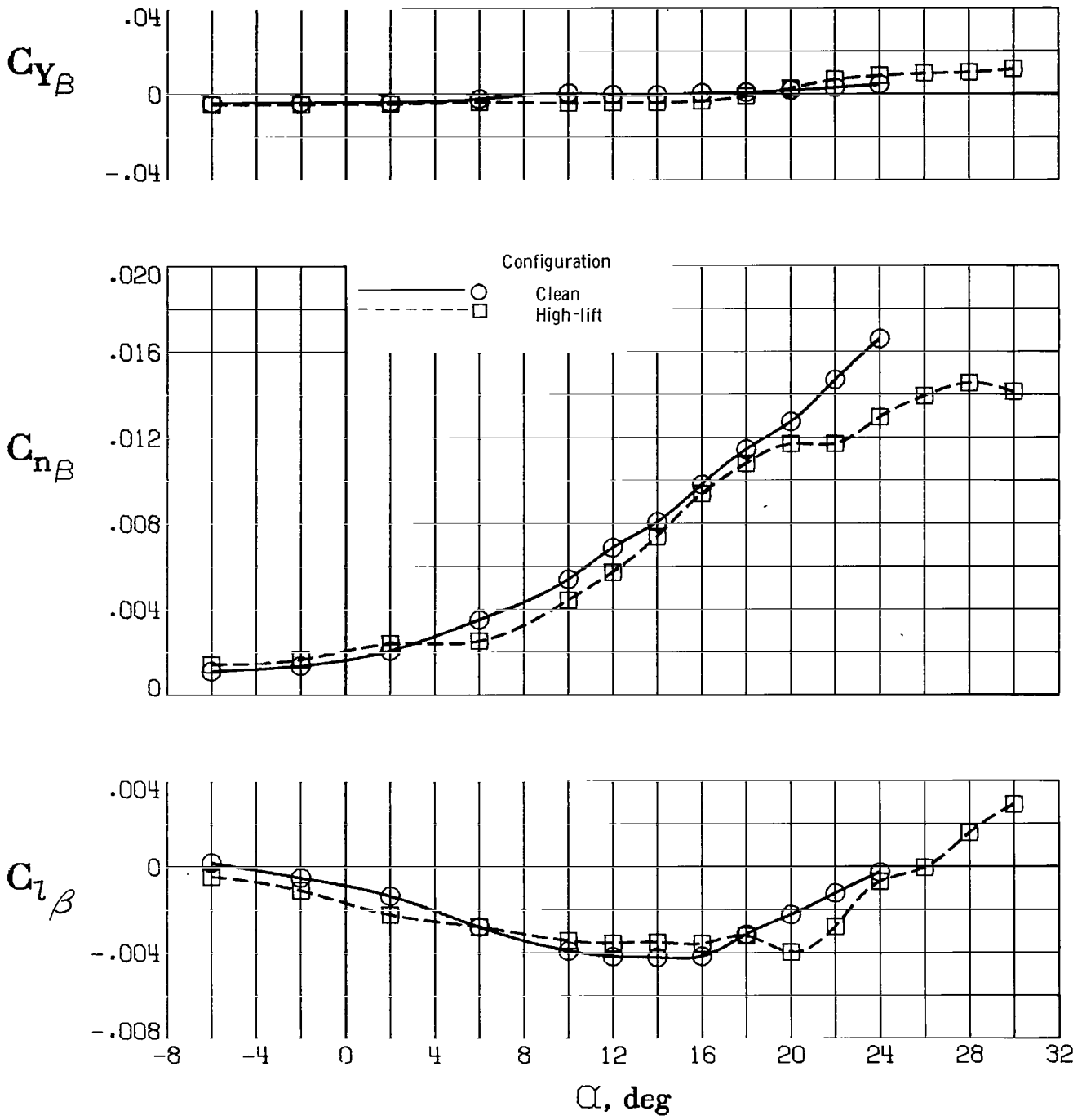

Figure 37.- Effect of leading- and trailing-edge flaps on lateral-directional stability derivatives. $(\delta_{f,te})_{1,2,3} = 20^o, 30^o, 30^o$; $(\delta_{f,le})_{1,2,3,4} = 45^o$; $(\delta_{f,le})_{5,6,7} = 60^o$; $C_T' = 0$.

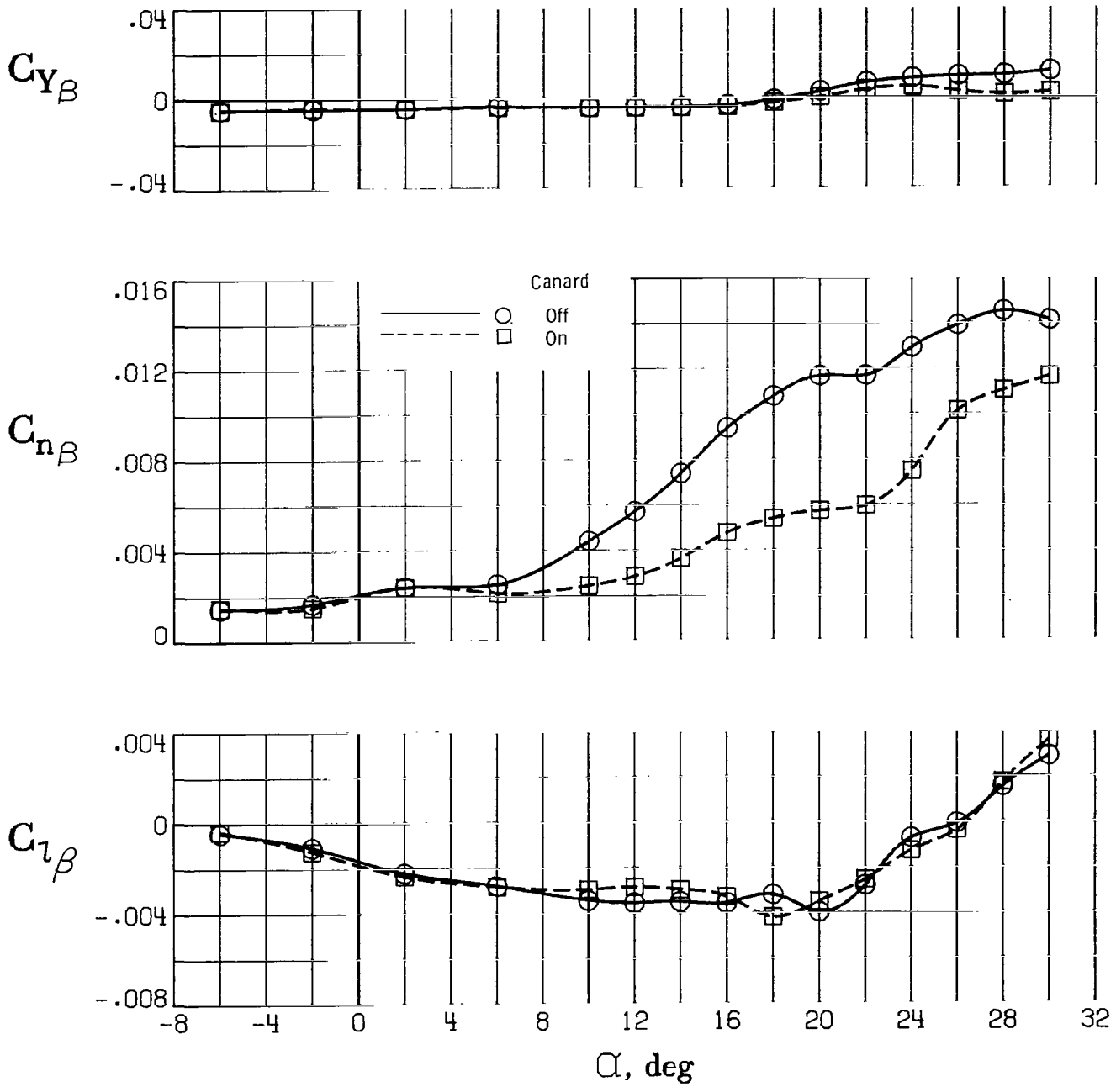

Figure 38.- Effect of 0.020S canard on lateral-directional stability derivatives of high-lift configuration. $(\delta_{f,le})_{1,2,3,4} = 45^o$; $(\delta_{f,le})_{5,6,7} = 60^o$; $C_T' = 0$.

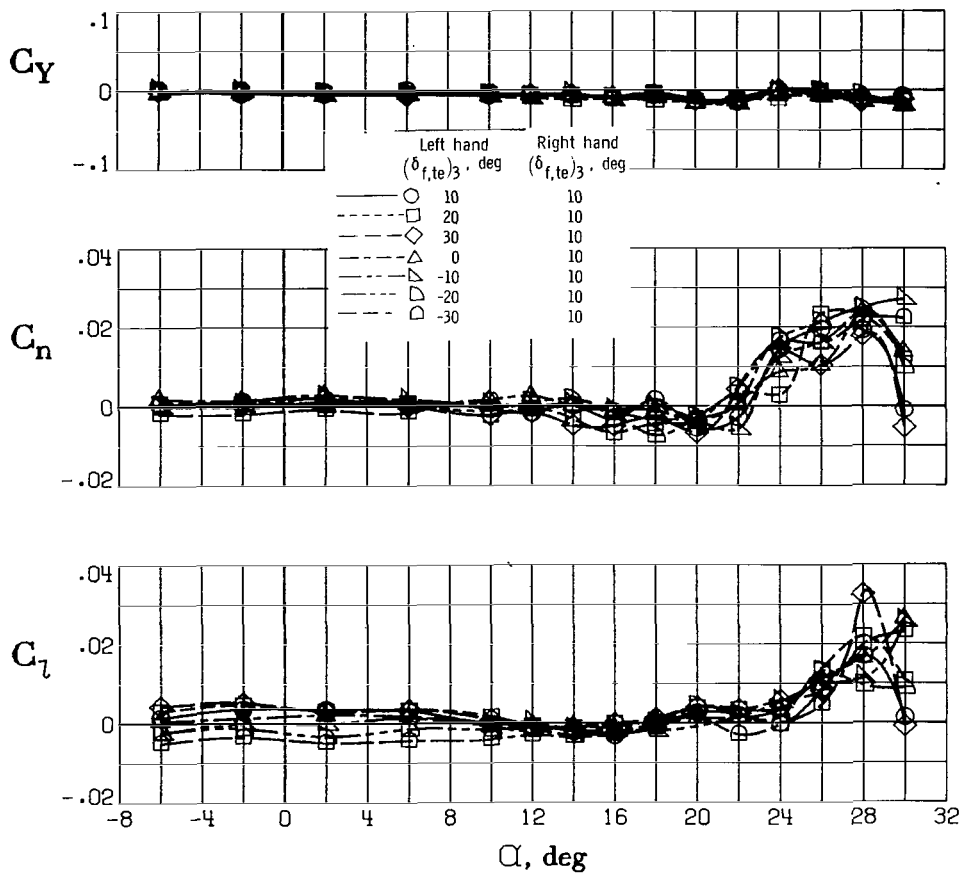

Figure 39.- Lateral control effectiveness of outboard trailing-edge flaps on lateral-directional aerodynamic characteristics of high-lift configuration. $(\delta_{f,te})_{1,2} = 30^o$; $(\delta_{f,le})_{1,2,3,4} = 45^o$; $(\delta_{f,le})_{5,6,7} = 60^o$; $\beta = 0^o$; $C_T' = 0$.

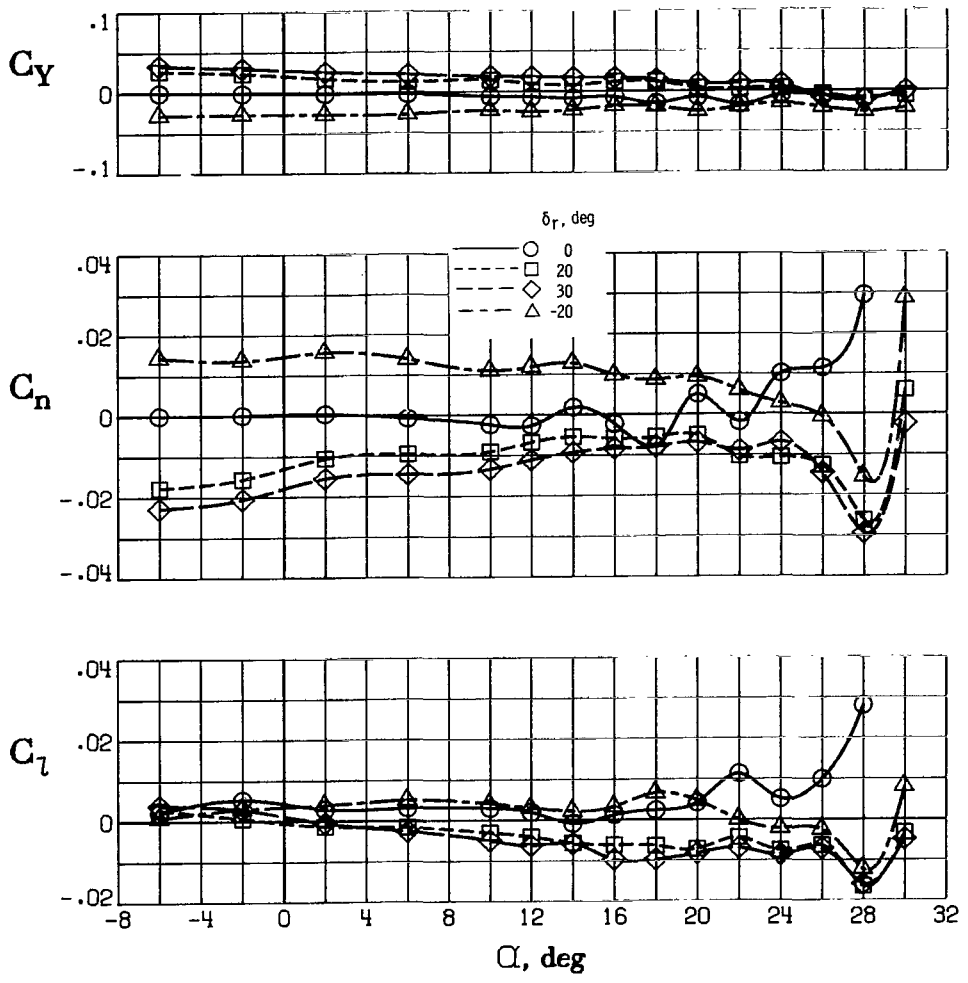

Figure 40.- Effect of rudder deflection on lateral-directional aerodynamic characteristics of high-lift configuration. $(\delta_{f,te})_{1,2,3} = 30°$; $(\delta_{f,le})_{1,2,3,4} = 45°$; $(\delta_{f,le})_{5,6,7} = 60°$; 0.025S canard; $\beta = 0°$; $C_T' = 0$.

NASA-Langley, 1977 L-11086

NATIONAL AERONAUTICS AND SPACE ADMINISTRATION
WASHINGTON, D.C. 20546

OFFICIAL BUSINESS
PENALTY FOR PRIVATE USE $300

SPECIAL FOURTH-CLASS RATE
BOOK

POSTAGE AND FEES PAID
NATIONAL AERONAUTICS AND
SPACE ADMINISTRATION
451

U.S.MAIL

406 CC1 C1 U A 770603 S00903DS
DEPT OF THE AIR FORCE
AF WEAPONS LABORATORY
ATTN: TECHNICAL LIBRARY (SUL)
KIRTLAND AFB NM 87117

MASTER: If Undeliverable (Section 158 Postal Manual) Do Not Return

"The aeronautical and space activities of the United States shall be conducted so as to contribute . . . to the expansion of human knowledge of phenomena in the atmosphere and space. The Administration shall provide for the widest practicable and appropriate dissemination of information concerning its activities and the results thereof."

—NATIONAL AERONAUTICS AND SPACE ACT OF 1958

NASA SCIENTIFIC AND TECHNICAL PUBLICATIONS

TECHNICAL REPORTS: Scientific and technical information considered important, complete, and a lasting contribution to existing knowledge.

TECHNICAL NOTES: Information less broad in scope but nevertheless of importance as a contribution to existing knowledge.

TECHNICAL MEMORANDUMS: Information receiving limited distribution because of preliminary data, security classification, or other reasons. Also includes conference proceedings with either limited or unlimited distribution.

CONTRACTOR REPORTS: Scientific and technical information generated under a NASA contract or grant and considered an important contribution to existing knowledge.

TECHNICAL TRANSLATIONS: Information published in a foreign language considered to merit NASA distribution in English.

SPECIAL PUBLICATIONS: Information derived from or of value to NASA activities. Publications include final reports of major projects, monographs, data compilations, handbooks, sourcebooks, and special bibliographies.

TECHNOLOGY UTILIZATION PUBLICATIONS: Information on technology used by NASA that may be of particular interest in commercial and other non-aerospace applications. Publications include Tech Briefs, Technology Utilization Reports and Technology Surveys.

Details on the availability of these publications may be obtained from:

SCIENTIFIC AND TECHNICAL INFORMATION OFFICE

NATIONAL AERONAUTICS AND SPACE ADMINISTRATION

Washington, D.C. 20546